METAL-SULFUR BATTERIES BASED ON SOLID-STATE REACTION

A Thesis
Presented to the Faculty of the Graduate School
of Cornell University
in Partial Fulfillment of the Requirements for the Degree of
Masters of Science

by
Shuya Wei
February 2016

ABSTRACT

Sulfur/Polyacrylonitrile composites provide a promising route towards cathode materials that overcome multiple, stubborn technical barriers to high-energy, rechargeable lithium-sulfur (Li-S) cells. Using a facile thermal synthesis procedure in which sulfur and polyacrylonitrile (PAN) are the only reactants, we create a family of sulfur/PAN (SPAN) nanocomposites in which sulfur is maintained as S_3/S_2 during all stages of the redox process. By entrapping these smaller molecular sulfur species in the cathode through covalent bonding to and physical confinement in a conductive host, these materials obviate polysulfide dissolution and shuttling between lithium anode and sulfur cathode. We show that in the absence of any of the usual salt additives required to stabilize the anode in traditional Li-S cells, Li-SPAN cells cycle trouble free and at high Coulombic efficiencies in simple carbonate electrolytes. Electrochemical and spectroscopic analysis of the SPAN cathodes at various stages of charge and discharge further show a full and reversible reduction and oxidation between elemental sulfur and Li-ions in the electrolyte to repeatably produce Li_2S as the only discharge product over hundreds of cycles of charge and discharge at fixed current densities.

The SPAN concepts have further extended to sodium-sulfur batteries, since research efforts have encountered more severed challenges, such as cathode material dissociation and dissolution, instable sodium deposition and insufficient cycle life with rapid capacity decay. We present a stable cycling room temperature Na-S battery that uses a sodium metal anode, a microporous carbon-sulfur composite, and a carbonate electrolyte with a hybrid ionic liquid silica nanoparticle (SiO_2-IL-ClO_4) as additive. The cell can stably cycle for over 100 cycles at 0.5C (1C = 1675 mAh/g) with 600 mAh/g reversible capacity and nearly 100 percent Coulombic efficiency

achieved. Spectroscopic and electrochemical analysis indicates a solid-state reaction probably happens only inside micropore on the cathode side, which contributes to the high stability and reversibility of the cell.

BIOGRAPHICAL SKETCH

Shuya Wei received her B.Eng. degree in Bioengineering from Nanyang Technological University, Singapore in 2013. Her research focuses on nanoparticle-polymer composite materials design and their applications in electrochemical energy storage technologies.

ACKNOWLEDGEMENTS

The author would like to express her deepest gratitude to her advisor, Professor Lynden A. Archer, whose help, continuous suggestions, invaluable teachings and guidance assisted her greatly in the completion of her master's research. The author is grateful to Prof. Archer who was willing to share his research experiences, enlightened the author in this field of research. Throughout the year project, Prof Archer's understanding, assistance and support had provided her with unconstraint learning opportunities. Moreover, Prof. Archer also ensures that works were going on well and regularly reviewed the author's research progress, enabling the author to complete her project successfully. Under his supervision, the author gained a lot of in-depth knowledge pertaining to this area of research and had decided to pursue research as her career path.

The author would also like to extend her gratefulness to her thesis committee member Professor Yong L. Joo for his assistance, teachings and valuable suggestions and all the Archer group members for their help.

TABLE OF CONTENTS

1 INTRODUCTION

1.1 Background

Among solid-state cathode materials under consideration for rechargeable lithium batteries, elemental sulfur offers the greatest promise for reversibly storing large amounts of electrical energy at moderate cost. As a cathode, sulfur hosts as many as two lithium ions non-topotactically via the following redox reaction: $16Li + S_8 \leftrightarrow 8Li_2S$. This reaction is attractive for electrochemical storage for a number of reasons. It can be used to reversibly store large amounts of electrical energy – up to 2500Wh/kg or 2800Wh/L of sulfur – a factor of ten or more higher than other electrochemical storage technologies (e.g. Ni-H (80Wh/kg, 120Wh/L), Li-ion (150Wh/kg, 250Wh/L), and Li-ion polymer batteries (180Wh/kg, 300Wh/L)) of contemporary interest (Figure 1) [1-5]. The reaction also occurs spontaneously, is fully reversible, and does not require intervention using catalysts or other means. Finally, the reaction can in principle occur entirely in the solid state and generates lithium-sulfur compounds as its only products. This can be contrasted with competing energy storage solutions based on combustion of fossil fuels, which irreversibly generate even larger amounts of energy on a gravimetric or volumetric basis (e.g. commercial coal: 6.7kW·h/kg, and a commercial-grade gasoline: 12kW·h/kg, 9kW·h/L), but with the added burden of managing harmful CO_2 and other gaseous emissions. The low cost of sulfur ($0.02 per g) and its availability in regions all over the world provides an additional incentive for development of Lithium-Sulfur (Li-S) electrochemical storage technology [6, 7].

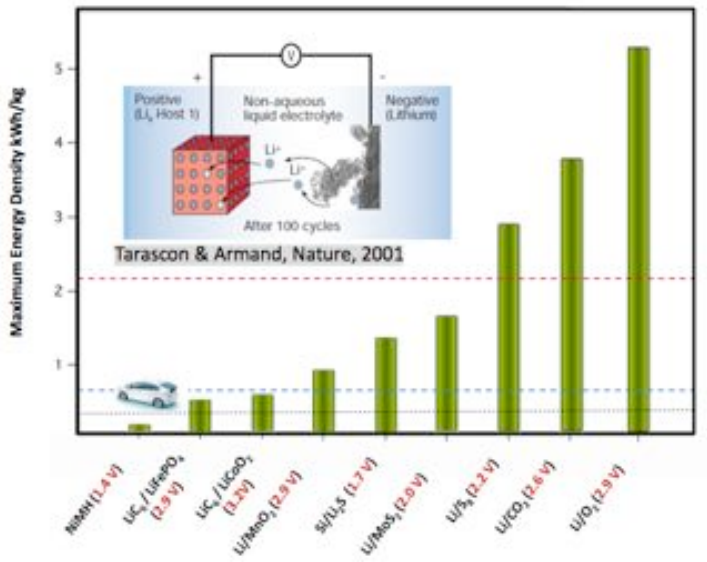

Figure 1. Comparison of the theoretical energy density and discharge voltages of different battery storage platforms. The inset illustrates the challenge with lithium dendrite growth and proliferation that limits adoption of storage technologies to the right of the plow that use metallic lithium as anodes for high overall cell energy densities. The red horizontal line represents the useful energy density of gasoline for transportation (i.e. the energy density of gasoline taking into account the 18% efficiency of the internal combustion engine). The dashed blue and black lines correspond to the US Advanced battery Consortium (USABC) long-term (2020) and short-term energy density targets, respectively [8].

Despite the considerable advantages offered by Li-S storage technology, commercial development of a practical Li-S rechargeable battery has been limited by multiple transport and thermodynamics-related challenges. A goal in writing this review is to show that the most important of these challenges provide opportunities for clever designs of the electrodes and electrolytes for Li-S cells using the toolset of nanomaterials science and engineering. A perhaps more practical motivation for writing the review is that despite the significant advances made over the last decade in improving Li-S battery performance, the actual storage delivered by even the best Li-S cells reported in the literature is still quite far away from the theoretical capacity upon which much of the promise of the Li-S battery lies. The best performing Li-S cells rarely deliver storage capacities above 60% of the theoretical value for this chemistry. This situation can be contrasted with the state of affairs in more traditional lithium ion batteries, where cell-

level performance approaching 90% of theoretical capacities are common. A Li-S battery that delivers 50% of its theoretical capacity over hundreds of cycles of charge and discharge already offers superior energy storage to the most energy-dense LIBs on a gravimetric storage basis, but substantially better performance is needed from Li-S cells to compete with LIBs for storage on a volumetric basis. The study carried out by Jie[9] (Figure 2) nicely illustrates this point. The study also underscores the need for Li-S cell designs in which high sulfur loadings in the cathode is achieved. Specifically, at low sulfur loadings, the volumetric energy density for the Li-S battery is noticeably lower than that of commercial lithium ion cells, even if one could realize the theoretical capacity of sulfur. Rechargeable Li-S cells that approach the theoretical capacity of the electrodes at high sulfur loadings are obviously desired.

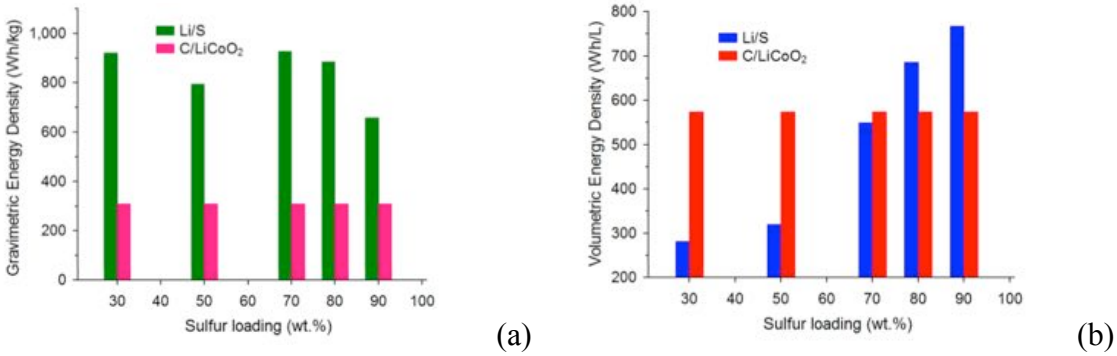

Figure 2. Gravimetric energy densities (a) and Volumetric energy densities (b) of lithium-sulfur cells with different sulfur loading percentages and their comparison to a $LiC_6/LiCoO_2$ cell[9].

In-depth understanding of the working mechanism, transport and other barriers that limit performance of Li-S cells are needed for further progress in the field. Such understanding is also essential to guide emerging efforts aimed at rationally designing each of the components in the Li-S cell towards the goal of full materials utilization. Sulfur is infamous for its poor electrical conductivity ($5x10^{-30}$ S/cm at 25°C) and ease with which it is able to form solid allotropes (over 30 are known) [10]. The first of these traits means that a pure sulfur cathode is intrinsically

insulating in nature, which limits the utilization of the active electrode material. High-surface area carbons are typically used as conductive additives within the cathode, but better charge transport in the cell often comes at the expense of storage capacity. Additionally, the volume of sulfur increases by around 80 % (density changes from 2.03 g/cm^3 for sulfur to 1.66 g/cm^3 for Li_2S) when it is fully lithiated. This means that synergistic cathode designs that can accommodate the volume change without compromising electronic connections with conductive additives, which do not expand, are critical for stable, long-term cell performance. A consequence of the second trait is that the preferred redox reaction product, Li_2S, is almost always accompanied by formation of various intermediate lithium polysulfides (LiPS = Li_2S_n, $2 \leq n \leq 8$) products (see Figure 3). Depending on the value of *n*, these intermediates can be either insoluble or soluble in the electrolyte, which leads to multiple challenges in managing active materials utilization and reuse. For example, the fully reduced product, Li_2S is insoluble in most electrolytes and is both electronically and ionically insulating. Thus, once Li_2S begins to form in the sulfur cathode, it can only grow by spreading outwards to cover the exposed surface of the conductive carbon particles in the electrode. Ultimately, this growth produces an insulating film on the carbon, which prevents further electronic and ionic access to the active material in the cathode, and the cell discharge voltage drops rapidly (Figure 4). Especially troublesome, are the soluble (Li_2S_n, $2<n<8$) polysulfide discharge products, which establish an internal shuttling pathway between the lithium anode and sulfur cathode that, if unchecked, will continuously consume the active material in both electrodes. Specifically, during the first discharge, the higher order LiPS ($n>2$) dissolve into the electrolyte, depleting sulfur from the cathode. Once in the electrolyte, polysulfides diffuse freely and ultimately reach the metallic lithium anode where they undergo chemical reaction to form lower order polysulfies, including Li_2S_{n-1} and Li_2S,

which may either deposit on the Li anode or diffuse back to the sulfur cathode, where they react with sulfur to reform higher-order polysulfides.

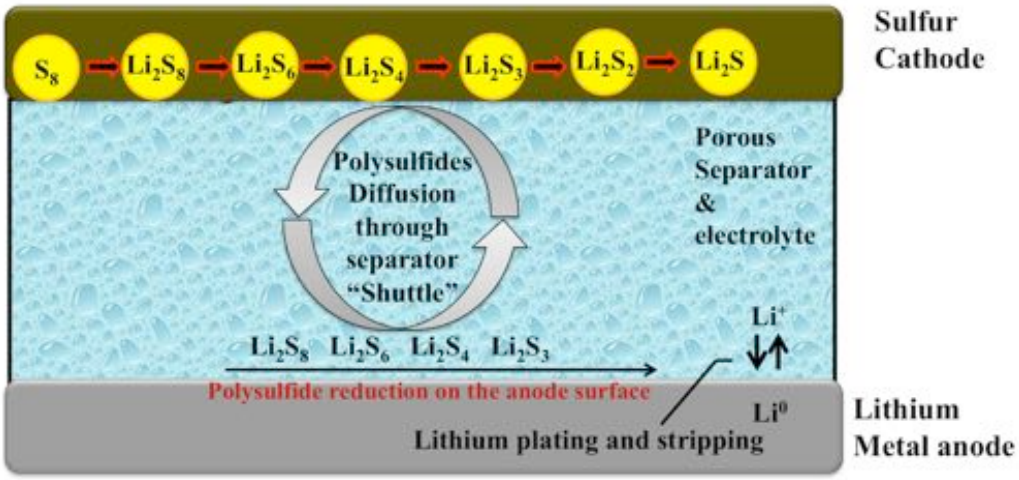

Figure 3. Illustration of polysulfides dissolution and shuttling process in a Li-S battery during the recharge processa [11].

The parasitic loop or 'shuttle' illustrated in Figure 3 is free to take place repeatedly and continuously during the cell recharge and not only depletes the active electrode materials, but continuously consumes electrical energy from an external circuit. It is easily visualized by the telltale asymmetry in the discharge and charge profiles (Figure 4a) of a Li-S cell and, lowers the Coulombic efficiency of the cell. Shuttling can also occur during cell storage and leads to self-discharge, which limits the shelf life of Li-S batteries. Sequestering the sulfur in carbon nanocapsules[12-14] is one of a handful of nanomaterials approaches that have been shown to completely remove this asymmetry (Figure 4a), underscoring its fundamental connection to LiPS dissolution. As illustrated in Figure 4b, without any other intervention strategies, this method completely eliminates the shuttle during the first cycle of charge and discharge for a range of Li-S cell discharge/charge current densities.

In addition to the intrinsically high storage capacity of sulfur, the high overall energy storage capacity of the Li-S cell stems from the use of metallic lithium as the anode. Li is readily ionized in a variety of aprotic liquids and as such provides an efficient complement to sulfur in an electrochemical cell designed to store large amounts of electrical energy. Unfortunately, even at low current densities, Li electrodeposition is sensitive to defects at the electrode surface and is prone to various transport and morphological instabilities[15, 16] that lead to growth and proliferation of rough electrodeposits collectively termed dendrites. Nucleated at the anode, these dendrites may grow as mossy deposits that react with the electrolyte and, if unchecked, will ultimately consume it all, drying out the cell. Dendrites may also grow and proliferate in the inter electrode space, ultimately short-circuiting the cell with potentially catastrophic consequences for safety. A remarkable, though poorly studied feature of the Li-S cell is that it possesses multiple internal safety measures that prevent catastrophic failure by dendrite-induced short circuits. LiPS dissolution and shuttling in the electrolyte provides an intrinsic mechanism for passivating dendrite tips by reaction with LiPS species in the electrolyte. Specifically, the tips concentrate electric field lines and the LiPS flux in the electrolyte, which leads to the reduction of LiPS and deposition of insoluble, insulating Li_2S on the tip surface limiting/eliminating further deposition of Li. This process also provides a high intrinsic overcharge tolerance for Li-S cells.

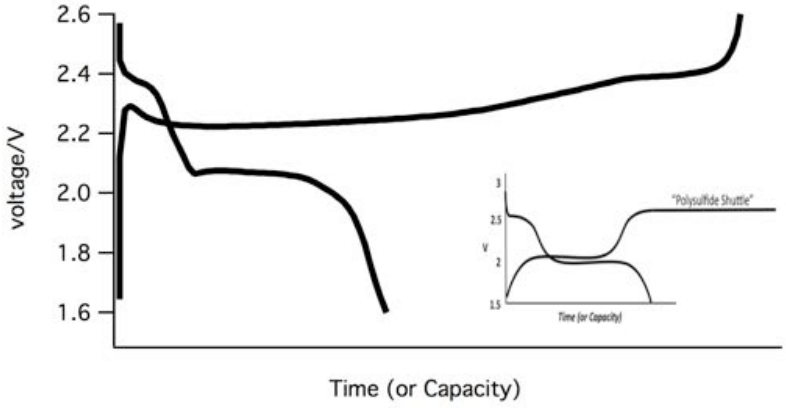

(a)

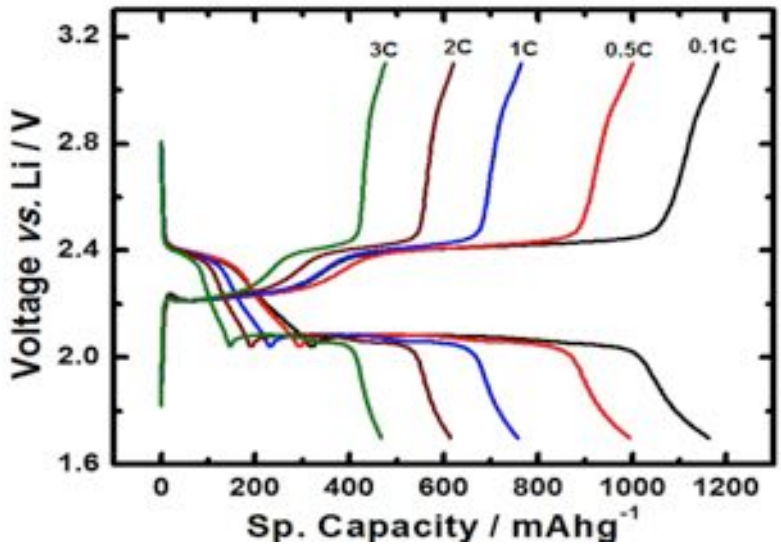

(b)

Figure 4. Discharge and Charge Profiles for Li-S cells: (a). Cell in which LiPS shuttling is dominant; inset is the drawing that shows the idea of 'polysulfide shuttling' **(**b). Cell in which sulfur is sequestered in carbon nanocapsules in which shuttling is eliminated over a wide range of current densities (0.1 – 3C) [13].

Through systematic application of nanotechnology to each component of the Li-S cell, significant improvements have been achieved in Li-S battery technology during the last decade. In particular, nanomaterials have been used to address the three most serious shortcomings outlined in the previous section: poor electrical conductivity of sulfur and sulfides; polysulfide-dissolution induced shuttling; and volume expansion. Nanomaterials can provide shorter

pathways for ions and electrons, which helps to solve the problem of poor electrical conductivity of the cathode [4, 5]. The intrinsically high surface-to-volume ratio of nanoparticles based on materials such as carbon with high affinity for sulfur has also been used to advantage to simultaneously provide kinetic barriers to LiPS loss to the electrolyte and to facilitate electronic transport in the cathode. Well-designed nanostructures can also be used as cathode additives to accommodate volume changes during discharge and charge, stabilizing the cathode in order to achieve greater performance.

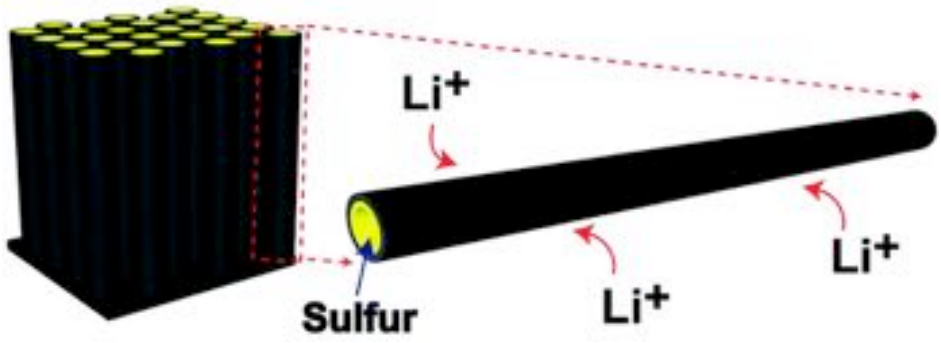

Figure 5. Illustration of nanostructured sulfur-carbon composite cathode; the diameter of the nanotube is 200nm and the length is 60 μm [17].

This effect is underpinned by a fundamental principle applicable to all nanomaterials: if a material of interest is expected to undergo a thermodynamic transition to an unfavorable state with critical nucleation radius r_c, confining the material to a rigid particle of radius $r_p < r_c$ eliminate such transitions [18]. Hollow nanostructures with anisotropic shapes (see Figure 5) are particularly advantageous because they can be designed to solve almost all three problems in a sulfur cathode using a single architecture. Specifically, such particles sequester the sulfur on

nanometer length scales; they dramatically reduce charge transport distances in the poorly conducting sulfur and sulfide phases contained in the nanometer sized pores; and provide an interconnected network of percolated surface contacts, which at relatively low particle contents, facilitates good electrical connections to an external circuit. An extreme example that illustrates the potential benefits of this strategy is the work by Cui and co-workers[17], which applied a hollow carbon nanofiber-encapsulated sulfur cathode.

1.2 Objective

Much interest has been aroused in the field of nanocomposite carbon materials owing to their beneficial attributes and widespread application. The chief objective here is to synthesize sulfur-polyacrylonitrile composite and microporous carbon polyhedron/sulfur nanocomposites as cathode materials for the application metal-sulfur batteries and fundamentally and systematically understand the chemistry and electrochemistry of these composites. This objective had been successfully achieved and problems were identified and solved in the following chapters.

2 LITERATURE REVIEW

2.1 Nanomaterials designs for sequestering sulfur in the cathode

Three of the four barriers to development of a practical Li-S cell that live up to the promise of the technology can be directly traced to the cathode. It is therefore unsurprising that development of functional cathode designs capable of overcoming these barriers has been a high priority for research. Cathodes based on components capable of achieving the necessarily electronic conductivity, of accommodating volume changes associated with the lithiation and delithiation reaction, and most importantly, which prevent polysulfide dissolution are an area of active study worldwide. Although largely driven by intuition the large improvements in capacity and cycling performance produced by even small changes in the electrode and electrolytes can be readily understood in terms of the mechanistic insights from in-situ analysis of the Li-S cathode. Incorporation of high-surface area and electrically conductive nanomaterials in the sulfur cathode have, for example, been demonstrated over the last decade lead to significant improvements in discharge capacity and lifetime. We focus first on the role nanostructures capable of trapping sulfur and polysulfides in the cathode using physical/kinetic and chemical/thermodynamic sequestration have played in improving the design and performance of the sulfur cathode in Li-S cells.

2.2 Sequestering sulfur in the cathode using physical forces

The strong interaction of sulfur with carbon and the synergetic effects the carbon brings in terms of enhancing the conductivity of the cathode has led to an upsurge in interest in cathodes based on sulfur-carbon nanocomposites[19, 20]. The morphology of the carbon-sulfur nanocomposite is now understood to influence everything from the cycling performance,[21, 22] propensity of

the cells to self-discharge,[23] and the LiPS shuttle.[24, 25]

2.2.1 Sulfur infused into porous carbon matrices

Carbonaceous materials with high porosity are widely used as conductive agents and as cathode hosts/matrices to trap the active polysulfide species in the cathode during cell operation. The perspective provided by the XANES studies by Abruna and co-workers provides straightforward justification for these efforts in terms of their ability to increase active material utilization. In addition, if the carbonaceous materials are engineered to contain sulfur in nanometer sized pores that can better accommodate volume expansion and strain they are expected to stabilize the mechanical properties of the cathode and hence enhance the Li-S cell lifetime. Thus in addition to its effect on sulfur sequestration and active material utilization, the pore size also affects other features such as the ease with which electrolyte can infiltrate the cathode and the rate with which electrons can be transported to/from the active material. Pore size and pore volume of the nanocomposite materials can therefore affect myriad aspects of the Li-S cell performance, including the plateau voltage, active material utilization, rate capability, discharge capacity, and capacity retention.

Porous carbon is classified as microporous (pore diameter less than 2nm), mesoporous (2 to 50 nm) or macroporous (larger than 50 nm). Reports on carbon-sulfur composites with a pore size greater than 10 nm show the typical two-plateau behavior of the sulfur electrode, which is similar to cathode without mesoporous carbon. In contrast, microporous carbon-sulfur composites have a slightly different voltage profile, with one plateau between 1.5 and 1.9 V vs. Li/Li^+ [26] which attains most of the discharge capacity. It is likely that sulfur is no longer in the S_8 cyclical structure in these composites; instead, small sulfur is formed due to the constrained pore volume

and sulfur and carbon are mixed at the atomic level [21, 27]. Consequently, the corresponding Gibbs free energy of the reaction is different because higher order polyfulfide formation process is excluded in the reaction.

Microporous carbon proves to be an effective sulfur immobilizer because it has extremely small pores to constrain sulfur and reaction by strong adsorption, which is able to prevent intermediate product polysulfides from outflowing into the electrolyte [28], as a result, long cycle life is often observed in the case [27, 29]. Zhang et al. [30] have obtained microporous carbon-sulfur composites with a narrow pore size distribution of about 0.7 nm after thermal treatment of sublimed sulfur and carbon spheres. This material delivers a large reversible capacity of 650 mAh/g even after 500 cycles at a current density of 400 mA/g, with a high coulombic efficiency as well. They have proposed that narrow micropores act as micro-reactors (shown in Figure 6) to confine all the electrochemical active species within the micropores and prevent sulfur and lithium polysulfides from releasing into the electrolyte such that the reversible capacity is improved. Guo et al. [21]have proved that, if the pore size of the carbon matrix is less than 0.5 nm, sulfur exists as smaller chainlike $S_{2–4}$ molecules due to limited pour volume. Thus, the higher order polysulfides that can dissolve into the electrolyte would not be formed during cycling process [31]. Smaller sulfur allotropes have become new starting active materials with the facilitation of microporous carbon materials. Despite exhibiting a good reversible capacity upon cycling, microporous carbon-sulfur composites have confined spaces that do not accommodate loaded active sulfur as well. It results in limited weight ratio of activate sulfur materials in the cathode and low practical capacity of the whole cathode materials.

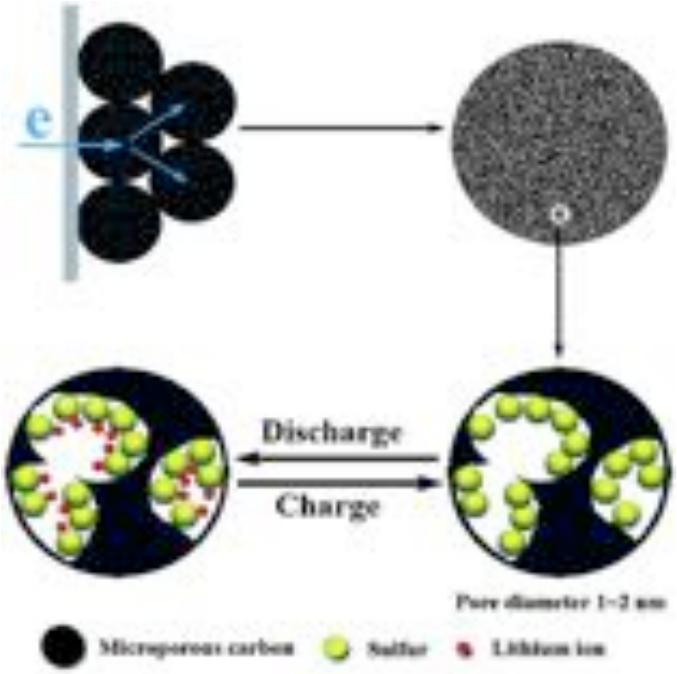

Figure 6. A scheme of the constrained electrochemical reaction process inside the micropores of the sulfur carbon sphere composite cathode. Reprinted with permission from[30]. Copyrights 2010 The Royal Society of Chemistry.

Porous carbons with an increased pore volume can be used to enhance sulfur loading. For this reason, mesoporous materials have been studied extensively as hosts for sulfur[32-35]. The large pore sizes over those of microporous materials allow for easier access to sulfur by liquid electrolytes such that it can facilitate Li ion migration. Thus, lithium sulfur cells with mesoporous carbon-sulfur cathodes show an increase in voltage plateau. Early work in this area was performed by Wang et al. [19, 36], who used an activated carbon with a pore size of around 2.5 nm as the conductive matrix and achieved a reversible capacity of 400 mAh/g. After that, Ji, Lee and Nazar [23] [37] have reported a highly ordered mesoporous carbon-sulfur cathode exhibiting high pore volume, uniform pore diameters and interconnected porous structure by employing a well-known mesoporous carbon material CMK-3, which is synthesized from a mesoporous silica template SBA-15. Their results show that this cathode renders a highly enhanced performance with reversible capacities up to 1320 mAh /g. The intake of sulfur within

the pores is accomplished by melt diffusion method, where sulfur and CMK-3 carbon mixture are heated together at 155 °C. The CMK-3/sulfur composite electrode was shown to exhibit a high initial discharge capacity of 1005 mAh/g, and it was improved to 1320 mAh/g by linking the carbon surface with polyethylene glycol (PEG) to further trap polysulfides. The highly porous carbon-sulfur composite reported by Lai [38] with 57 wt % sulfur loading delivers the initial high specific capacity up to 1155 mAh/g and a stable capacity of 745 mAh/g after 84 cycles at the current density of 40 mA/g. On the basis of the analysis of the microstructure and electrochemical performance, they confirmed that the composite could effectively prevent the shuttle behavior of the lithium-sulfur battery.

In designing mesoporous carbon-sulfur cathodes, factors such as pore size, pore volume and sulfur loadings are essential for improving the performance. The pore size and volume effects have been investigated by Li et al. [35], who studied a series of mesoporous carbon materials with tunable pore sizes ranging from 3 nm to 22 nm and pore volumes ranging from 1.3 to 4.8 cm^3/g. The authors reported that the overall electrochemical performance of Li-S cells based on electrodes containing carbon with different pore sizes are very similar if the sulfur loading is sufficiently high to fill the pores with sulfur. However, by partially filling the pores with sulfur, they observed improved utilization of the active material and enhanced cycling performance. This finding can be rationalized in terms of the competing beneficial effects of sulfur sequestration and optimized electrical contact with the mesoporous substrate with the less attractive features of a sulfur-filled pore, such as limited access to the electrolyte, reduced dissolution/diffusion of polysulfides and sluggish transport of lithium ions.

Carbons with bimodal pore structure, which combines microporous with mesoporous elements

were first reported as cathode hosts for Li-S cells by Liang et al. [28]. Other researchers have recently performed more in-depth studies of Li-S cells incorporating this type of carbon [32, 34, 39]. In general, carbon with a bimodal pore structure is believed to offer multiple advantages. The small pores can confine polysulfide species to prevent their outflow, while the large pores are in favor of accommodating the liquid electrolyte where lithium ions have high conductivity. He et al. [39] have synthesized sulfur bimodal porous carbons as the cathode for lithium sulfur cells cycled at high rate with an evaporation-induced self-assembly approach. They have obtained the desired bimodal distribution by optimizing the carbon: silica: surfactant ratio and demonstrated an initial capacity of 995 mAh/g and a capacity of 550 mAh/g after 100 cycles at 1675 mA/g rate. In addition, mesoporous silica, which is believed to increase hydrophilicity and help trap more polysulfides, has been applied in this work to enhance the cycle stability. Liang et al. [28] reported a carbon-sulfur nanocomposite based on a hierarchically structured micro-mesoporous carbon formed by a post-activation treatment. Sulfur was loaded solely into the microporous wall by a wet-impregnation method. The empty mesopores function as reservoirs for the soluble polysulfide ions formed during cycling. They also find that utilization of sulfur is strongly affected by the active mass fraction. A composite containing 11.7 wt% sulfur exhibits a first discharge capacity of 1584 mAh/g even at a very high current rate of 2500 mA g^{-1}. Increasing the composite's sulfur content to 51.5% gives a decreased discharge capacity of 818 mAh/g at first cycle. Rapid capacity fading is observed in all cases. A core-shell structure, in which sulfur cores are encapsulated by carbon shells, can improve sulfur loading without compromising cycleability. Li et al. [32] reported an ordered meso-microporous core-shell (MMCS) carbon as a sulfur container(shown in **Figure 7**). The core part of the composite with large pore volume and highly ordered porous structure promises a sufficient sulfur loading and a

high utilization of the active material, while the shell containing microporous carbon and smaller sulfur acts as a physical barrier and stabilizes the cycle capability of the entire composite. The composite exhibits a capacity as high as 837 mAh g^{-1} at 835 mA/g after 200 cycles with a high capacity retention of 80% vs. the second cycle. This bimodal structure can greatly reduce the diffusion of polysulfides into the bulk electrolyte.

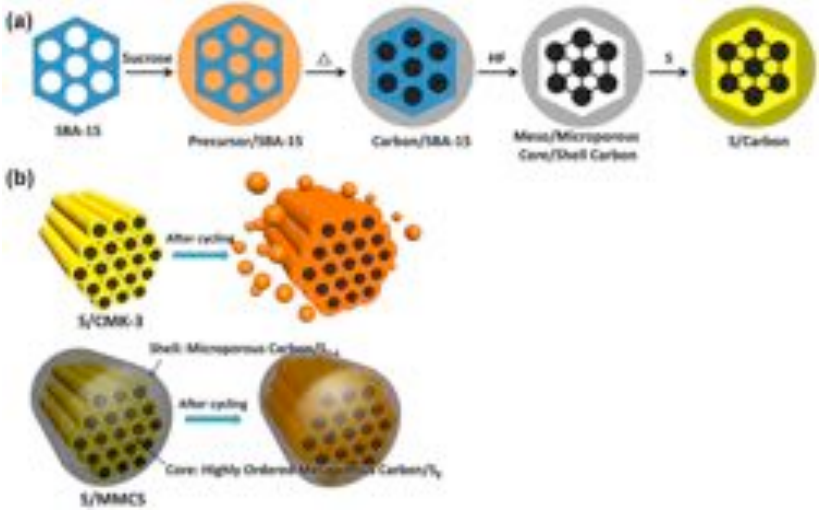

Figure 7. (a) Schematic for preparation of highly ordered meso-microporous core–shell (MMCS) carbon and sulfur/carbon composite. (b) Schematic of the mesoC/S_8-microC/S_{2-4} core–shell structure [32].

Macroporous carbons with pore sizes greater than 100 nm show no advantage on preventing shuttling upon cycling and have been investigated less as cathode for lithium sulfur system. Macroporous carbon has open structures that cannot effectively retain sulfur and intermediate polysulfides within pores. Wei et al. [40] have adopted KOH activation to obtain hierarchical porous structure including macropores derived from pig bone. Despite a high initial capacity of 1265 mAh /g is observed, the capacity decreases to 643 mAh /g only after 50 cycles. The substantial decay in capacity suggests that macroporous carbons are not ideal candidates for lithium sulfur cathodes.

2.2.2 Sulfur infused into anisotropic carbon nanostructures

One-dimensional (1-D) carbon nanostructures offer unique features for addressing problems related to conductivity and active material retention and utilization in a sulfur cathode. The conductive matrix created by the one-dimensional percolated carbon network provides better electrical connection to the active materials. In addition, novel designs of the 1-D nanostructured carbon can potentially address the previously mentioned difficulties in mechanical durability of sulfur cathodes. Ahn et al. [41] reported sulfur-containing multiwalled carbon nanotubes (MWCNTs) via a direct precipitation method for the cathode. In this case, sulfur is not trapped by or bonded strongly to nanotubes. As a result, a very low discharging capacity was observed upon 30 cycles. To achieve a stronger interaction between MWCNTs and sulfur, Yuan et al. [42] have taken advantage of the capillary effect between the sulfur and MWCNTs to construct a novel electrode with carbon nanotube as the core. This composite shows a good cycle life compared to the counterpart made by simply mixing sulfur with MWCNTs. However, a low initial capacity with only 650 mAh/g is observed. The reason is probably that sulfur is directly coated on the surface of the MWCNT host, resulting in the easy dissolution of polysulfide during cycling.

Chen et al.[43] have developed three dimensional (3D) multi-walled carbon nanotubes to house sulfur or lithium sulfide, and achieved much enhanced capacity with 780 mAh/g remaining after 200 cycles at a current density of 500 mA/g. They believe that 3D carbon nanotube structures can buffer the stress caused by the volume expansion of sulfur upon discharging [43], and retard the out-diffusion of sulfur-based materials from electrodes [44]. Besides, the pores existing in such 3D structures can facilitate electron diffusion while allowing fast ions transport. Recently, a

novel tube-in-tube carbon nanostructure (TTCN) with MWNTs confined within hollow porous carbon nanotubes is synthesized for Li-S cells by Zhao et al. [24]. MWNTs were encapsulated into hollow porous carbon nanotubes through a step-by-step strategy (shown in **Figure 8**). This structure is designed to enhance the electrical conductivity, hamper the dissolution of lithium polysulfide, and provide large pore volume for sulfur impregnation. As a cathode material for Li-S cells, the S-TTCN composite withholds a high sulfur content of 71 wt%. At a current density of 500 mA g^{-1}, a high discharge capacity of 918 mAh/g remained after 50 cycles, demonstrating high reversible capacity and good cycling performance as well as excellent rate capabilities.

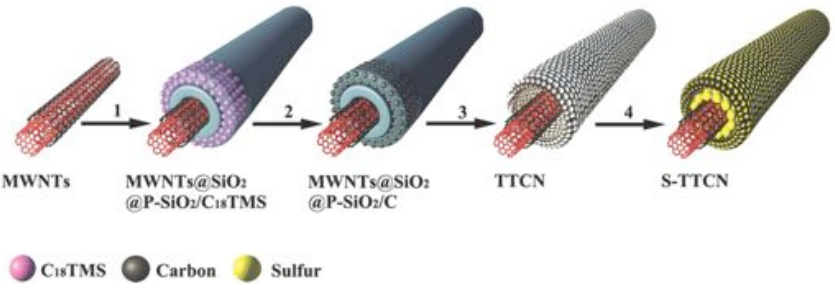

Figure 8. Schematic illustration for the formation of S-TTCN composite: (1) Uniform coating a solid SiO_2 layer and a porous SiO_2 layer embedded with $C_{18}TMS$ molecules on MWNTs; (2) formation of porous carbon nanotube by carbonization of $C_{18}TMS$; (3) etching SiO_2 layers to obtain tube-in-tube carbon nanostructure (TTCN) with MWNTs encapsulated within hollow porous carbon nanotube; (4) sulfur infused into TTCN to fabricate S-TTCN composite. Reprinted with permission from [24]. Copyrights 2014 Wiley-VCH Verlag GmbH & Co. KGaA, Weinheim.

Porous carbon nanofibers have also recently been used for sulfur electrodes to reduce the amount of exposed sulfur. In this approach, carbon nanofibers from commercial activated carbon cloth [45] or electrospun polymeric precursors [46] were impregnated with sulfur. The commercial activated carbon fibers have a narrower pore size distribution, with a majority of the microporous

structures smaller than 2 nm. Hollow carbon nanofibers with a high aspect ratio have been shown to be effective in trapping sulfur. Moon and co-workers [17] have encapsulated sulfur into thin-walled carbon nanowires, which were obtained with the assistance of anodic aluminum oxide templates, demonstrating high-rate electrochemical behaviors. They avoid of adding binders and other additives in cathodes, which increase the utilization of composite materials but results in continuous capacity fading. Zhang et al. [47] also reported the Li-S cells composed of colloidal microporous carbon nanofiber-encapsulated sulfur structures with unprecedented electrochemical performance and high specific capacity and good cycling stability (950 mA h g^{-1} after 50 cycles of charge-discharge). The excellent electrochemical performance of the battery is attributed to their high-quality fiber morphology, controlled porous structure, large surface area, and good electrical conductivity.

One-dimensional nanotubes/nanofibers have to date proven insufficient for retarding polysulfide dissolution and shuttling due to their open-ended structure. Although nanostructures with open-ends are beneficial for the access of electrolytes and ion migration, these same structures also result in polysulfide leakage. Core/shell structures have been explored to address the challenge of open-end structures. In most core/shell structures, sulfur or sulfur-based compound acts as the core. Furthermore, high sulfur contents of approximately 85% embedded in the shell can be achieved [48]. In particular, the sulfur-carbon sphere composite with 42 wt% sulfur presents a long electrochemical stability up to 500 cycles, based on the constrained electrochemical reaction inside the narrow micropores of carbon spheres due to strong adsorption. Therefore, the electrochemical reaction constrained inside the micropores proposed here would be the dominant factor for the enhanced long stability of the sulfur cathode [30].

2.2.3 Sulfur infused into hollow carbon nanostructures

Modifying the core/shell carbon framework also provides some approach towards preventing polysulfide dissolution. This can be achieved either by making a hollow shell to allow easy access of electrolyte or by making double shells to increase the effectiveness of preventing polysulfide dissolution. Jayaprakash et al. [13]. reported a hollow carbon-sulfur nanocomposite, where the hollow carbon capsule was generated by a template-based approach (shown in **Figure 9**). They display outstanding electrochemical features (high capacity retention of 91% after 100 cycles) attributed to sequestration of elemental sulfur in the carbon capsules and to its favorable effect in limiting polysulfide shuttling as well as to enhanced electron transport from the sulfur. Zhang et al.[25] reported a novel carbon-sulfur nanocomposite synthesized by confining sulfur in double-shelled "soft" carbon hollow spheres with high surface area and porosity. With void space between the core and double shells, the volume expansion can be buffered. The double shell structure facilitates ion and electron transport as well. This carbon–sulfur nanocomposite shows an initial discharge capacity of 1020 mA h g^{-1} and a reversible capacity of 690 mA h g^{-1} after 100 cycles.

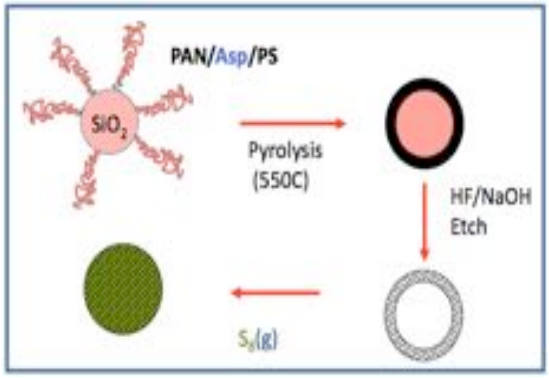

(A)
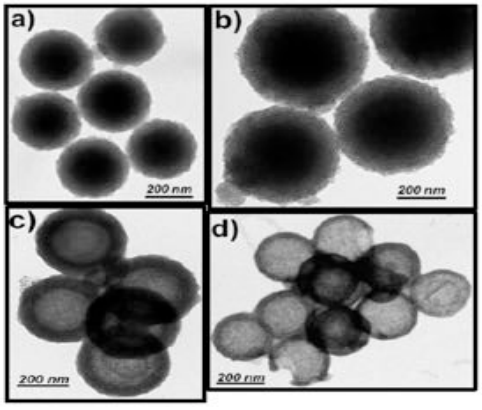

(B)

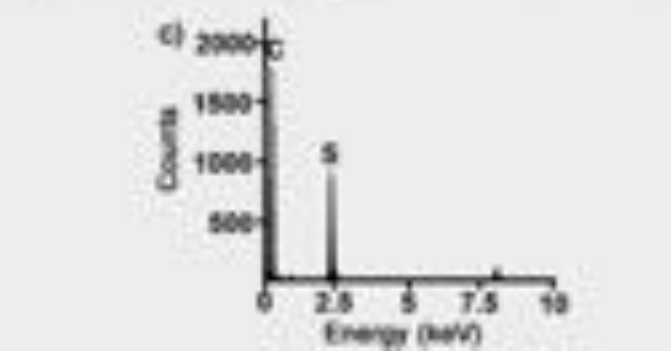

(C)

Figure 9. (A). Illustration of procedure to create C@S nanocomposites by infusion sulfur into carbon capsules. (B). TEM images of a) mesoporous carbon hollow spheres b) C@S nanocomposite and (C). EDX analysis of C@S nanocomposite showing the presence of sulfur [13].

Nanoporous carbon–sulfur composites represent a clever method to improve the performance of the sulfur cathode, as shown in the examples above. To realize enhanced performance, the following aspects should be carefully considered: (1) optimized pore size and closed structure to trap polysulfides and minimize pulverization, (2) large pore volume to increase the content of sulfur for practical applications and (3) maximized amount of sulfur loading inside carbon pores. Given the tremendous potential of porous materials in Li-S battery applications, it will be highly beneficial if the kinetics associated to ion migration inside the nanoporous materials can be studied in more detail. It is also equally important to further study a variety of techniques to construct optimized porous materials.

2.3 Sequestering sulfur in the cathode using specific chemical interactions

Previously, sulfur cathodes have been designed to absorb polysuflides (PS) via various carbon matrices with optimal porosity and high surface area. However, the physical barrier created by carbon only delays the rate at which PS diffuse into the electrolyte. As a result, the kinetics associated with PS dissolution are only slowed initially and over time PS leach out of the electrode. Consequently, low capacity fade is often observed. Considering the weak Van der

Waals interactions associated with the non-polar and hydrophobic carbon, these elements are too weak to contribute any appreciable adsorption effects. Furthermore, such methods often rely on expensive energy intensive methods to infuse the sulfur into the pores of the host material. As such, considerable attention to the use of surface-functionalized carbon materials as cathode material or metal oxides as cathode additive is currently being investigated. These materials possess polar chemical bonds and hydrophilic surfaces that provide chemical bonding with lithium polysulfides. In this way, the polysulfides produced during discharge is thermally sequestered in the cathode rather than temporarily capsuled.

Metal oxides have been utilized as either adsorbents or coatings to hinder the diffusion of LiPS. Nazar group has reported the use of porous SiO_2 as a polysulfide reservoirs [49]. The polysulfide shuttle mechanism is suppressed to a large degree by incorporating SBA-15 as an effective internal polysulfide reservoir, which permits adsorption/desorption in a reversible manner during the electrochemical reaction. Similar results were reported using mesoporous titania as an additive to the cathode [50]. Three types of mesoporous titania with different surface area, pore volume and pore size were investigated. The cathode was probed by FTIR and Raman to confirm the interaction between the Ti atom and sulfur species. The cathode with α-TiO_2 as additives maintained discharge capacities above 750 mAh/g after 200 cycles, achieved with less than 4 wt% content of additives. Other metal oxides, such as Al_2O_3, La_2O_3, and $Mg_{0.6}Ni_{0.4}O$ were also reported to be effective as additives in immobilizing the sulfur and retarding polysulfide shuttling [51-53]. Even as early as 2004, Hwang has patented several inorganic additives for Li-S cells, which included metal oxides, metal sulfides or a mixture thereof. Example metals include V, Al, Zr, and Ti. Preferred are V_2O_5, Al_2O_3, ZrO_2, and TiS_2 [54]. A recent work published by Archer group [55] took advantage of molecular sorbents (TMS-PDTA and ionic liquid IM-Cl) to

thermodynamically sequester sulfur species. The molecule were chosen because of the anchoring silane group which can tether to the carbon surface, and also because of the high binding energy towards LiPS calculated by DFT. This work is actually inspired by the former study carried out by the same group, which showed the ability of the PAN chains to pull Li_2S_x species out of solution, implying that the binding forces between Li_2S_x and PAN are strong and specific (**Figure 10**).

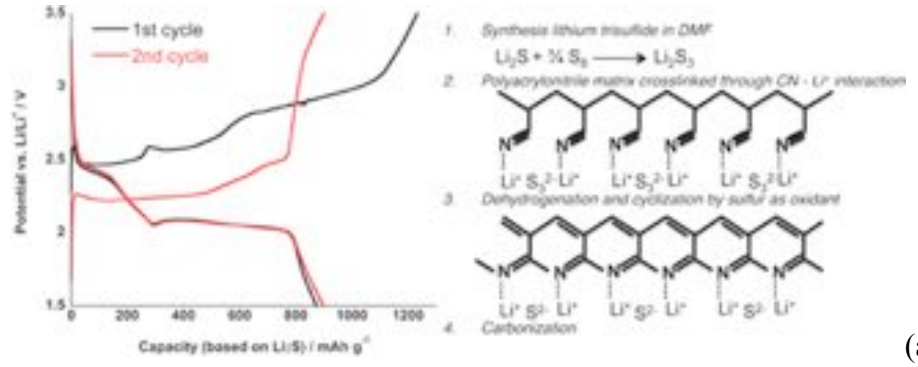

(a)

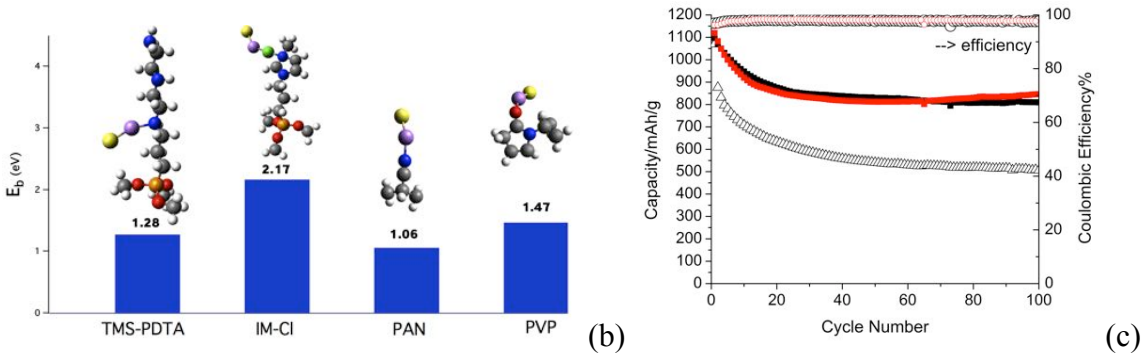

(b) (c)

Figure 10. (a) PAN as a host for Li_2S cathode and the corresponding voltage profile. Reprinted with permission from [56]. Copyrights 2012 American Chemical Society. (b) DFT calculation of binding energy of different additives with polysulfide species. (c) Cycling performance of Li-S cell with additives of TMS-PDTA (black circle); IM-Cl (red circle); and no additives (black triangle) [55].

Such studies have confirmed the importance of chemical interactions in hindering the migration

of soluble polysulfides. Although they are effective in reducing dissolution of LiPS, oxides and molecular sorbents, are often inherently insulating, which means that complementary painstaking steps are required to establish their optimal loadings. They impede electron transport and Li^+ ion pathways resulting in limited sulfur utilization and rate capability. Thus researchers are trying to look for a two-in-one strategy: a bifunctional sulfur host material that combines high conductivity with the ability to chemically bind LiPSs on the surface. The study of Ti_4O_7 as a sulfur host material was reported by two groups [57, 58]. The inherently polar, high surface area metallic oxide cathode host combines electronic conductivity for redox electron transfer with a polar surface for strong LiPSs/Li_2S binding, enabling low capacity fade rates to be sustained. The findings can be generalized to other kinds of Magnéli-phase metal oxides (V_nO_{2n-1}, W_nO_{2n-1}, Mo_nO_{2n-1}, etc.) and some other matrix materials with abundant low coordinated metal sites on surface (**Figure 11**).

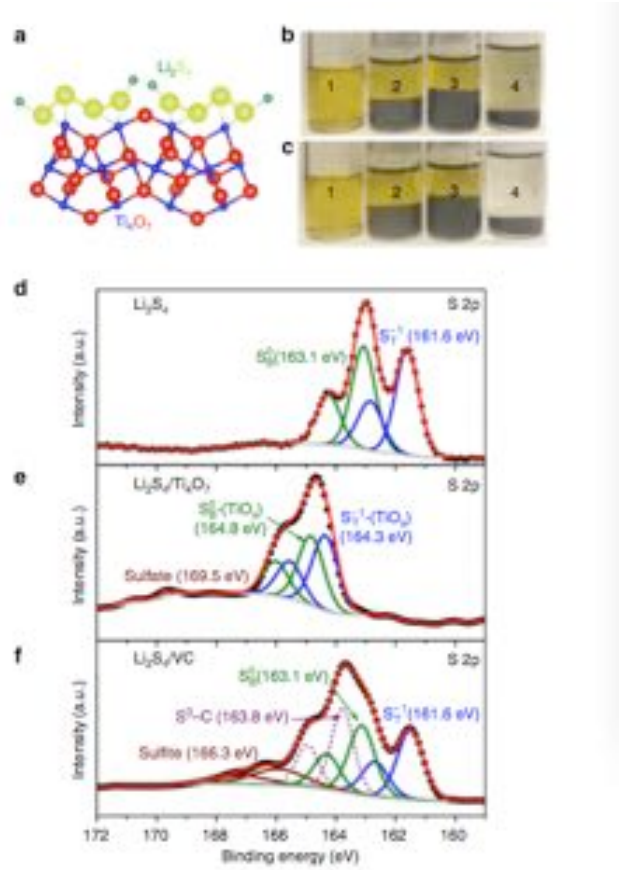

Figure 11. Demonstration of the strong interaction of LiPS with Ti_4O_7. (a) A schematic showing the electron density transfer between Li_2S_4 and TiO_x (yellow 1⁄4 S, green 1⁄4 Li, blue 1⁄4 Ti, red 1⁄4 O). (b,c) Sealed vials of a Li_2S_4/THF solution (1), and after contact with graphite (2), VC carbon (3) and Ti_4O_7 (4), immediately upon contact (b) and after 1 h stirring (c). (d–f) High-resolution XPS S 2p spectra of (d) Li_2S_4, (e) Li_2S_4/ Ti_4O_7 and (f) Li_2S_4/VC (black dotted line 1⁄4 experimental data, red line 1⁄4 overall fitted data, solid/dotted lines in other colours 1⁄4 fitted individual components)[58].

An alternative method to sequester sulfur during cycling with high conductive matrix is to apply graphene oxide (GO) [59-62]. Zhang et al. [60] used a chemical reaction-deposition strategy to immobilize Sulfur on quasi-two-dimensional GO to prepare graphene oxide-sulfur (GO-S) nanocomposite cathodes for Li-S batteries. This approach obtained a uniform and thin sulfur coating on GO sheets and enabled the strong interaction between graphene oxide and sulfur or polysulfides, leading to a reversible capacity of 950-1400 mAh/g and stable cycling for more than 50 deep cycles at 0.1C. A detailed study of the electronic structure and chemical bonding

between GO and S by X-ray Photoelectron Spectroscopy (XPS), Near-edge X-ray Absorption Fine Structure (NEXAFS) and X-ray Emission Spectroscopy (XES) was done to better understand the property of this nanocomposite [63]. They found the incorporation of Sulfur can partially reduce the GO and thus improve the conductivity of the GO. The existence of both C-S and O-S bonds was confirmed by the XPS and NEXAFS results. Also, the mild interaction between GO and S can not only preserve the fundamental electronic properties of GO but also stabilize the S by direct bonding with the GO sheet, which can prevent the diffusion of LiPS formed during the cycling into the electrolyte. Nazar et al[59] also used partially oxidized graphene as both an electrical conduit for insulating sulfur and as a barrier to retard polysulfide dissolution. Highlighted by the high sulfur content (87 wt%), it demonstrated that large amounts of conductive carbon additives are not required to obtain an efficient working Li-S cell. The slightly hydrophilic quality of the graphene surface, a result of the oxygen groups, will aid in polysulfide binding.

The mechanism of polysulfide binding is investigated by Pantelides et al. [64] by first-principles molecular dynamics simulations and density functional calculations. They find that oxygen on the graphene basal plane can bind to the Li_2S_8 cluster with an adsorption energy of 1.1eV, which is larger than the binding energy on pristine graphene (~0.8eV). Thus, oxygen enhances the interfacial interaction between LiPS and graphene. This study also points out that the interaction energy between OH and graphene is rather weak. Therefore, oxygen at the vacancies and similarly at the edges may serve as stable oxygen-containing functional groups for the purpose of stabilization of polysulfide, which is important for the improvement of the cycle stability.

2.4 Sequestering sulfur in the cathode using a combination of chemical and physical interactions

To overcome characteristically low capacity and quick fading, a combination of physical traps and chemical bonds are introduced to suppress shuttling and improve performance. While physical trapping often employs high surface area conductive carbon, the gains in performance are short lived. Similarly, the introduction of favorable chemical bonds is an effective method to sequester PS but low utilization of the active material is often achieved. As such, previous methods that utilize metal oxide frameworks are limited because the insulating nature of the functional groups limits full capacity utilization. To combine these two methods effectively the framework must be conductive. Therefore, a variety of multifunctional nanomaterials are applied to serve both as the physical barrier and thermal adsorbents.

Recent findings have demonstrated heteroatom-doped carbon as a feasible method to combine high surface area carbon matrices and the polar surface for Li-S cells [65-68]. Among various dopants (phosphorus, sulfur, boron, nitrogen), nitrogen is most attractive for substantially improving the carbon surface polar, wettability, and conductivity. The first work of applying N-doped carbon to Li-S battery was reported by Sun et al. [66]. The electrochemical impedance spectroscopy results showed that the charge-transfer resistance in nitrogen-doped carbon cathode was much lower than that of activated carbon without doping. They concluded that nitrogen-doping could enhance activity towards sulfur reduction, providing higher discharge potential and initial capacity. However, surface doping by high temperature treatment limited the doping content to 3.3 wt%. In contrast, a homogeneous incorporation of nitrogen into the carbon was realized by a controlled chemistry through in situ doping of carbons using nitrogen containing precursors, reported by Ling et al. [65]. The results show that the nitrogen doping could assist mesoporous carbon to suppress the shuttling phenomenon, via an enhanced surface interaction between the nitrogen functionalities and polysulfide species. It is also shown that nitrogen

doping can improve the electronic conductivity of the carbon matrix within an appropriate content range (4-8 wt%), offering faster charge-transfer kinetics. The cathode composite delivers a high discharge capacity of 758 mAh/g at 0.2C and 620 mAh/g at 1C rate after 100 cycles. A more recent work reported by Chen [67], designed and synthesized a novel N-doped carbon-sulfur (NCMSs-S) composite by confining sulfur in porous NCMSs. The S-immobilized NCMs showed very slow decay at 2.0C (0.030% per cycle for 500 cycles) with a reversible capacity of ~605 mAh/g. The authors contributed the results to the confinement of sulfur by porous structure and the ability of the electron-donating atoms (N and O) to absorb the polysulfide produced during the electrochemical reaction. These results would shed light on developing more novel N- or other elements-doped carbon spheres with suitable porous structures for an ideal sulfur-hosted matrix. A detailed study of the effect of carbon-heteroatom bonds in Li-S cells was carried out by Li et al. (Figure 12)[69]. Carbon black substrates were prepared by various treatments to introduce nitrogen or oxygen surface species. The XPS study revealed that the defect sites of nitrogen-doped carbon are favorable for the discharge product deposition, leading to a high utilization and reversibility of sulfur cathodes. For oxygen functional groups, they found negative effect on the sulfur cathode due to the reduced conductivity and unwanted side reactions occurring between sulfur and surface oxygen species. This study indicated the important correlation existing between carbon-heteroatom bonds and battery performance.

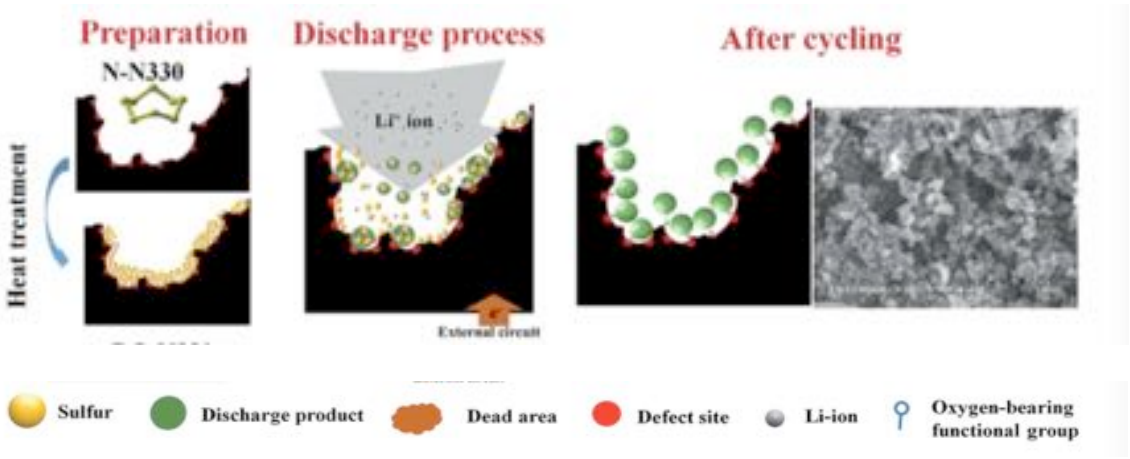

Figure 12. Schematic diagram showing effects of carbon–heteroatom bonds on sulfur cathodes[69].

One method to increase the sulfur loading is to uniformly distribute a thin-layer of sulfur in conductive materials through the strong interaction between S and conductive host. Transition metals (e.g. Co, Ni, and Cu, etc.) have been shown to react with sulfur to form sulfides at moderate temperatures, and these sulfides have been investigated as cathode materials for lithium batteries. Researchers are also applying the transition metals to Li-S systems, taking advantage of conductive transition metal-sulfur species [33, 70-72]. Wang [71] reported a design of copper-stabilized sulfur-microporous carbon (MC-Cu-S) composite with S loading of 50% as sulfur cathode by an ultrasonic-assisted multiple wetness impregnation and synchro-dry technique (Figure 13). The unique structural MC-Cu-S composite cathode shows Coulombic efficiency close to 100% (1.0M $LiPF_6$ + EC/DEC (1:1 v/v)), and maintains capacities of around 630 mAh/g at the current density of 100 mA/g with cycling up to 500 cycles. The authors attributed the good performance to the enhanced electronic conductivity of the MC-Cu-S cathodes and the formation of solid Cu-polysulfide clusters through strong interaction between Cu and S. Also, the porous structure carbon matrix provides a physical barrier to sulfur species and free space for volume change of S/LiPS during cycling. Manthiram et al. [72] and Li et al. [33] both reported using 3D Ni foams as either a cathode or a current collector. The Ni foam

matrix works as an electron transport network to improve the electrical conductivity of the cathode, as a container to accommodate the active material, and as a cage to retain the polysulfides in the cathode region during the charge/discharge process. Though the authors didn't point out the chemical bonding between Ni and S, we believe that the interaction also contributed to the good performance of Li-S cells.

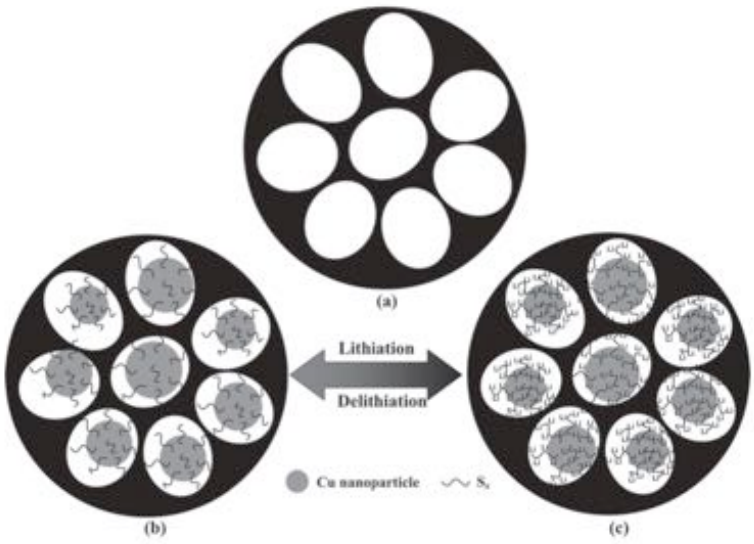

Figure 13. Schematic illustration of lithiation/delithiation process of the MC-Cu-S cathode[71].

Another method to combine the physical barrier and chemical interaction in Li-S cells is to use metal-organic frameworks (MOFs) [73, 74] [75, 76]. MOFs are attractive for their high porosity and chemical stability. Tarascon et al. [73] first proposed to use mesoporous chromium trimesate MOF, MIL-100 (Cr) as an improved confined matrix for sulfur impregnation. Electrodes containing sulfur impregnated within the pores of the MOF were found to show a marked increase in the capacity retention of Li-S cathodes (Figure 14). The XPS studies demonstrated the reversible capture and release of the polysulfides by the pores of MOF during cycling, and a weak binding between the polysulfides and the oxygenated framework was

evidenced. However, due to the poor conductivity of the MOFs and sulfur particles, a large amount of carbon is needed to ba added in order to ensure the conductivity of the cathode. Thus Li et al[75] coated the MIL-101 (Cr) with graphene oxide, and the MIL-101 (Cr) @rGO improved the electronic conductivity of meso-MOFs effectively, rising the capacity from 458mAh/g of the bare MOFs to 650 mAh/g. A more recent work done by Xiao[74] demonstrated that a novel Ni-based metal organic framework (Ni-MOF) can remarkably immobilize polysulfides within the cathode structure through physical and chemical interactions at the molecular level, and they described the binding as Lewis acid-base interactions, which involves the electron-donating S_x^{2-} ions and electron-accepting metal ions. The hierarchical porous structure with high surface area of Ni-MOF serves as a sulfur holding matrix to prevent the 'leaking' of soluble species from cathode by physical trapping. More critically, the strong interaction between Lewis acidic Ni (II) center and the polysulfide soft Lewis base successfully trap the soluble species within MOF scaffold, which is confirmed by both theoretical calculations and experimental characterization.

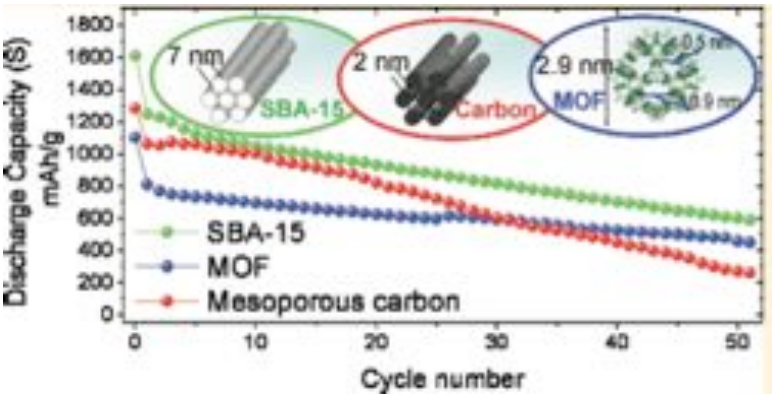

Figure 14. Comparison of battery performance with SBA-15, MOF and Mesoporous carbon[73].

Polymers, especially conductive ones, can be tailored or used to modify the surface of cathodes,

facilitating ion and charge transport [77]. In addition, they are soft and self-healing so that polymer-sulfur composite can accommodate volumetric expansion during discharge [78]. The studies in polymer-sulfur composites have revealed two general approaches that can enhance the electrochemical performance of polymer-sulfur composites. First, the sulfur size should be small in nanometers to achieve homogeneous interaction between sulfur and polymer. The second approach is based on the belief that simple physical confinement on the electrode surface is not sufficient for retarding polysulfide dissolution and thus not effective in achieving a long cycle life. Certain atoms such as N, S, O and some functional groups on the polymer can form stronger chemical bonds towards sulfur such that they can better trap intermediate products and thus superior cycling life[36, 79-83].

Fu et al. [84] have developed a polypyrrole/sulfur composite with the core/shell structure. A cell using this composite as the cathode exhibited a high initial capacity of 1050 mAh/g and exhibits a high capacity upon 50 cycles at 835 mA/g. Despite this advantage, it only has 67% capacity retention after 50 cycles. Similar results can be found in other reports with the same-engineered polypyrrole/sulfur composition and structures [79, 84-87]. Xiao et al. [78] have proposed a facile and environmental friendly synthesis process with self-assembling polyaniline nanotubes (PANI-NT) (Figure 15) for sulfur encapsulation. The polymer treated with sulfur at 280 °C forms a cross-linked, 3-D and structurally stable polyaniline nanotube-sulfur composite (PANI-NT/S) (shown in Fig). This polymer framework offers strong chemical confinement to sulfur-based components, alleviating the loss of active materials greatly. Additionally, the soft polymer matrix and nanostructured sulfur components have provided cushioning for volume changes during electrochemical reactions. Although relatively low initial discharge capacities occurred at

different charge/discharge rates, the electrodes showed a gradual increase in discharge capacities during the initial several tens of cycles, which indicates that SPANI-NT/S composite electrode requires an activation step due to the limited surface area of polyaniline compared to porous carbon. Other polymer/sulfur nanocomposites such as PVP-encapsulated hollow S nanospheres [82], poly(pyrrole-co-aniline) (PPyA) copolymer nanofibers[88], core/shell structured polythiophene[80], Sulfur/Poly(acrylonitrile) composite[81], poly(3,4-(ethylenedioxy)thiophene) (PEDOT) /poly(styrenesulfonate) (PSS)-based conductive polymers [83] were also studied extensively by other researchers.

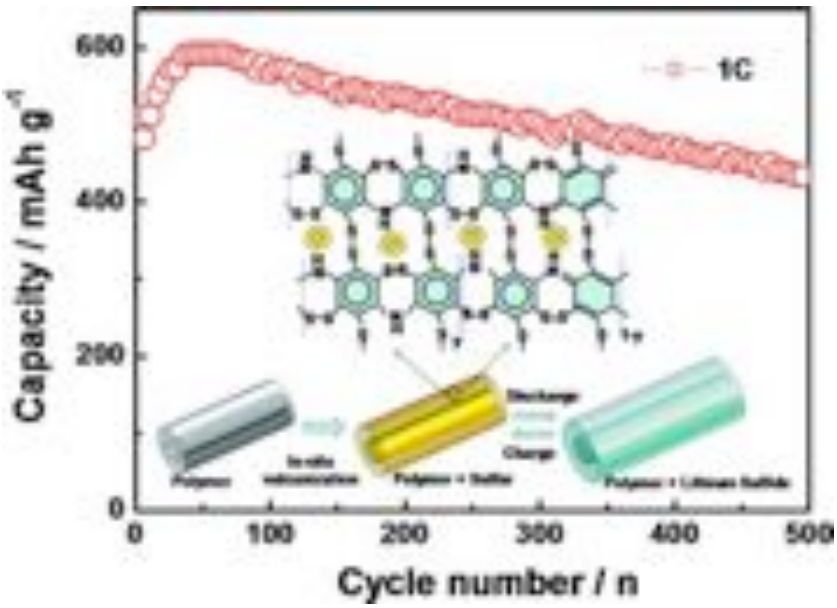

Figure 15. Schematic illustration of the construction and discharge/charge process of the SPANI-NT/S composite and prolonged cycling performance of the electrode up to 500 cycles at 1 C rate[78]

3 METAL-SULFUR BATTERY CATHODES BASED ON PAN-SULFUR COMPOSITES

3.1 INTRODUCTION

Sulfurized polymer composites have attracted recent interest as cathode materials for Li-S batteries due to the opportunities they appear to offer for employing both of chemical and physical interaction discussed in previous chapter. In 2002, Wang and co-workers appear to be the first to report that SPAN composites possess good-enough charge and ion transport properties to be used as cathodes in rechargeable lithium batteries[89]. Although the composite cathode exhibited good stability in electrochemical cycling studies, no evidence of C-S bonds was observed from FTIR studies, suggesting that sulfur exists mainly in elemental form. Fanous et al. used TOF-SIMS to characterize SPAN composites subjected to different thermal synthesis protocols and report CNS-fragments in the materials treated at elevated temperature[81]. Hwang et al. recently reported that these SPAN composites processed in a fiber morphology exhibit good electrochemical stability when employed as cathodes for sodium-sulfur cells[90]. There have been numerous follow-on type studies of electrochemical properties of this composite, however the electrochemical lithiation and delithiation process are still largely unknown[91-99]. The details of how sulfur interacts with the conductive polymeric host material during charging and discharging are understood to be important, but so far scarcely studied.

1. Ball Milling of PAN and Sulfur;

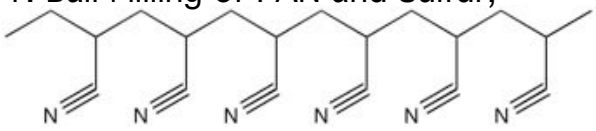

2. Dehydrogenation with S as oxidant and cyclization;

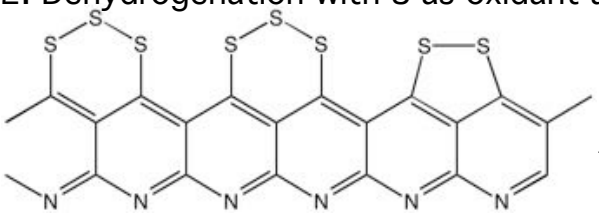

3. Carbonization to form honeycomb C structure (partial N removal)

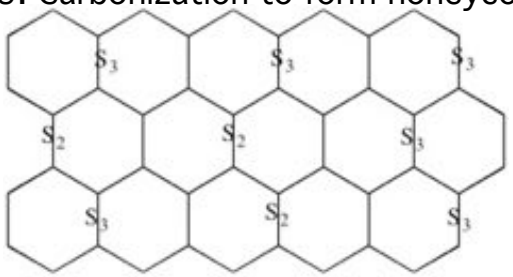

Scheme 1. Proposed synthesis route for creating sulfur-polyacrylonitrile (SPAN) nanocomposite cathode materials.

Herein we report a facile synthesis scheme and on chemistry and electrochemical properties of a family of sulfur/polyacrylonitrile (SPAN) composites that utilize specific interactions with nitrile groups on the polymer backbone and S_8 to destabilize PAN and to promote dehydrogenation and ring formation (Scheme 1). Thermal treatment of the material is shown to lead to metastable, covalently bound sulfur species S_x (x = 2-3) that are integrated throughout the composite. The approach builds on the two most successful strategies – physical confinement and chemical sequestration reported for improving electrochemical activity of sulfur in Li-S cells. Cathodes based on porous carbonaceous materials have, for example, been proposed previously for physically trapping LiPS and improving electronic transport. Of these approaches, microporous carbon materials are thought to provide the strongest physical confinement/immobilization of sulfur and its reduction products due to extremely small pore sizes. Notably, cyclic voltammetry analysis of cells based on this cathode design have been reported to exhibit an absence of the

higher (2.35 V) reduction process associated with formation of high-order LiPS by reaction of Li^+ and S_8, and subsequent loss of LiPS to the electrolyte. This implies that in such cathodes sulfur may exist in other forms than S_8. Xin, for example, has argued in favor of *smaller* S_x (x = 2-4) molecules that upon reduction with Li^+ cannot form soluble high-order LiPS[100]. Although this argument is a reasonable interpretation of the electrochemistry data, support from thermodynamic analysis of the electrode has so far been lacking.

Various approaches for chemically sequestering LiPS, by affinity particles/molecules/functional groups incorporated as additives in the sulfur cathode, have also been studied with differing degrees of success. Graphene oxide[60-63, 95, 101], metal oxides (SiO_2, TiO_2, V_2O_5, Al_2O_3, TiS_2) particles[31], nitrogen-doped polymers such as polypyrrole, polyaniline and polyacrylonitrile (PAN) have for instance all been used as additives or protective coating layers, where the high binding energy between LiPS and O, N containing molecules are thought to be beneficial. Guo et al., have provided the most direct evidence in support of this concept by showing that addition of soluble LiPS to stable PAN/dimethylformamide (DMF) solutions lead to rapid gel formation, in which PAN chains swollen by DMF are cross-linked by LiPS[102]. The strong affinity between LiPS and nitrile-containing molecules has also recently been confirmed both by density functional theory and diffusion experiments. An important result from the study by Guo et al. is that sulfur species associated with nitrile groups in the cross-linked polymer solutions remain well dispersed in carbon materials derived from the PAN component, by first removing the DMF solvent and pyrrolizing the PAN in an inert environment. A key conclusion from this study is that when proper attention is given to removing physically adsorbed S_8, a similar process leads to the spontaneous formation of S_2 and S_3 species linked to a conductive, PAN-derived carbon framework.

In this work, we report on the thermal synthesis of sulfur/PAN nanocomposites and employ electrochemical and spectroscopic tools to evaluate various hypotheses (Scheme 2) for lithiation and delithiation processes in these materials. Reaction 1 and 2 assume that S-S linkages that covalently bond to organic polymer materials can reversibly cleave and reform by analogous redox chemistry as reported for thiolates (RS^-). It is known that these reactions involve one-electron transfer per sulfur atom, which gives a theoretical specific capacity of 837 mAh/g_S. In Reactions 3 and 4, the R-S bond completely breaks during the lithiation process, resulting in the formation of Li_2S as the only sulfur-containing lithiation product. This reaction involves two-electron transfers per sulfur atom, yielding a theoretical capacity of 1675 mAh/g_S.

Reaction 1:	$RSSR+2Li^+ \leftrightarrow 2RSLi$
Reaction 2:	$RSSSR+4Li^+ \leftrightarrow 2RSLi+Li_2S$
Reaction 3:	$RSSR+4Li^+ \leftrightarrow 2R+2Li_2S$
Reaction 4:	$RSSSR+6Li^+ \leftrightarrow 2R+3Li_2S$

RSSR, RSSSR: Organosulfur-based materials

Scheme 2. Proposed lithiation mechanisms for SPAN nanocomposite.

3.2 RESULTS AND DISCUSSION

The specific synthesis route used in the study is shown in Scheme 1 and detailed in the experimental section. Briefly, to prepare SPAN, a simple one-step procedure involving thermal treatment of physical PAN/sulfur blends at a low temperature ramp rate of 5 ^oC/min and under continuous nitrogen gas flow. In the following sections, materials prepared using thermal

treatment of the blends at 250, 350, 450 and 600 °C are denoted as SPAN2, SPAN3, SPAN4 and SPAN6, respectively. As a control, PAN without sulfur was heat-treated at 450 °C and denoted as PANC. It is believed that cyclization of the polymer backbone carbons is facilitated by sulfur coordination with and subsequent cleaving of the CN triple bonds. It is further hypothesized that cyclic sulfur (S_8) is in the process cleaved into smaller chain sulfur radicals, which are able to react with and covalently bond to the PAN carbon backbone and dehydrogenate the material to form H_2S. A similar scheme for the dehydrogenation and cyclization of PAN in the presence of sulfur has been reported previously[91-93, 96, 97, 99]. At high temperature, PAN may further carbonize to produce pyridinic-N carbon ring structures encapsulating sulfur species.

Figure 16a and c report typical STEM images for the as-synthesized SPAN4. The figures indicate that the material exists in a nanosphere morphology with average diameters between 100 nm and 150 nm. To determine the distribution of S, N and C in SPAN4, energy dispersive X-ray (EDX) maps based on the area shown in the annular dark field (ADF) image (Figure 16c) reveals that SPAN4 contains 45.6% sulfur. This composition is higher than previous literature reports, and we attribute it to the low thermal ramp rates used in the pyrolysis step. The sulfur and carbon maps in Figure 1d and e match the result shown in the ADF image (Figure 16c), indicating that carbon and sulfur are homogeneously distributed throughout the materials. The nitrogen map (Figure 16f) shows that SPAN4 contains 8.59 % N, indicating only partial removal of N atoms during heat treatment. Electron energy loss spectroscopy (EELS) was performed on the composite to investigate the distribution of elements along the line shown in Figure 16a. Figure 1b reports the normalized EELS intensities with respect to position for the S-, C-K, and N-K edges. The results show more sulfur intensity along the middle of the line, indicating that the sulfur is most probably encapsulated by carbon rings.

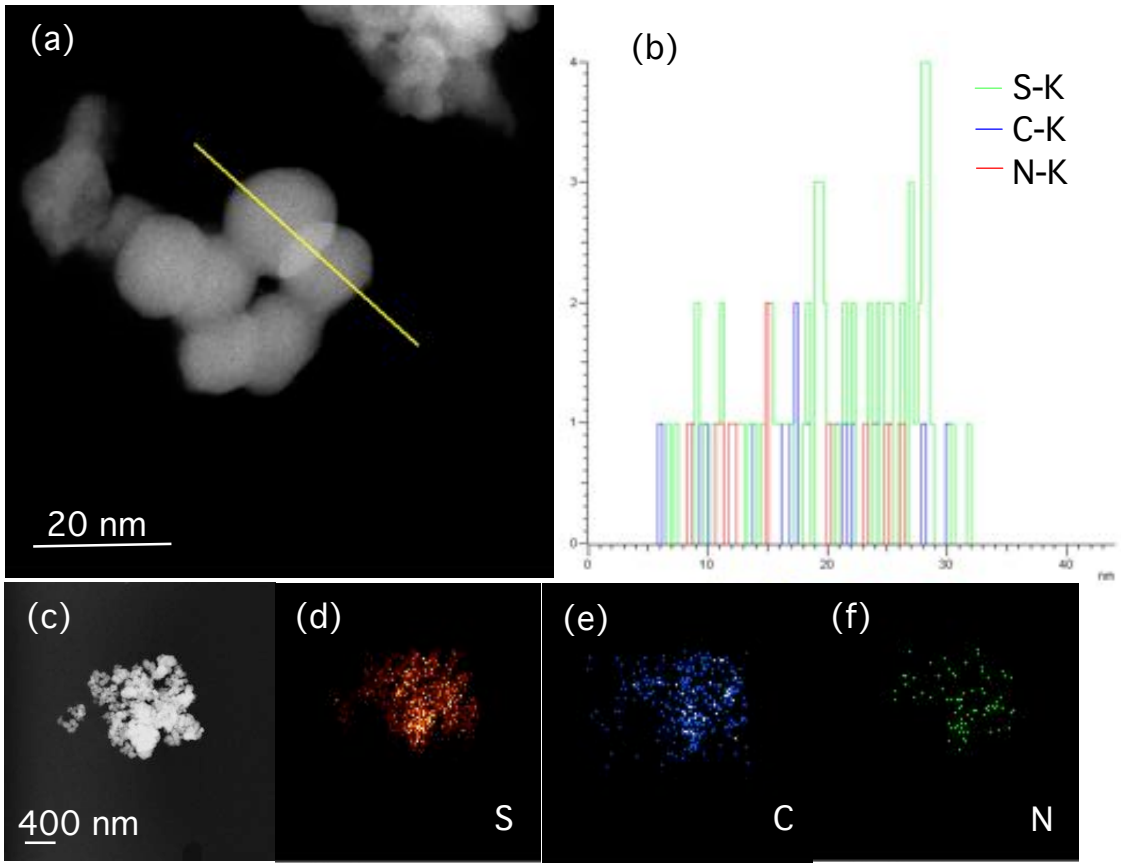

Figure 16. STEM (a and c) images of the SPAN4 composite; EDX sulfur (d), carbon (e) and nitrogen (f) maps based on the area shown in (c); and (b) normalized EELS intensity along the line in (a).

The thermal stability of the various SPAN materials, PANC, and PAN is accessed by thermal gravimetric analysis (TGA) in the temperature range from 25 to 1000 °C (Figure 17). SPAN2 exhibits a significant weight loss of 42 % in the range 200 and 400 °C, which is ascribed to sublimation of unreacted elemental sulfur. For the other SPAN materials, more significant and distinctive weight loss is observed at much higher temperature, beyond 500 °C. It reflects the strong bonding between carbon and sulfur, and is consistent with the higher dissociation energy of the C-S (272 kJ/mol) bond, compared to the S-S bond (251 kJ/mol). XRD analysis (Figure 18) reveal that sulfur in orthorhombic S_8 state only exists in SPAN2, the material synthesized at the lowest temperature; no sulfur peaks can be observed in any of the other SPAN materials,

suggesting that the sulfur embedded at higher temperatures loses all crystallinity. A broad diffraction peak at 2θ = 26.5° corresponding to the graphitic (002) plane is also apparent in the SPAN materials, verifying the carbonization of PAN. A signature peak at 2θ = 17°, corresponding to the (110) plane of the PAN crystal, completely disappears after carbonization with sulfur. To analyze the chemical structure of the SPANs, Raman (Figure 19) and FTIR (Figure 20) spectra for composites were performed, with PANC, PAN and sulfur as controls. Specific peak assignments are summarized in SI. Based on the information, the structure of the SPAN can be confirmed as turbostratic carbon configuration via dehydrogenation and efficient π-π stacking, and with sulfur covalently bonded to the carbon backbone.

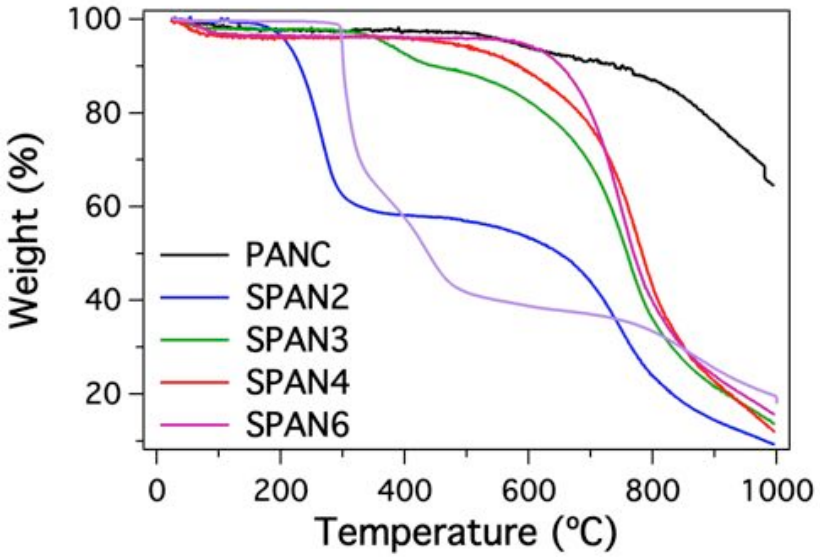

Figure 17. TGA profiles for SPANs, PAN and PANC from 25 to 1000 °C at a rate of 5 °C/min.

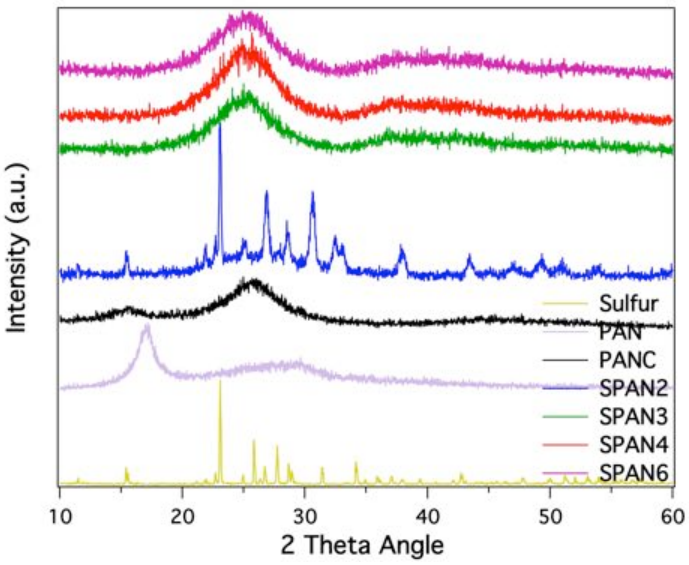

Figure 18. XRD patterns of PANSs, PANC, PAN, and elemental sulfur.

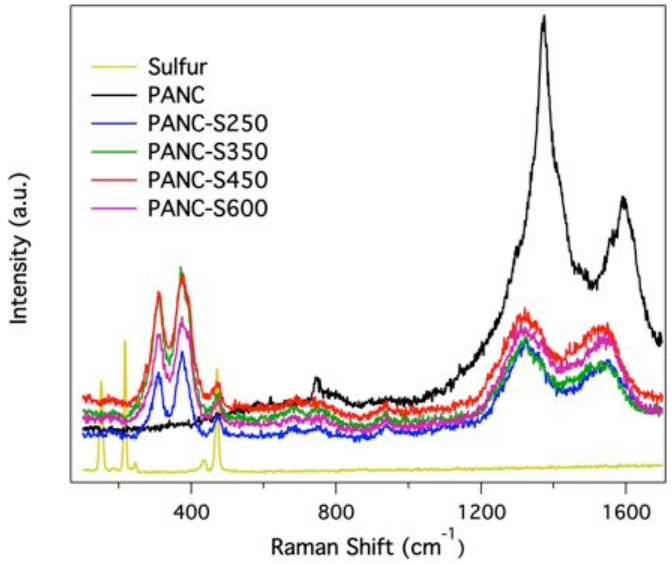

Figure 19. Raman Spectra of PANSs, PANC, and elemental sulfur.

Table 1. Raman shifts (cm^{-1}) and assignments for SPAN and sulfur. [2,3]

SPAN	Sulfur	Assignments
	150	Characteristic peak of S8
176		C-S
	219	Characteristic peak of S8
298		C-S in plane bending
370		C-S Deformation
	471	Characteristic peak of S8
460		S-S
926		Ring (containing S-S bond) Stretch
1143		Ring (containing S-S bond) Stretch
1360		D Band
1577		G Band

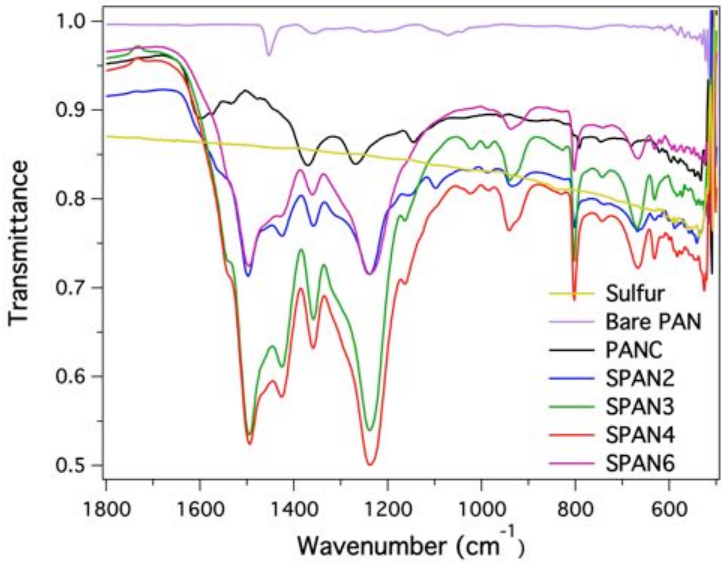

Figure 20. FTIR spectra of SPANs, PANC, PAN and sulfur.

Table 2. FTIR wavenumbers (cm^{-1}) and assignments for SPANs.[2,4,5]

SPAN	Assignments
1549	C=C Asymmetric Stretch
1502	C=C Symmetric Stretch
1431	C=N Asymmetric Stretch
1363	C-C Deformation
1250	C=N Symmetric Stretch
943	Ring Breath (Side-chain Containing S-S)
804	Ring Breath (Main-chain Hexahydric-ring)
671	C-S Stretch
513	S-S Stretch

Electrochemical characteristics of the SPAN composites were characterized in 2032 coin cells with the composite as the active cathode material and lithium foil as the counter electrode. We studied SPAN4 in detail as it exhibited superior electrochemical properties among all the SPAN materials, as well as acceptable sulfur content. To illustrate, the first discharge voltage profile for different SPAN-based cathodes in Figure 21. It is seen that discharge voltage plateau decreases with an increase in the preparation temperature for the SPANs. However, the sulfur content in the materials generally decreases as the temperature increases, thus there is a clear trade-off between sulfur content and binding strength between S and C atoms, with optimal results for both features of the materials found in SPAN4. Two types of electrolytes, 1M $LiPF_6$ in EC/DEC and 1M LiTFSI in DOL/DME with $LiNO_3$ as additive were used in the study to assess the electrodes. This assessment revealed unexpected results that appear critical for understanding the chemistry of the SPAN4 material and the exceptional electrochemical properties of sulfur cathodes based on this material. Figure 22a reports the galvanostatic charge/discharge profile in a cell cycled in the former electrolyte. Comparison of the discharge profiles between the 2^{nd} and 200^{th} cycle reveal negligible changes in both the shape and specific capacity. Figure 22b shows that the material exhibits exceptionally stable cycling stability for over 1000 cycles at 0.4 C (1 C= 1675 mA/g) based on sulfur. The capacity degradation/fade upon repeated cycles of

discharge and charge is only 0.027 % per cycle from the 2nd to 1000th cycle. The figure shows that SPAN4 delivers a capacity of over 1000 mAh/g even after 1000 cycles, the highest reported for a Li-S cell cycled at moderate high rate.

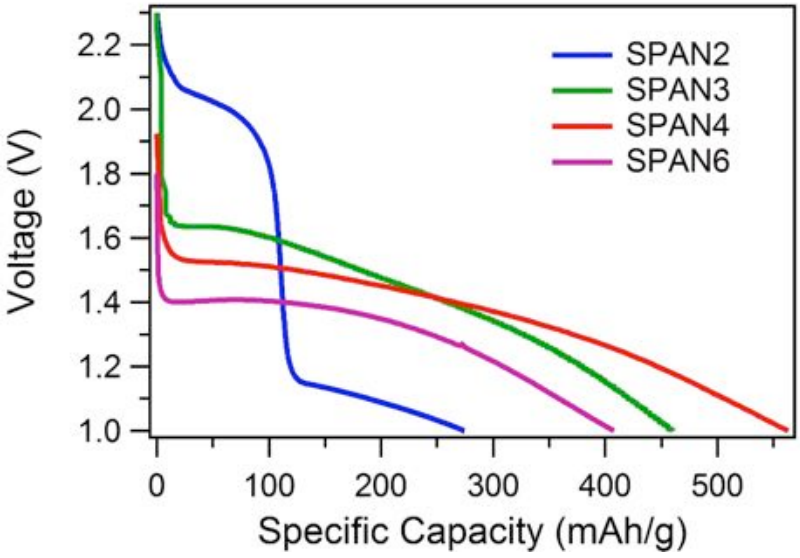

Figure 21. First discharge profiles of different SPANs at 200 mAh/g in 1M $LiPF_6$ in EC/DEC (capacity based on whole cathode weight).

Figure 22a shows that the voltage plateau during the first discharge cycle (~1.5 V) is lower than the values observed in subsequent cycles. This implies that the reduction reaction and transport in the cathode involves different processes, probably cleavage of S-S bonds in the composite, compared to the subsequent cycles. The capacity (1843 mAh/g_{sulfur}) estimated for the initial discharge is higher than the theoretical capacity of sulfur. This means that the π-conjugated pyridinic carbon framework likely makes a contribution, probably a combination of Faradic processes in forming the solid-electrolyte interlayer (SEI) on carbon during the first cycle and a non-Faradic pseudocapacitance that may persist over many cycles. During the following cycles of discharge, the voltage plateau increases and remains stable between 1.6 V and 2.1 V over hundreds of cycles of charge and discharge. This observation is evidently distinct from what is

typically found in Li-S cells where a two-step discharge plateau is observed. In the first step at (~2.35 V), the plateau is associated with the reaction of Li^+ and S_8 to form LiPS. The second plateau at (~2.1 V) is attributed to reversible reactions between smaller sulfur species (e.g. LiS_3 and Li_2S_3)[20]. The fact that only the latter of these two voltage plateaus is observed in electrodes based on SPAN4 is significant because it means that in the material sulfur exists in a form that prevents it from achieving its bulk thermodynamically favored form S_8, even when the Li-S cells are in the fully charged state. The result is also significant because it means that LiPS cannot form in these cells, which eliminates complications such as shuttling associated with formation and dissolution of LiPS in the electrolyte. The plausibility of this conclusion will be supported more fully in the sections to follow, however the high coulombic efficiencies evident in Figure 2(b) over extended cycling of the cells, without any of the usual $LiNO_3$ additive in the electrolyte, provides additional proof that shuttling has been arrested in this cathode design. Figures 22c and 22d report the effect of current density on performance of Li-S cells that utilize a SPAN4 cathode. Current densities from 0.08 mA/cm^2 (=0.2 C) to 0.63 mA/cm^2 (=1.6 C) were investigated. In each cycle, the rates were the same for both charge and discharge. The similarity of the charge and discharge profiles, irrespective of rate, is clearly apparent from the figures. As illustrated in Figure 2d, the SPAN4 cell also shows high capacity retention at different C rates with only an average of 4.13 % capacity decay through high C rate (1.6 C) to low C rate (0.4 C). Importantly, once the C rate is reduced to the original value of 0.2 C, the capacity recovers to its previous steady value.

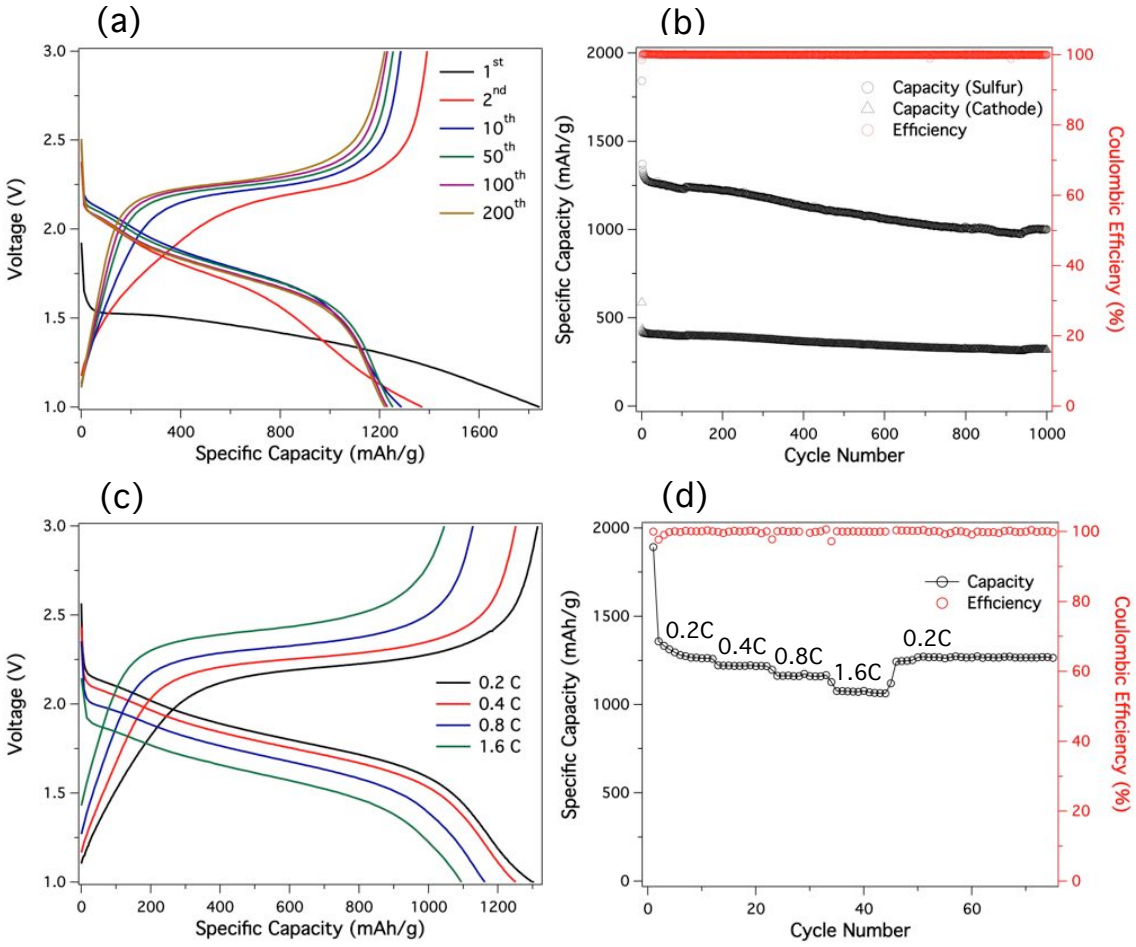

Figure 22. (a) Electrochemical discharge and charge curves of SPAN4 at various cycles. The tests were performed at 0.4 C for both charge and discharge in the potential range of 1–3 V vs Li/Li^+. (b) Capacity and Coulombic efficiencies versus cycle number for PANS4. The black circles report capacities relative to the weight of the active sulfur species in the cathode, whereas the data represented by black triangles are the corresponding capacities based on the overall cathode mass. (c and d) Rate performances of the SPANS measured at various C-rates. The C-rates were same for both charge and discharge in each cycle.

Reaction of sulfur with PAN at high temperature is expected to produce S_x cross-links covalently linked to the carbon rings. After the initial discharge, however, the S-S bond may be expected to break and, upon cell recharge, any sulfur species present in the cathode may spontaneously transform into high order LiPS and S_8, which would remove the benefits of covalently linking the sulfur to carbon in the cathode. The absence of the characteristic 2.35V discharge plateau after hundreds of discharge cycles of the SPAN4 cathode is somehow able to

avoid this fate. Moreover, the charge profile and discharge profile are more symmetric compared to Li-S cells made with elemental sulfur as cathodes, which again indicates that there is excellent utilization of sulfur in the cathode and very little if any losses to the electrolyte.

The inability of unbound smaller sulfur species produced in the cathode after the first recharge to transform to S_8 and, in the subsequent discharge, to LiPS, implies that the smaller sulfur species are perhaps isolated/encapsulated in the cathode. To understand the nature of the interactions that hold the smaller sulfur species in the cathode, we compared the electrochemical behavior of cells in which the commonly used 1M LiTFSI in DOL/DME with $LiNO_3$ (See Figure 23) electrolyte is substituted for the 1M $LiPF_6$ in EC/DEC electrolyte used in the studies reported in Figure 2. It is apparent that this change has dramatic and negative consequences on cell performance. Specifically, while the discharge profile and specific capacity for the first discharge cycle are comparable for SPAN4 cycled in the two electrolytes, it is clear that by the second cycle a two-step discharge profile, analogous to what is seen in a conventional Li-S cell, is observed and that this is accompanied by shuttling and significant deterioration in cell performance upon charging. Even if Guo et al.[102] used solid Li_2S encapsulated in PAN as cathode, a two-step discharge plateau is still observed in a LiPS-soluble tetraethylene glycol dimethyl ether electrolyte. It is evident then that the electrolyte plays a large role, as well as that the smaller sulfur species trapped in the cathode are likely held in place by physical interactions with the carbon host.

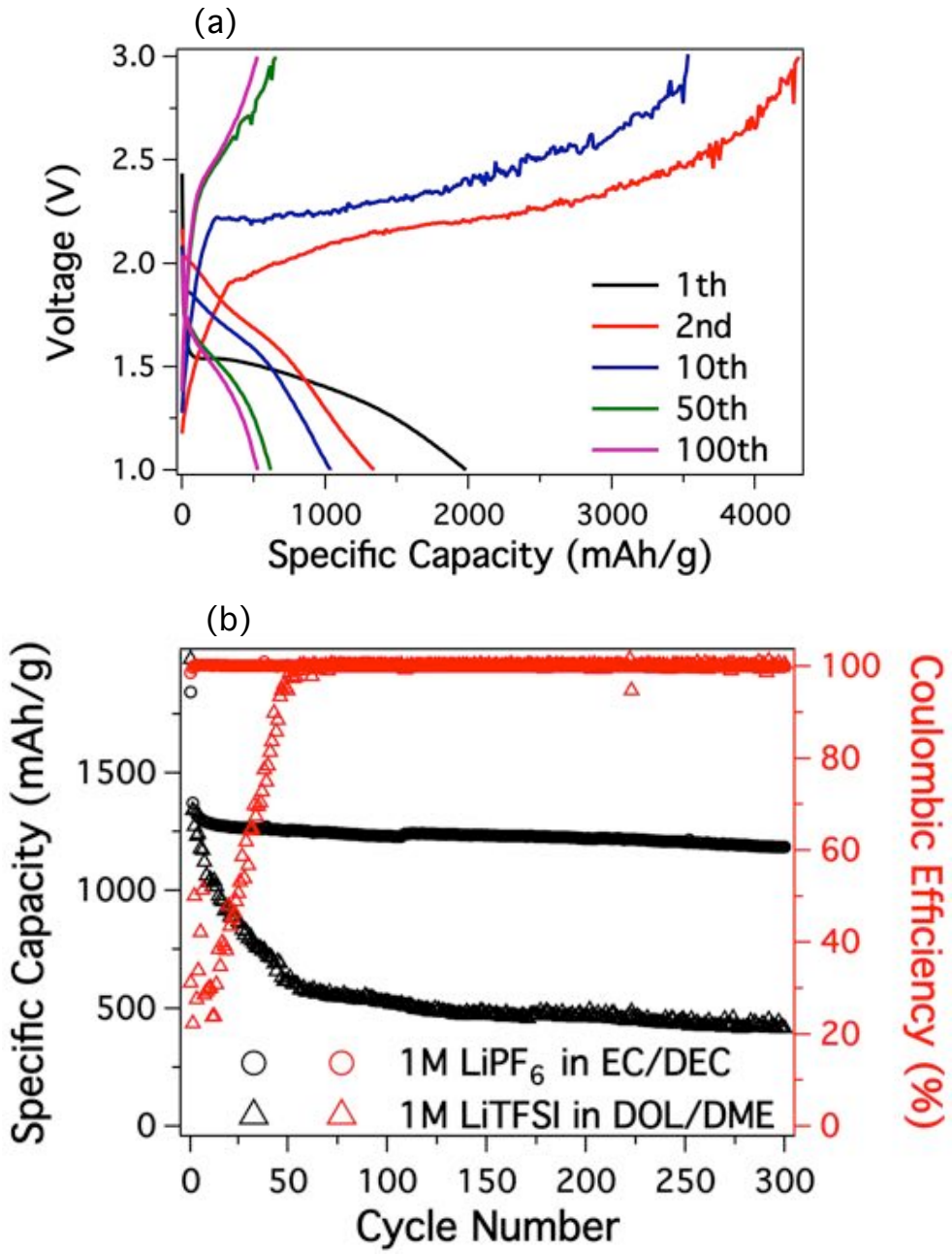

Figure 23. (a) Electrochemical discharge and charge curves of SPAN4 at various cycles in 1M LiTFSI in DOL/DME with $LiNO_3$. The tests were performed at 0.4C for both charge and discharge in the potential range of 1–3 V vs Li/Li^+. (b) Capacity retention and Coulombic efficiencies of PANS4 in two types of electrolytes.

Carbonate-based electrolytes are broadly considered incompatible with Li-S batteries because of the nucleophilic addition reaction between LiPS and the electrolyte, which irreversibly consumes the active sulfur in the cathode and electrolyte solvent. Our finding that Li-S cells based on

SPAN cathode materials cycle more stably in a carbonate-based electrolyte than in electrolytes based on DOL/DME provides additional confirmation that LiPS and its deleterious effects on carbonate electrolytes are somehow avoided when SPAN materials are used as cathodes for Li-S cells. Three hypotheses can be applied to explain these observations: 1) After the first recharge cycle, sulfur exists mainly as S_2 or S_3 in the composite, and cannot form larger S_8 or reactive LiPS species in electrolyte solvents in which the smaller sulfur species or Li_2S have poor/no solubility. This would mean that Li_2S would be the only discharge product in a fully discharged cathode. 2) In the 1-3V voltage window used $LiNO_3$ decomposes and is irreversibly reduced on the cathode surface when the cell is discharged below 1.7 V, the minor plateau in Figure S6a would be the evidence. 3) The higher solubility of LiPSs in DOL/DME promotes recombination and loss of high-order polysulfides to the electrolyte during recharge process.[41] If correct this would confirm common, but heretofore largely untested wisdom, that an electrolyte based on a non-solvent for LiPS with high ionic conductivity would be an ideal choice to confine sulfur in the cathode and ensure electrochemical reaction in the cathode occur all in solid state.

Quantitative experiments were carried out to assess each of these hypotheses. Li_2S was either mixed with elemental sulfur or pristine SPAN4 in desired stoichiometric ratios to form a polysulfide with formula Li_2S_8. EC/DEC and DOL/DME based electrolytes were added to the LiPS species to evaluate their solubility and physical properties. Sulfur concentrations in the resultant four solutions were recorded as a function of time using ICP-AES (Figure 24a) and UV-vis spectra of the solutions recorded after 10 days, are shown in Figure 24b. It can be clearly seen that whereas sulfur is undetectable in the carbonate-based electrolyte it is readily observed in DOL/DME. What's more, none of the characteristic UV-vis absorption peaks associated with LiPS can be identified in the carbonate electrolyte and no color change is noticed. In contrast, in

DOL/DME, irrespective of the source of sulfur, the sulfur concentration in the electrolyte increases with time and a color change from yellow to dark brown can be observed, which are consistent with UV-vis absorption for LiPS. In the case of elemental sulfur, both sulfur concentration and LiPS absorption in UV-vis spectra are much higher than SPAN4, even at comparable sulfur loadings. It means that in the pristine SPAN, electrolyte access to sulfur is limited and that SPAN4 is an effective material for sequestering LiPS. An even broader inference from these observations is that whether the source of sulfur is SPAN or elemental sulfur, the expected polysulfide with lithium sulfide is not formed in the carbonate electrolyte solvent.

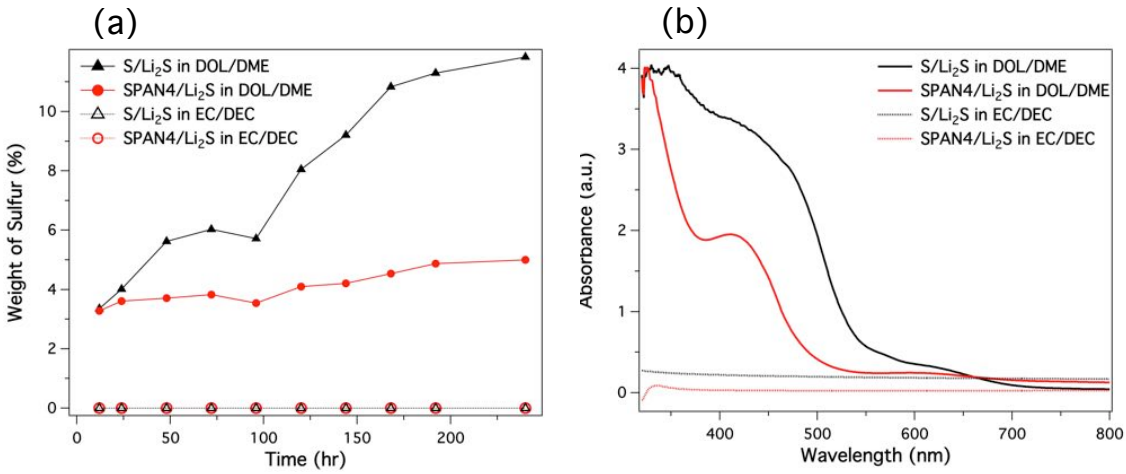

Figure 24. (a) Sulfur content in the electrolyte for four different cases; (b) UV-vis spectra of the solutions for the four samples after 10 days, which are equally diluted with the corresponding electrolyte.

The capability of SPAN4 to hold sulfur can be indirectly assessed in a simple electrochemical measurement that reports the open-circuit potential (OCP) and self-discharge behavior for PAN4 and sulfur in DOL/DME (Figure 25). The OCP for cell based on elemental sulfur as the cathode is seen to gradually decrease during the two-week time duration of the experiments. The drop in the OCP is accompanied by the LiPS dissolution and a large decrease (~53%) in capacity after

two weeks. However, the OCP for the two cells employing cathodes based on SPAN4 show only slight initial decreases followed by a slow stabilization towards the OCP of SPAN after two weeks. It suggests that the cells may need longer time for electrolyte to penetrate the separator and wet the cathode in order to reach interfacial equilibrium caused by surface tension and strain.[46] The relatively small initial decrease in capacity again suggests that even in the DOL/DME-based electrolyte, SPAN4 has strong ability to hold sulfur and prevent LiPS formation and dissolution in the electrolyte. The decrease in capacity (~25%) is less than half compared to the elemental sulfur cathode after two weeks.

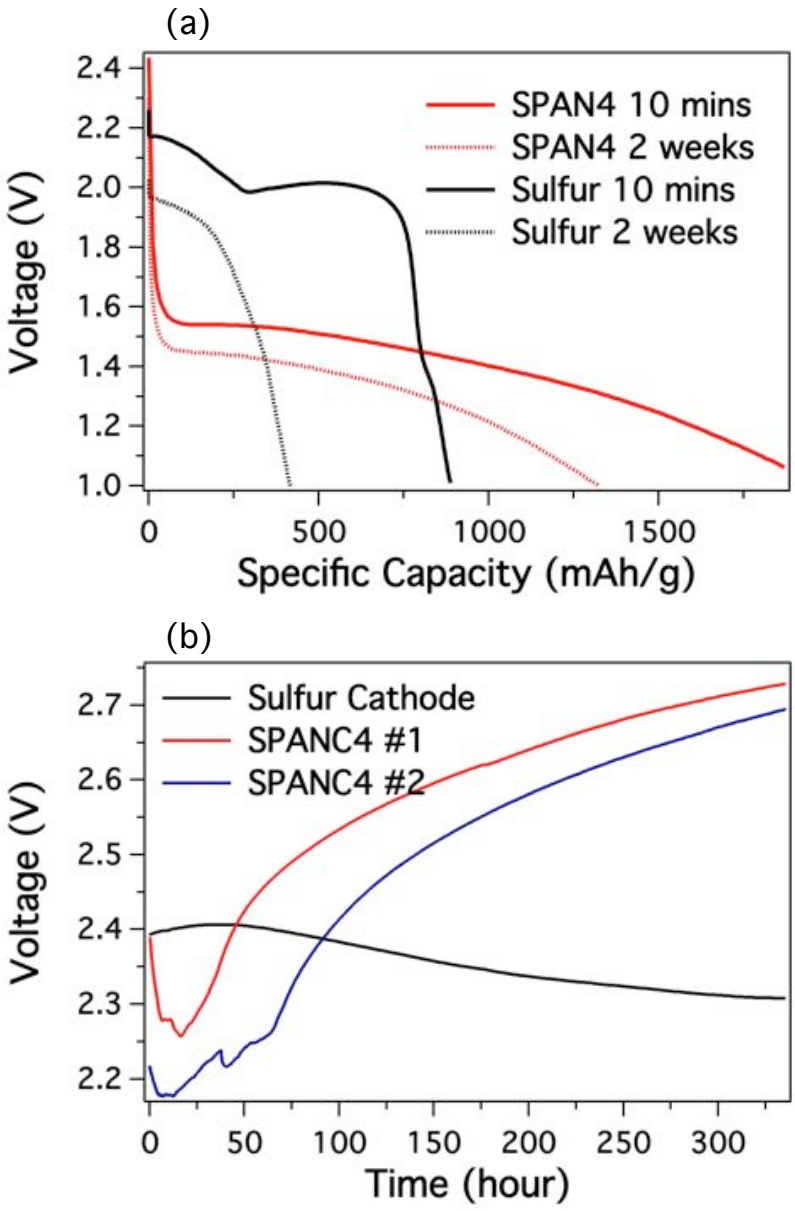

Figure 25. (a) Discharge plateaus of SPAN4 and pristine sulfur cathodes with different resting times in 1M LiTFSI in DOL/DME with $LiNO_3$; (b) Change in open-circuit potential of Li-S and Li-SPAN4 cells with storage time.

In order to better understand the electrochemical reactions in SPAN4 cathodes with carbonate electrolytes, the materials were studied during and post electrochemical cycling using nuclear magnetic resonance (NMR), X-ray photoelectron spectrum (XPS), Raman spectroscopy, scanning electron microscope (SEM), and energy dispersive spectroscopy (EDS). It is known that the intermediate reaction species in Li-S cells, LiPS, are able to exist in a variety of allotrope

forms due to the low energy barriers for recombination and disproportion reactions that transform higher order LiPS to lower order LiPS and vice versa (eg. $Li_2S_6 \leftrightarrow 2LiS_3$).[47] Moreover, due to their atmospheric sensitivity, it is difficult to interrogate these materials using some of the most powerful chemical characterization techniques. Here, we employ an organic conversation method, wherein chemical reaction of LiPS with benzyl chloride is used to transform pure or mixed LiPS into their more stable benzyl polysulfide (BzPS) analogs, without changing the order of the LiPS.[48] High nucleophilicity of thiolate anion makes it possible to achieve nearly 100% conversion of LiPS to BzPS. Systematic application of the method coupled with NMR analysis has been used to characterize the NMR spectra of different BzPS, allowing peak assignments for different BzPS. Figure 26a and b are the NMR spectra obtained by reacting a mixture of DME and benzyl chloride with Li_2S powder, Li_2S_3 solution, and the cycled SPAN4 cathodes; respectively. Distinctive peak assignments for Bz_2S_3 Bz_2S_4 Bz_2S_5 at 4.02 ppm, 4.15 ppm and 4.20 ppm can be found from the spectra, which are in accordance with previous literature. A single Bz_2S peak at 3.60 ppm can be found, for example, in the Li_2S case. On the other hand, the spectrum for Li_2S_3 (obtained by reacting Li_2S and S_8 in a 4:1 molar ratio) clearly shows that this material is a mixture of multiple species. Based on the reference spectra, we conclude that Bz_2S is the only BzPS species that exist in the discharged SPAN4 cathode. This clearly means that Li_2S is the only or the dominant discharge product in the cell. Significantly, once the cell is charged to 3 V, the chemical shift for Bz_2S disappeared and a broadened curve arises between 3.80 and 4.0 ppm, consistent with expectations for sulfur interacting/bonded to a polymeric species. After the 10^{th} cycle of discharge, the peak for Bz_2S is seen to still exist. NMR spectra of the cathodes cycled at intermediate stages of discharge and charge are shown in Figure S10 with Bz_2S signal detected only. Our results therefore lend support to the hypothesis that the improved

sulfur utilization of the SPAN4 cathodes is a result of the fact that elemental sulfur is fully reduced to Li_2S upon discharging. As no intermediate LiPS are found in the spectrum, it is also apparent that higher order sulfur species do not exist in the SPAN4 composite cathode.

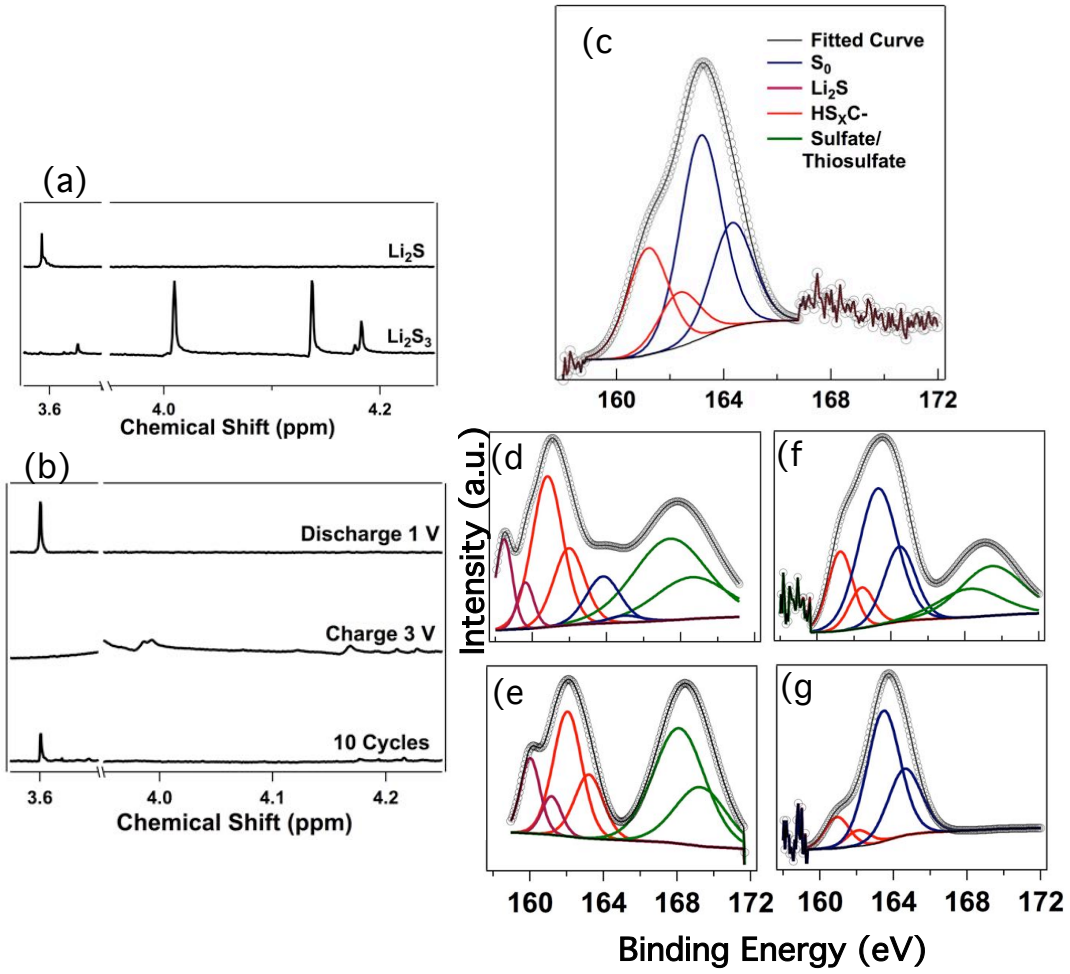

Figure 26. ^{1}H NMR spectra of the converted BzPS from (a) Li_2S powder and Li_2S_3 solution and (b) SPAN4s at different cycling states; Ex situ XPS spectra of S 2p in SPAN4s at (c) pristine and different cycling states (Cell was discharged to (d)1.25 V and (e) 1V and cell was recharged to (f) 2.25 V and (g) 3 V at the first cycle respectively).

XPS analysis of SPAN cathodes evaluated at different states of discharge and charge provide additional insights into the electrochemical mechanisms through which these cathodes are able to achieve their exceptional cycling performance. XPS spectra in the C 1s region (Figure 27a) for

the pristine SPAN4 reveal that C1s band can be split into three peaks. The main peak at 284.6 eV corresponds to the sp^2 type C-C component. The peak at 286.4 eV can be partially ascribed to C-S or C-N bond. The minor peak at 289.3 eV represents extended delocalized electrons in the composite, resulting in a satellite structure. Figure 4c to g presents S 2p spectra for the pristine SPAN and cathode at different galvanostatic cycling states. S 2p spectra for pristine cathode show an overlapped band with two shoulder bands. The main S2p 3/2 peak at 163.4 eV (Figure 26c), slightly lower than binding energy of elemental sulfur (164.0 eV) is consistent with the presence of C–S bonds in the composite. Another S2p 3/2 peak at 161.2 eV can be attributed to adsorbed HS_xC- byproduct generated in the sulfurization reaction on the surface of the composite.[12] Upon discharging (Figure 26d and e), the peaks for elemental sulfur are seen to disappear and new peaks at 168.2 eV arise from the sulfate/thiosulfate complex species most likely formed by the oxidation of Li_2S when processing the cathode for XPS characterization.[52,53] As the peak attributed to Li_2S around 160 eV appears when discharging and disappears during charging, and no other LiPS could be found, we attribute that Li_2S is the final discharge product in the cathode, which is consistent with our earlier study. We also found that peaks represent delocalized electrons in C 1s spectra increased dramatically upon discharging (Figure 27b), suggesting sulfur has interaction with conjugated carbon backbone during lithiation. When the cell is charged (Figure 26f and g), the oxidized sulfur peaks gradually disappear, and peaks for elemental sulfur reappear, suggesting sulfur recovers to elemental state. Based on the fact from XPS C 1s spectra and Raman spectra (Figure 28) that S-C bond recovers upon charging, we conclude that carbon in SPAN is able to reform strong bond with sulfur.

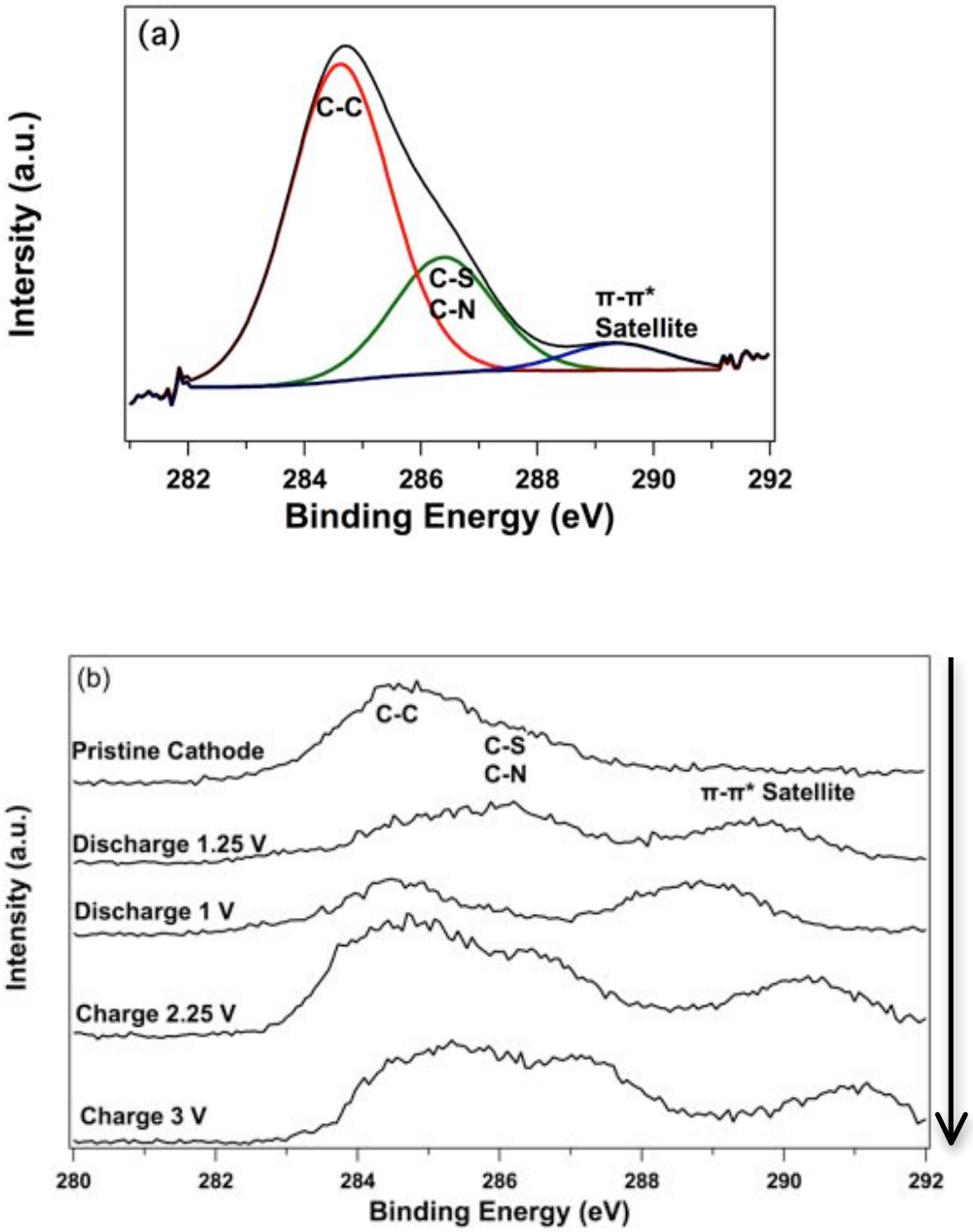

Figure 27. Ex situ XPS spectra of C 1s in SPAN4s at (a) pristine state (Black lines are the fitted curves) and (b) different cycling states (cell was discharged to 1.25 V and 1V, then cell was recharged to 2.25 V and 3 V at the first cycle respectively).

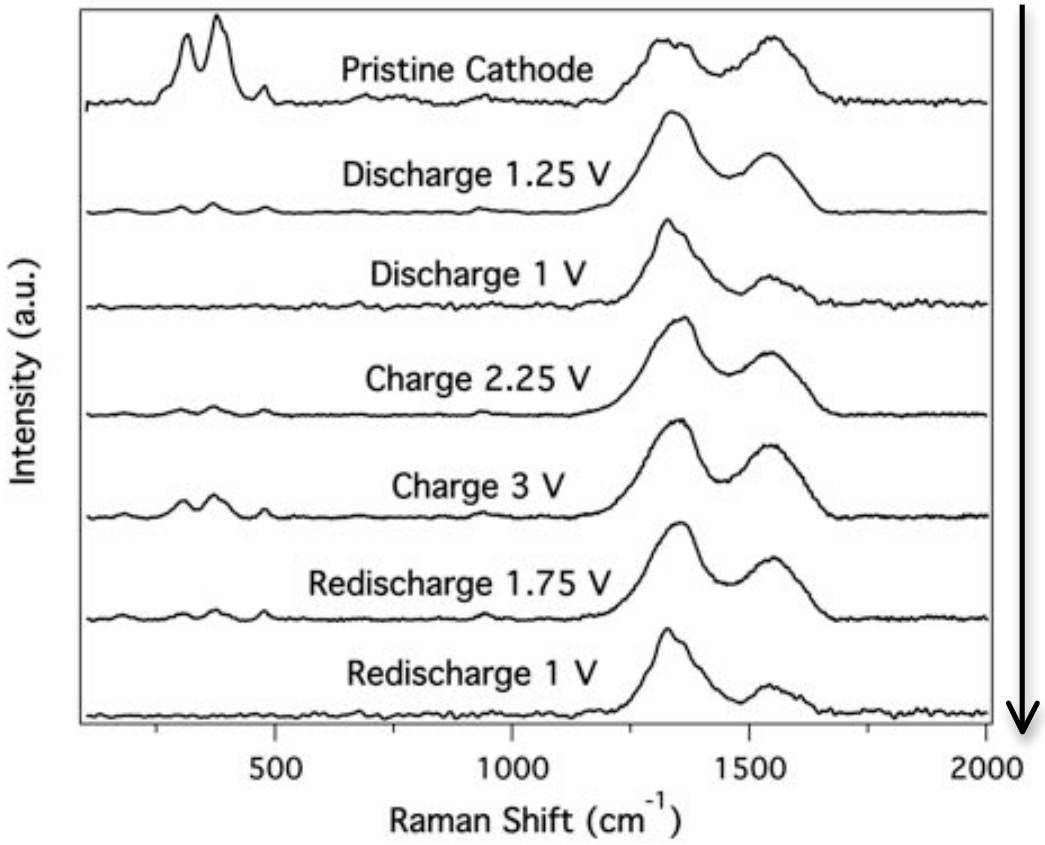

Figure 28. Ex-situ Raman spectra in the range of 100–2000 cm-1 during the first two cycles of SPAN4s.

Additional insights about the electrochemical characteristics of the SPAN4 cathodes can be deduced from cyclic voltammetry (CV). In particular, by using CV to interrogate behaviors in multiple electrochemically active sulfur compounds containing sulfur species similar to what we hypothesize to exist in the SPAN4 cells, it is possible to confirm that sulfur in the form of S_2 and S_3 are the dominant species in the cathode. In particular, Li_2S_3 cross-linked to PAN (obtained using the method reported by Guo et al.[102]) (Figure 29b); tetramethylthiuram disulfide (TMTD) (Figure 29c); bis(p-tolylsulfonyl) trisulfide (BPTT) (Figure 29d); dipentamethylenethiuram tetrasulfide (DPMTT) (Figure 29e) containing oligosulfides covalently linked to organic molecules were each employed as cathode vs. lithium and their

electrochemical behaviors compared with those for SPAN4 (Figure 29a). CV curves for SPAN4 for multiple redox cycles are shown in the graph. It displays a lower plateau for the first reduction process, which agrees well with the voltage profile deduced from galvanostatic cycling studies shown previously.

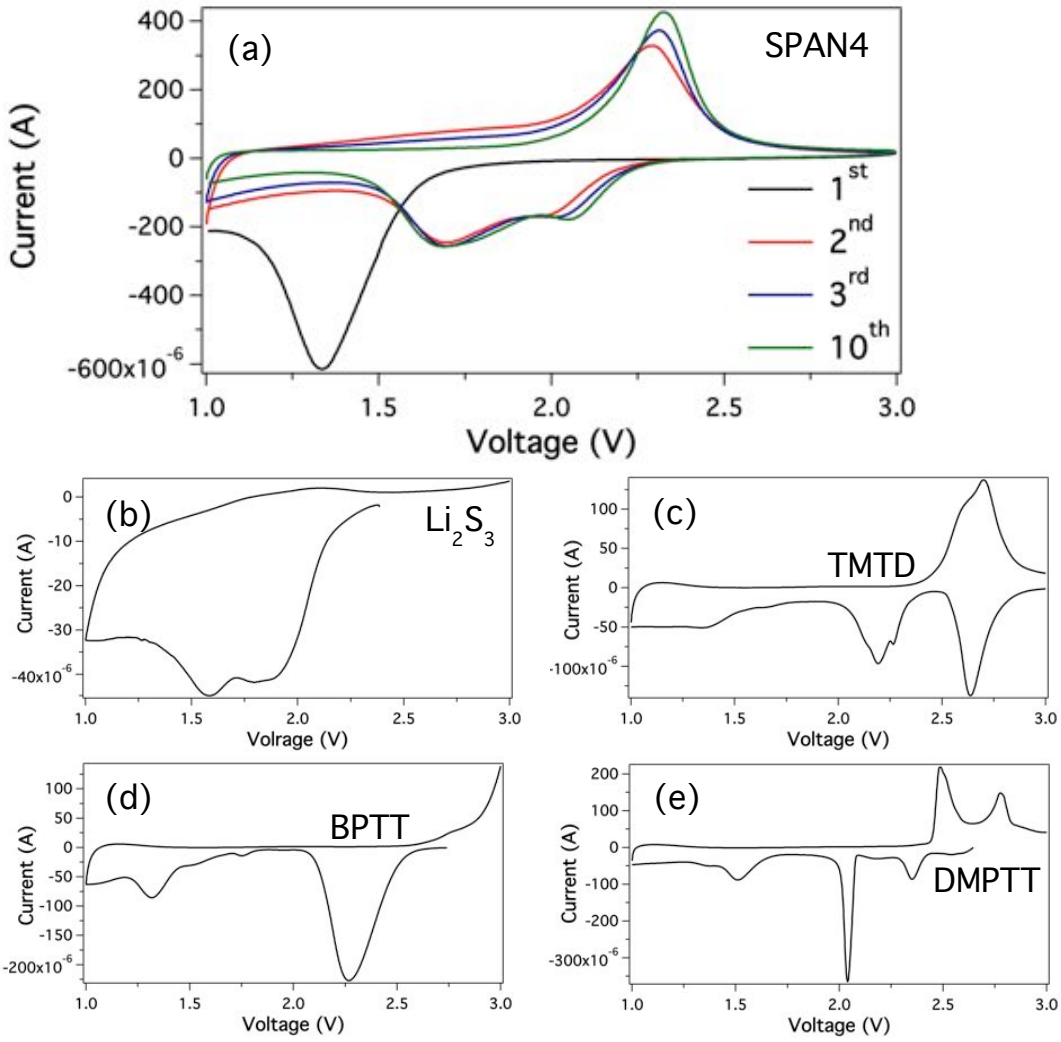

Figure 29. Cyclic voltammograms of the (a) as-prepared SPAN4 composite cathode; (b) Li_2S_3 cross-linked to PAN cathode; (c) tetramethylthiuram disulfide (TMTD) cathode; (d) bis(p-tolylsulfonyl) trisulfide (BPTT) cathode; (e) dipentamethylenethiuram tetrasulfide (DPMTT) cathode at a scan rate of 0.1 mV/s.

It is known that organosulfur-based polymer materials with S-S linkages are capable of

reversibly cleaving and reforming based on the redox chemistry of thiolates (RS^-), which can be oxidized to the corresponding radical (RS) and in turn, couple to form disulfides (RSSR). This process involves one electron transfer such that the capacity is not high compared to elemental sulfur. As these molecules contain other functional groups like thiuram and sulfonyl terminals, the reduction peaks at higher voltage can be ignored, as they are probably related to the reduction of these complex functional groups that are not related to the bond cleavage in sulfides. The reduction peaks at voltages below 2.1 V are thought to arise from S-S bond breakage. And, there is a clear relation between the number of peaks in this section of the CV spectrum and the number of S-S bonds in the materials. TMTD for example shows one broad reduction peaks at ~1.3 V, similar to the initial reduction peak for SPAN. This suggests that during the first discharge, the S-S bond that adjacent to carbon ring breaks in SPAN4 composite and it requires higher energy input.

During following cycles of discharge, CV profile for SPAN shows similarity with Li_2S_3, these can be explained that sulfur that detached from the carbon ring maintains its two-electron transfer properties. A two-electron process is also consistent with the high specific capacity of this material. The absence of a similar sharp reduction peak for SPAN4 compared to DMPTT at 2.05 V, is thought to provide additional evidence that during the first discharge, the S-S bond adjacent to carbon ring breaks in the SPAN4 composite and requires higher energy input. Thus, based on these organic sulfide compound analogues, we propose that in SPAN4, electrochemically active sulfur exists principally as S_3 or S_2 attached to the adjacent carbon backbone. The complete reduction of either species is achieved in a two-electron transfer process, which is likely responsible for the high specific capacity of the material.

We close by considering the effect of a SPAN-based cathode in the Li-S cell on the metallic

lithium anode. As discussed earlier, carbonate electrolytes exhibit minimum solubility for LiPS and Li-S cells based on SPAN cathodes exhibit high coulombic efficiency and no evidence of shuttling. We examined the morphology of lithium anodes for the Li-SPAN4 cells after 500 cycles of galvanostatic charge and discharge in both EC/DEC and DOL/DME electrolytes. Figure 30a shows the SEM image and EDS mapping of the lithium anode in carbonate electrolyte. A very dense and uniform SEI layer can be observed on the anode for cells cycled in EC/DEC electrolyte. The time-dependent growth of the SEI can explain the increase in interfacial resistance in impedance spectra (Figure 31) of the cell upon cycling, as the diffusion length is longer. This SEI can protect lithium and probably minimize lithium dendrite formation, enable stable cycling capability. Remarkably, EDS mapping of the SEI shows no evidence of sulfur, meaning that shuttling can be eliminated when using a non-solvent electrolyte for LiPS in the cell. Thus complete sequestration of electrochemically active sulfur in the cathode not only facilitates complete reduction and high specific capacity, but also provides a well-protected anode, which contributes the cycling stability for the Li-SPAN4 cell. The morphology of cathode after cycling is well maintained and no obvious change can be identified from SEM images (Figure 32). However, when the cell was cycled in DOL/DME, a loose and cracked SEI was observed on lithium anode with abundant sulfur signal being detected shown in Figure 30b, explaining the shuttling phenomena where LiPS attack lithium metal and result in the loss of active cathode mass.

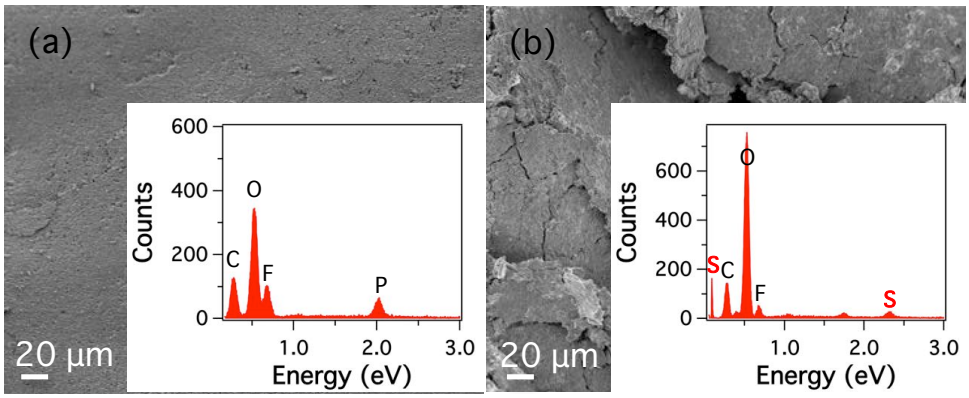

Figure 30. SEM images and EDS mapping of the lithium anode after 500 cycles in (a) EC/DEC; (b) DOL/DME based electrolyte.

Experimental Section

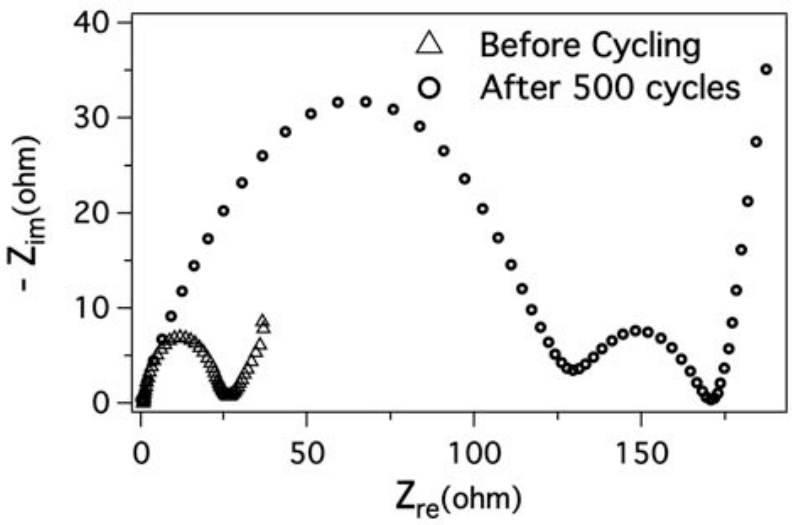

Figure 31. Nyquist plots of the Li-SPAN cells before and after 500 cycles.

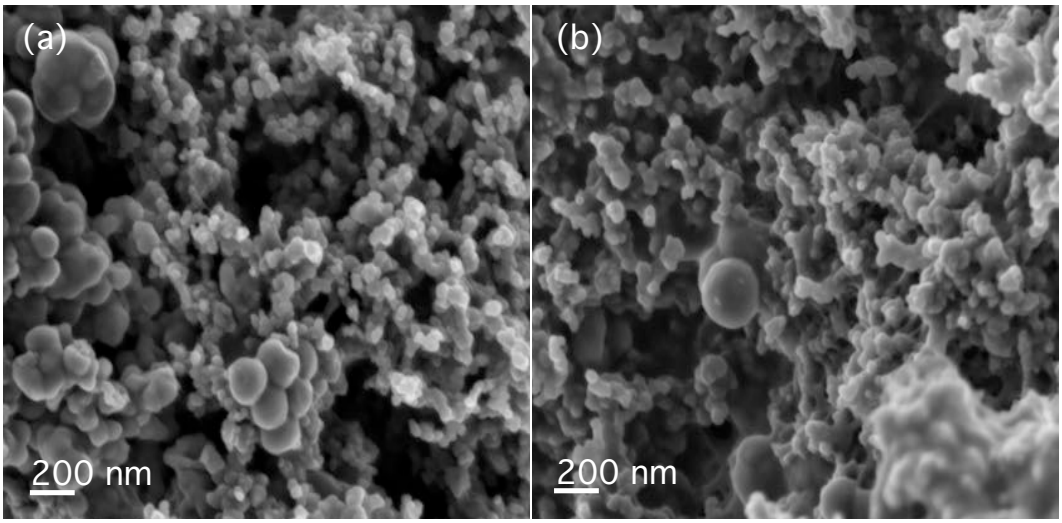

Figure 32. SEM image of the SPAN4 cathode before and after 500 cycles.

3.3 CONCLUSIONS

We have used a straightforward thermal synthesis process to create sulfur/PAN (SPAN) nanocomposites in which sulfur is so strongly linked to a conductive polymer host that its solution state electrochemistry is different from that of bulk S_8. By means of spectroscopic and electrochemical methods, we deduce that in these SPAN composites sulfur exists as S_3/S_2 units covalently attached to a carbon backbone containing pyridinic-N units. When used as cathodes in lithium-sulfur cells, the SPAN nanocomposites exhibit high active materials utilization, exceptional stability in extended cycling, and none of the shuttling behaviors characteristic of cathodes based on elemental sulfur. We show that the beneficial electrochemical attributes of the materials are not only a consequence of the strong interactions between sulfur and its conductive host, but is also a consequence of the host's ability to prevent formation of S_8 after complete oxidation during the cell recharge.

The most impressive electrochemical performance of the SPAN nanocomposite cathodes is

achieved in carbonate electrolytes with minimum solubility for high-order lithium polysulfide (LiPS). In Li-SPAN cells containing these electrolytes and none of the usual salt additives (eg. $LiNO_3$) required to stabilize the anode in conventional Li-S cells, we find no evidence of such reactions or of LiPS shuttling. We find instead that the electrochemical reactions between elemental sulfur in the cathode and Li ions in solution occur fully and with high efficiencies, yielding Li_2S in the solid state as the only discharge product. In contrast, Li-SPAN cells based on electrolytes containing DOL/DME solvent exhibit poor cycling, LiPS shuttling, and low efficiencies. Although more work is needed to fundamentally understand the structure evolution of sulfur in PAN during redox processes in the cathodes, our results support our hypothesis that sulfur exists stably as smaller S_2/S_3 species in the SPAN nanocomposites even after the materials are subjected to galvanostatic cycling for hundreds of cycles.

3.4 Experimental Section

3.4.1 Synthesis

All chemicals were purchased from Sigma-Aldrich unless otherwise specified and used without purification. To synthesis SPANs, polyacrylonitrile (PAN, M_w=150,000) was mixed with sulfur powder in a mass ration of 1:4 and ball milled for one hour to ensure homogeneous mixing. The mixed samples were heated in a nitrogen-filled furnace at 250 °C, 350 °C, 450 °C, 600 °C for 6 hours with a ramping rate of 5 °C/min to carbonize PAN and to yield final products respectively. A control sample PANC was created by the same process but without mixing with sulfur powder and heated to 450 °C.

3.4.2 Characterization

The morphologies of SPAN4 were studied using FEI Tecnai G2 T12 Spirit Transmission Electron Microscope (120kV) and elemental mapping (EDX and EELS) was performed using

FEI Tecnai F20 Transmission Electron Microscope (200kV). Thermogravimetric analysis was performed using TA Instruments Q5000 IR Thermogravimetric Analyzer. The crystal structures of the products were characterized using Scintag Theta-theta X-Ray Diffractometer (Cu Kα, λ=1.5406 Å). Raman spectra were collected using a Renishaw InVia Confocal Raman Microscope (laser wavelength = 488nm). Fourier Transform Infrared Spectra were taken using a Bruker Optics Vertex80v Infrared Spectrometer. Inductively coupled plasma atomic emission spectroscopy (ICP-AES) was used to quantify sulfur content in the electrolytes as a function of time. UV-vis spectra were collected by Shimadzu UV-Vis-NIR Spectrometer. ^{1}H NMR spectra were taken by Inova-400 Spectrometer. X-ray photoelectron spectroscopy (XPS) measurements were performed with a Surface Science SSX-100 spectrometer using a monochromatic Al Kα source (1486.6 eV). Non-linear least squares curve fitting was applied to high-resolution spectra, using CasaXPS software. A LEO 1550 high resolution scanning electron microscopy (HRSEM) with elemental mapping (EDS) was employed to characterize the morphology of the composite electrodes.

The lithium polysulfide dissolution experiments were carried out in the following: Due to the sensitivity of LiPS to air, all the following procedures were performed in an argon-filled glovebox (MBraun Labmaster). Li_2S and S with a molar ratio of 1:7 (49.5 and 224 mg) were mixed and added in 2 ml of the two electrolytes (1M $LiPF_6$ in EC/DEC and 1M LiTFSI in DOL/DME with $LiNO_3$ as additive). Li_2S and SPAN4 were done in the similar method with equal sulfur content in the mixture. 10 μL solution from the four samples was timely collected and subjected to ICP-AES test to quantify sulfur content in the electrolyte. Sulfur contribution from LiTFSI was excluded.

Organic conversion experiments were performed by the following: To convert lithium sulfide (Li_2S) to benzyl sulfide (Bz_2S), 5 mg Li_2S was added in 1 mL mixture of benzyl chloride and 1, 2-dimethoxyethane (BzCl/DME) (v:v = 1:1) and allowed to sit for four days for the conversion to complete. To convert LiPS solution to BzPS, 20 μL 1 M Li_2S_3 in DME (synthesized by mixing Li_2S and S with stoichiometric ratio of 2 : 3 between Li and S in DME) was added in 1 ml mixture of BzCl/DME and allowed to sit for three hours. The LiPS solution becomes transparent and colorless immediately after mixing with BzCl/DME, suggesting quick conversion from LiPS to BzPS. To convert the intermediate species in the cathode, the Li-SPAN4 cells cycled at different stages were opened and the cathodes were soak in the mixture of BzCl/DME and sonicated for 3 hr and kept in the solution for 4 days as more time is needed to convert Li_2S to Bz_2S than LiPS to BzPS.[1] After that, solvents were allowed to evaporate from the samples. The samples were then mixed with chloroform-d and filtered out of impurities (mainly carbon black on the cathode). They were then transferred to NMR tube and subjected to NMR test.

3.4.3 Electrochemical Characterization

Electrochemical characterization of the SPAN nanocomposites as cathode materials in rechargeable lithium batteries was performed at room temperature in 2032 coin-type cells. The working electrode consisted of 70 wt% of the active material, 15 wt% of carbon black (Super-P Li from TIMCAL) as a conductivity aid, and 15 wt% of polymer binder (PVDF, polyvinylidene fluoride, Aldrich). A carbon-coated aluminum foil (0.004 in thick, Alfa Aesar) was used as the current collector. Typical thickness of the active material film is ~0.02 mm and mass per unit area is ~0.85 mg SPAN/cm^2. Lithium foil (0.03 in thick, Alfa Aesar) was used as the counter and reference electrode. Celgard 2500 polypropylene membranes were used as the separator. 40 μL

1M Lithium hexafluorophosphate in a mixture ethylene carbonate (EC) and diethyl carbonate (DEC) (v:v = 1 :1) or 1 M lithium bis(trifluoromethanesulfone) imide (LiTFSI) and 0.2 M $LiNO_3$ in 1, 3-dioxolane and 1, 2-dimethoxyethane (DME) (v:v 1:1) were used as electrolyte for the cells. Cell assembly was carried out in an argon-filled glove-box (MBraun Labmaster). The room-temperature cycling characteristics of the cells were evaluated under galvanostatic conditions using Neware CT-3008 battery testers and electrochemical processes in the cells were studied by cyclic voltammetry using a CHI600D potentiostat. Electrochemical impedance Spectroscopy tests were conducted by using a Solartron Cell Test System model 1470E potentiostat / galvanostat.

4 A STABLE CYCLING ROOM TEMPERATURE SODIUM SULFUR BATTERY

4.1 Introduction

Advance in rechargeable lithium batteries has successfully dominated portable electronics and electric vehicles as energy storage systems since their discovery[2, 3, 103, 104]. Various efforts on developing lithium-sulfur (Li-S) batteries are being devoted due to the high theoretical energy density (2500 W h kg^{-1}), the nature abundance as well as the environmental benignity of sulfur electrode, with great progress being achieved during the past decade[20, 23, 101, 105-108]. However, the cost and feasibility of lithium anode hinder the implementation of lithium-based technology for large-scale storage such as automotive transportation and grid-related application. In such way, new chemistry is needed[109-111], and sodium, the second lightest and smallest alkali metal with much less cost and unlimited everywhere resources, is one of the most appealing alternatives for lithium[112, 113].

Quite surprisingly, although the commercialized stationary energy storage systems - high temperature sodium-sulfur (Na-S) batteries operated at > 300 °C with molten electrodes suggest a large scale and feasible rechargeable battery based on sodium metal[114, 115], room temperature (RT) Na-S batteries, the analogues of Li-S batteries, seem to be hardly understood and investigated. This indicates more obstacles related to RT Na-S batteries need to be solved and different cell chemistries between Li and Na based batteries. The differences are probably related to the larger size of the sodium ion that affects the phase stability, the solubility, the transport properties and the interphase formation as well as the less reducing nature of Na ions compared to Li ions[113]. In addition to more severed challenges facing Li-S batteries such as insulating nature of sulfur and discharge product lithium sulfide (Li_2S), intermediate soluble lithium polysulfides (LiPS) induced shuttling, and volume expansion upon discharging on the

sulfur cathode side of RT Na-S batteries[20, 116-118], sodium metal is seen to less likely form a stable solid-electrolyte interphase (SEI), which easily causes defects on the surface and parasite dendrites at higher current densities, resulting in cell instability during Na electrodeposition. The phenomena have been observed in Na-O_2 batteries[119] and even in Na metal anode when operated at molten state in high temperature Na-S batteries[114], leading to instable charging and low Coulombic efficiency. Therefore, in order to construct a stable cycling RT Na-S battery, solutions on both sulfur and sodium electrodes sides are necessary.

Generally, to construct a performing RT Na–S battery, the utilization of active cathode material is directly dependent on the accommodation ability of the conductive cathode host due to the insulating nature of both fully charged and discharged products (S and Na_2S) and the soluble nature of the intermediate sodium polysulfides (NaPS) produced during cycling[120]. In this regard, sulfur infused in microporous carbon materials with high surface area for chemical and electrochemical reaction and strongest physical confinement for polysulfides with nonpolar interaction between carbon host and sulfur are preferred[26, 100, 121]. These types of sulfur cathodes are compatible with carbonate electrolytes, which has been demonstrated to react with soluble high-order polysulfides (PS) in traditional Li-S batteries[122]. This indicates a solid-state reaction directly from sulfur to solid sulfur species in the cathode without forming reacting and soluble PS, which can diffuse and dissociate in electrolyte and subsequently induce shuttling. On the anode side, techniques for preventing dendrite formation in lithium metal batteries should necessarily be involved. Some of the successful methods in Li batteries, for examples, adding hybrid silica particles[123, 124] or LiF in electrolyte[125] or coating a protective hollow carbon sphere layer[126] on lithium metal, to allow stable Li deposition and prevent dendrite formation could perhaps work in Na battery system.

We herein construct a stable cycling RT Na-S battery in coin cell (Figure 33a), using an Na metal anode, a microporous carbon polyhedron-sulfur composite cathode (MCPS) by infusing sulfur into microporous carbon which is derived from metal-organic framework (MOF), and a liquid electrolyte made by dissolving $NaClO_4$ salt in carbonate electrolyte with hybrid ionic liquid silica nanoparticle (SiO_2-IL-ClO_4) additives as stabilizing agent. The large difference in size between Na atom and Na ion and less reducing nature of Na ion results in non-even electrodeposition upon charging in Na-metal batteries. This phenomenon, which is seen to be independent of cell discharge and related to higher current density, however remains unsolved, and as a result, leads to very low Coulombic efficiency and cell failure. Therefore, unlike Li-S batteries, where Coulombic efficiency plays a critical role to evaluate cell performance, research on Na-S batteries rarely reports Coulombic efficiency.

By adding IL nanoparticles, our cell is able to achieve excellent cycling performance with nearly 100 % Coulombic efficiency at higher current density and with higher sulfur loadings, suggesting stable Na deposition. In addition, by applying the composite cathode, we could get a reversible capacity of over 860 mAh/g at 0.1C (1C=1675 mA/g) and 600 mAh/g at 0.5C based on active sulfur mass. The battery is able to cycle stably for over 100 cycles at 0.5C with 0.31 % capacity decay per cycle. The electrochemical properties on sodiation and desodiation of the constructed Na-S cell were investigated based on spectroscopic tools and analysis. Moreover, the low diffusivity of Na^+ into the composite cathode calculated from electrochemical data suggests a solid-state diffusion, indicating a different reaction mechanism compared to traditional metal-sulfur batteries, as no soluble PS species are formed when using microporous carbon-sulfur composite, which also contributes to the stability and high capacity retention upon cycling.

4.2 Results and Discussion

We start by looking at the effect of particle additives on electrochemical stability of the cell. An electrochemical floating test was performed in the potential range from 3.0 V to 5.0 V. As shown in Figure 33b, electrolytes without particles start to show an increase of current as the potential increases and exhibit an unstable time-dependent current response when the potential reaches 4 V. In contrast, electrolytes containing particles exhibit much lower current response and display attractive stability at least up to 4.5 V. It suggests that, higher leak current caused by higher potential leads to instable charging, while particle additives have beneficial effects on stable sodium electrodeposition, as well as enhances the potential limit of the electrolyte, which can lead to the improved cycling performance. Ionic conductivity (Figure 33c) of the cell with different amount of particle additives is presented as a function of temperature. It can be noticed that temperature-dependent ionic conductivities are found in electrolytes with particles, where local segmental motion, chain relaxation, and crystallinity probably play important roles that increase the stability of the cells. Cell with 10 vol % particles in electrolyte can maintain this feature just below the melting point of Na metal (97.72 °C), which could also indicate the enhanced stability of the cell. However, cells with no particle additives show irregular increased conductivity with temperature, suggesting less stability of the cells. Based on both analysis, we proposed that SiO_2-IL-ClO_4 additive may probably play two roles to stabilize the cell: ionic liquid helps chemically form a stable SEI layer by decomposing on the surface of sodium metal[123], while silica particle can physically reduce electric field by increasing the length scale of the electric field to the size of the particle and the viscosity of the electrolyte which is indicated by the increase in interfacial resistance of the cell.

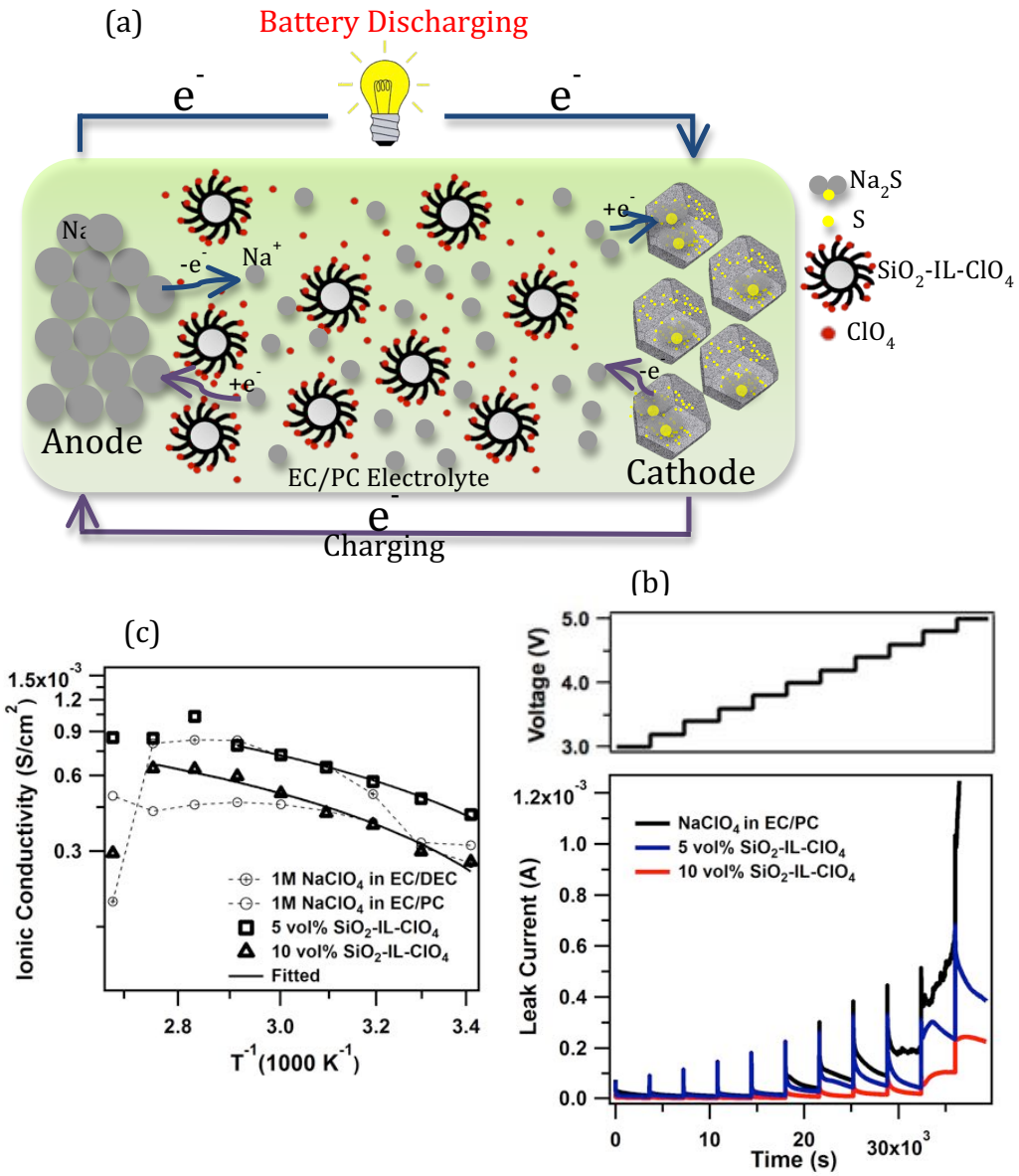

Figure 33. a, Schematic drawing of the Na-S cell during galvanostatic cycling, using SiO_2-IL-ClO_4 as additive in 1M $NaClO_4$ in a mixture of ethylene carbonate and propylene carbonate (EC/PC) (v:v = 1:1). On the anode side, sodium atom loses electron to form sodium ion during discharge. Sodium ion diffuses inside the microporous carbon-sulfur composite (MCPS) and reacts with sulfur to form sodium sulfide (Na_2S) on the cathode side, and the reverse reaction took place during charging, where SiO_2-IL-ClO_4 helps stabilize sodium anode. b, constant voltage-charge profile of the Na-S cells with different volume fraction of SiO_2-IL-ClO_4 in the electrolyte mentioned in a

maintained at 3.0, 3.2, 3.4…5.0 V for 1 h at room temperature. c, Ionic conductivity of the Na-S cells with different volume fraction of SiO_2-IL-ClO_4 in the electrolyte as a function of temperature. EC/DEC represents a mixture of ethylene carbonate and diethyl carbonate (v:v = 1:1). The solid lines are linear Vogel–Fulcher–Tammann fits for the temperature-dependent ionic conductivity.

In metal-sulfur batteries, cathode design plays an important role in improving the cycling performance of the cell. Due to the highly reactive nature of sodium, reaction between sodium and sulfur would be stronger compared to lithium and sulfur, indicating that cathode materials having stronger interaction with sulfur to hold PS species should be applied in Na-S cathode. Microporous carbon materials are thought to provide the strongest physical confinement/immobilization for sulfur and its reduction products due to their extremely small pore sizes. This material has been successfully applied in Na-S cathode with lower sulfur loadings (32 %)[121]. Increasing sulfur loading in microporous carbon need special design in porous carbon host, such as homogeneous pore size distribution and increased pore volumes[127]. We applied a facile synthesis of microporous carbon polyhedrons (MCPs) using unique chemically and thermally robust and highly porous zeolite-type MOF (ZIF-8) rhombic dodecahedra as both the template and precursor, and use them as host to incorporate sulfur for Na-S battery cathode. The as-prepared MCPs show very high surface area and uniform microporosity, which can facilitate Na^+ transport and immobilize sulfur inside the pores homogeneously.

The composite MCPSs are prepared based on the reported method[26, 128]. Figure 34a shows the STEM and TEM images of the MCPs, indicating a uniform microporous spongy like texture. The abundant micropores give rise to a high Brunauer–Emmett–Teller (BET) surface area of 833 m^2/g calculated from the N_2 adsorption-desorption isotherm of the MCPs (Figure 34b and Table 3), which also give rise to a 708.5 m^2/g microporous surface area and pore size distribution

ranging from 0.4 nm to 1.8 nm. Different amount of sulfur is infused in MCPs and the composites are denoted as MCPS1 and MCPS2 with 47 % and 65 % sulfur loading respectively (verified by TGA curve Figure 35). The weight loss for MCPS1 due to the evaporation of sulfur occurs in a wide temperature range up to 450 °C, indicating strong nonpolar interaction between sulfur and carbon matrix, while MCPS2 shows a two-step weight loss, representing sulfur vapor outside and inside the MCPs respectively. SEM image (Figure 2c) of the as-synthesized MCPS suggests well-maintained rhombic dodecahedra morphology from ZIF-8 after carbonization and after sulfur infusion process, most of sulfur is trapped inside the micropores. Raman spectra (Figure 2d) of MCPs and MCPSs indicate carbonization of ZIF-8 and well dispersion of sulfur in micropores in MCPS1 as no crystalline sulfur peaks can be observed.

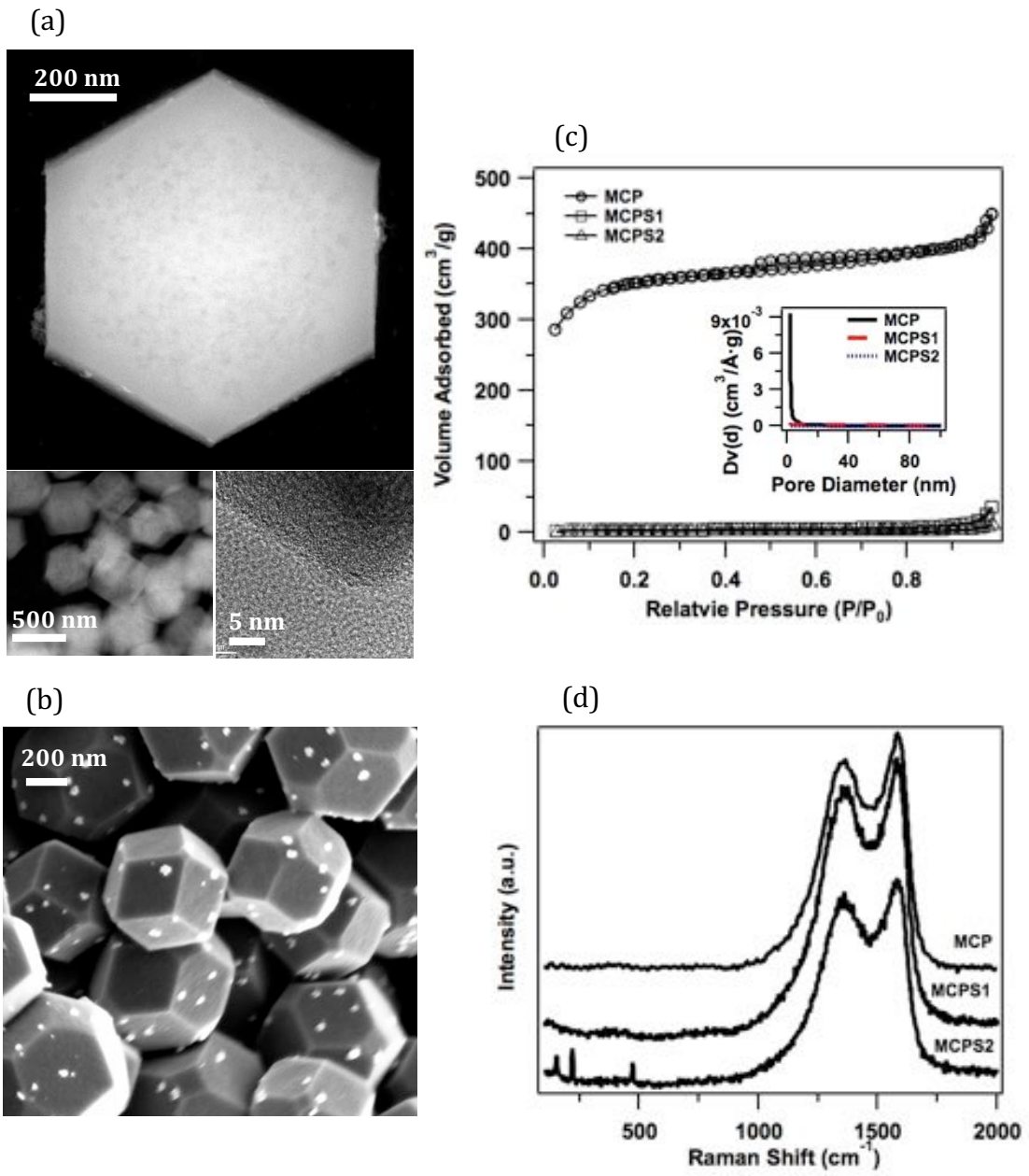

Figure 34. a, Scanning transmission electron microscopy (STEM) and transmission electron microscopy (TEM) images of MCP. The right bottom TEM image shows the edge of the MCP, indicating uniform porous structure of the MCP. b, Scanning electron microscopy (SEM) image of MCPS1. The small dots on the surface of the MCPS1 are trace amount of sulfur. c, N_2 adsorption–desorption isotherm and the corresponding BET pore size distribution (inset) of MCP and MCPS composites . d, Raman Spectra of the MCP and MCPS composites.

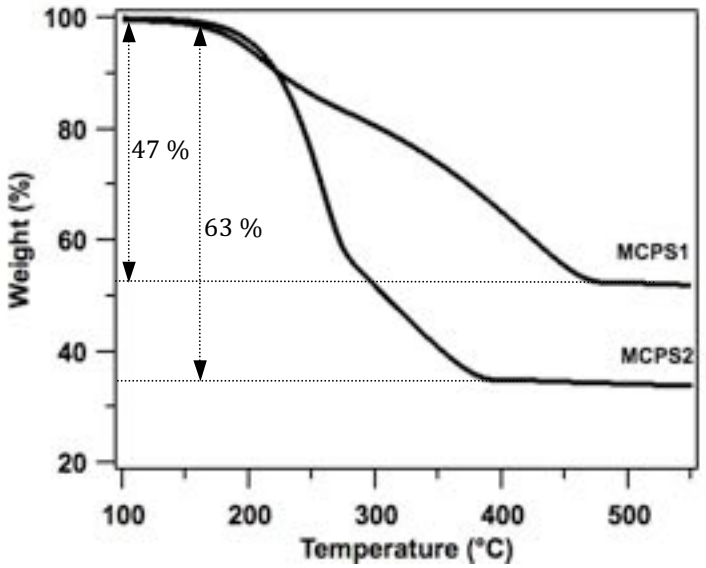

Figure 35. Thermogravimetric analysis (TGA) of the MCPSs with different sulfur loadings under N_2 flow.

Table 3: Physical characteristics of the MCP and MCPS composite. DFT: Density function theory method used to determine microspores. I_g/I_d is the ratio used to determine the amount of graphitic carbon verse disordered carbon in the composite, which are the normalized peak ratio of G band to D band in Raman Spectra.

Samples	BET Total Surface	Pore Volume	Micropore Surface	DFT Pore Size	Conductivity(S/cm)	I_g/I_d

	Area (m^2/g)	(cm^3/g)	Area (m^2/g)	Distribution (nm)		
MCP	833.3781	0.695505	708.4812	0.4~1.8	$9.66*10^{-3}$	1.14
MCPS1	11.5262	0.054189	2.3499	n.a.	$6.13*10^{-3}$	1.14
MCPS2	3.2628	0.017352	1.1322	n.a.	$5.22*10^{-3}$	1.08

Galvanostatic cycling performance of the cell by using a MCPS1 as cathode, a Na metal foil as anode and a carbonate electrolyte is shown in Figure 36a. The cell exhibits a high initial discharge capacity of 1614 mAh/g at a current density of 0.1C (1C = 1675 mAh/g). The dimple and the lower voltage plateau at the beginning of discharge compared to the following cycles indicates that Na ions need to go through a barrier which is probably related to desolvation or solvation shell distortion[129, 130] to accommodate extremely small pore size in order to diffuse inside the micropores. This higher irreversible capacity is partially attributed to initial SEI formation and electrolyte decomposition. The reversible discharge plateau in the following cycles ranges from 1.6 V to 1 V. The lower voltage suggests formation of Na_2S/Na_2S_2 directly without intermediate soluble PSs species, while higher order NaPSs may formed and react with carbonate electrolyte when MCPS2 is used as cathode (Figure. 37). A reversible discharge capacity of 800 mAh/g is stably achieved for 50 cycles (Figure 36b). For comparison, a TEGDME electrolyte, which has high solubility for NaPS is applied and shuttling is observed by post mortem study (Figure 38 and 39). To investigate reduction and oxidation mechanism, cyclic voltammgram at various scan rates are conducted and shown in Figure 36c. Two reduction peaks are observed, indicating a two-electron reduction. The reduction peaks shift towards a more negative value and oxidation peak shift towards a more positive value with increasing scan rate, indicating a mixed kinetics of charge transfer process and diffusion of electro-active species

control[131]. The peak current is found to increase with scan rate as well, which shows a linear growth with square root of scan rate (Figure 36d), suggesting a diffusion process. Furthermore, the almost the same cathodic and anodic peak currents indicates good reversibility and similar reaction mechanism occurring during charge and discharge.

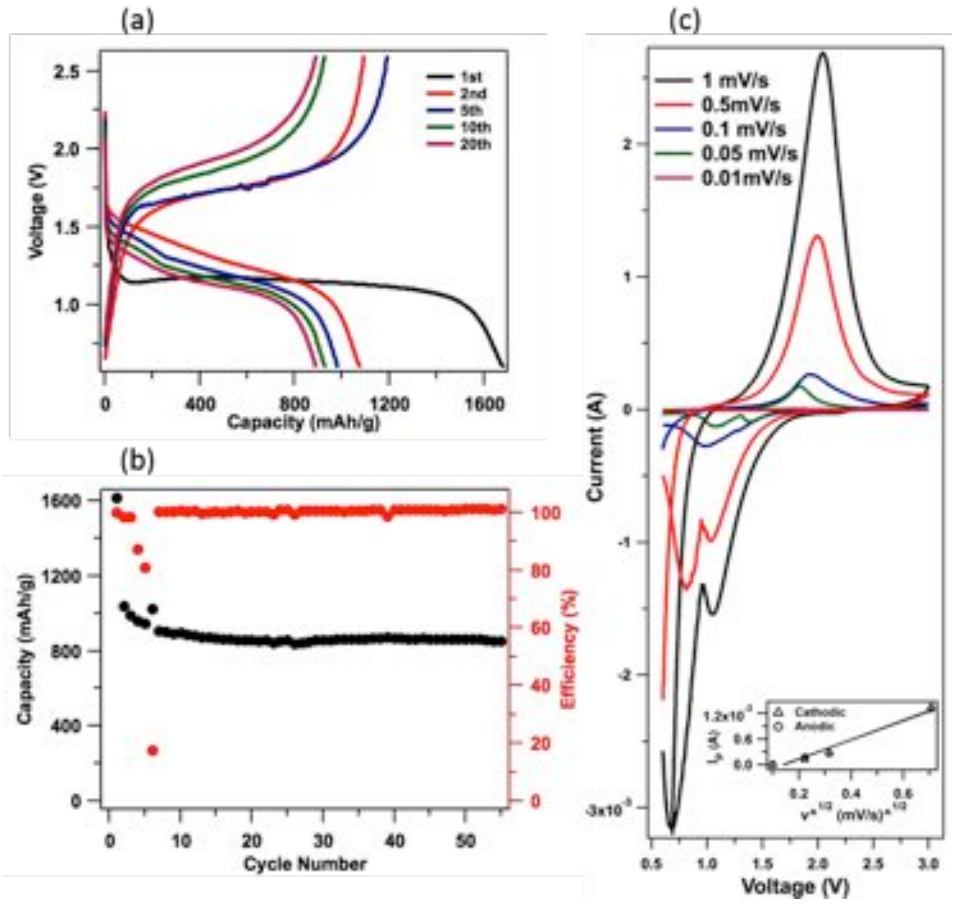

Figure 36 a, Electrochemical discharge and charge curves of the cell at various cycles. The tests were performed at 0.1 C for both charge and discharge in the potential range of 0.6–2.6 V vs Na/Na^+. b, Capacity and Coulombic efficiencies versus cycle number for the cell. c, Cyclic voltammograms (CV) of the Na-S cells at various scan rates. d, Relation between peak cathodic and anodic currents verse square root of scan rate derived from c.

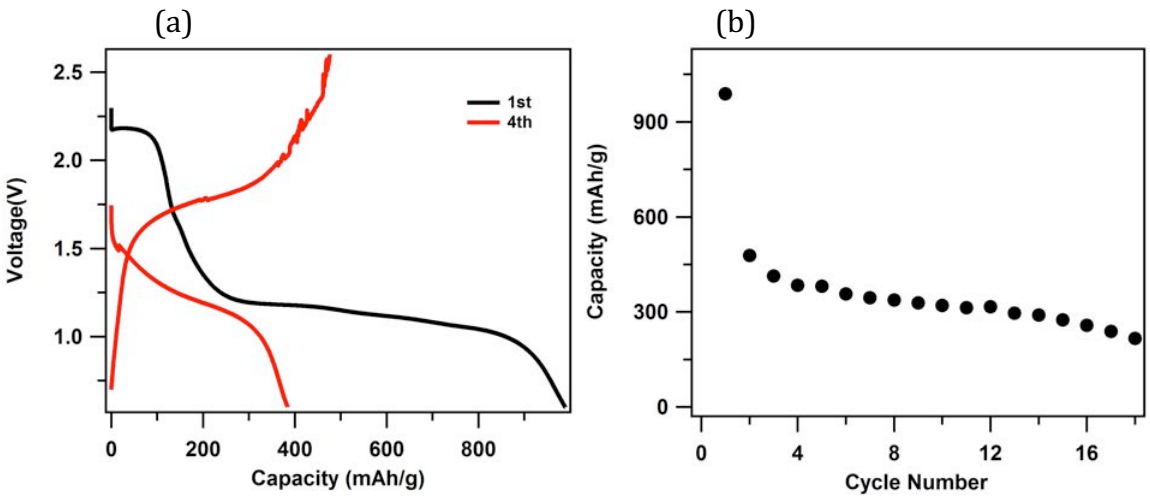

Figure 37. a, Electrochemical discharge and charge curves of the cell at 0.1C. The two discharge plateau in the first cycles indicates sulfur outside and inside the MCP. The disappearance of the higher discharge voltage plateau suggests that the elemental sulfur outside MCP reacts irreversibly with carbonate electrolyte. b, Capacity verses cycle number by using MCPS2 as the cathode.

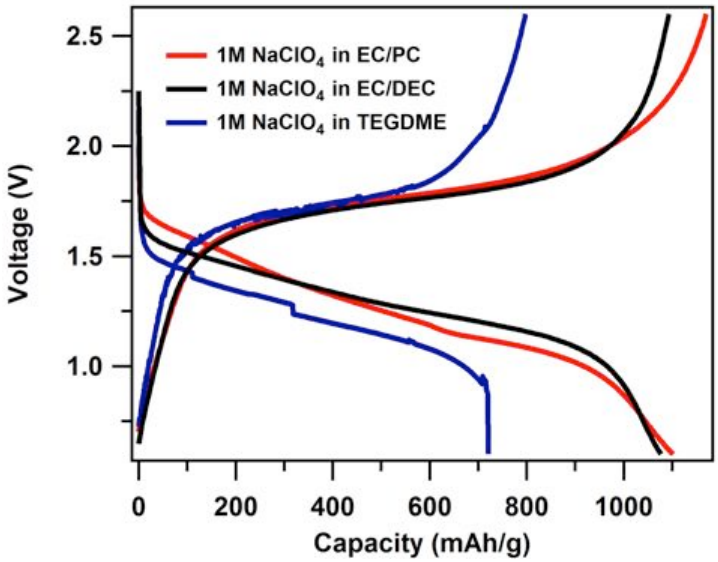

Figure 38. Tetraethylene glycol dimethyl ether (TEGDME) is a commonly used ether-based electrolyte in Li-S batteries due to its higher solubility to LiPS, however, carbonate electrolytes are suggest to be non-solubility to PS. The cathode is MCPS1. When usin MCPS2 as cathode in TEGDME electrolyte, server shuttling is observed during charging. The current density is 0.1C for both charge and discharge.

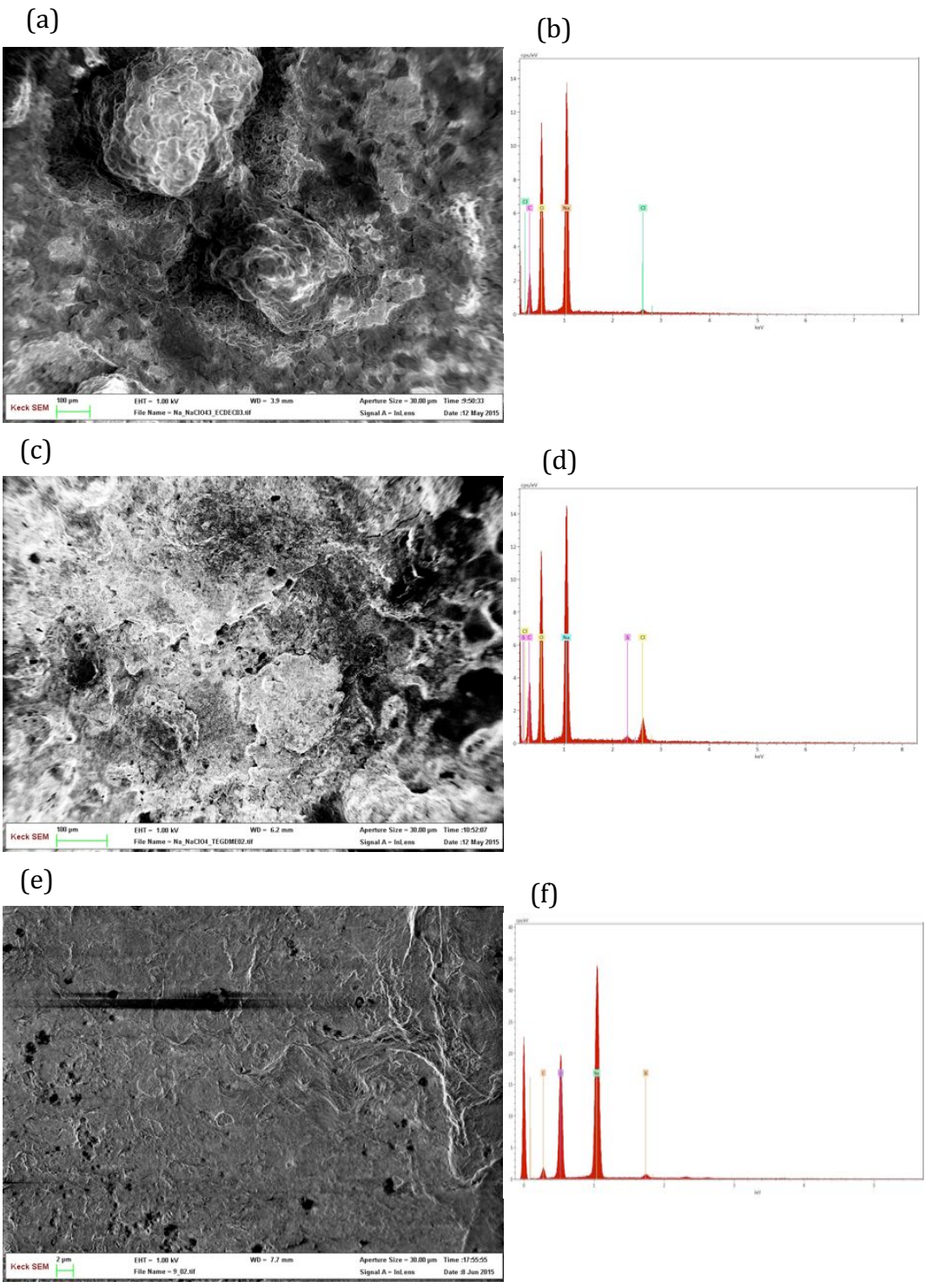

Figure 39: Scanning electron microscopy (SEM) image and energy dispersive spectra (EDS) maps of the sodium anodes after 10 cycles. a and b, SEM image and EDS maps of the sodium anode in 80 µL 1M NaClO4 in EC/DEC electrolyte. c and d are in 80 µL 1M NaClO4 in TEGDME electrolyte. e and f are in 1M NaClO4 in EC/PC electrolyte with 10 vol% SiO_2-IL-

ClO_4. The cells were dissembled after 10 cycles of charge and discharge at 0.1C in a argon filled glovebox and the anodes were washed with electrolyte solvent before characterization.

However, we found that, although the battery can cycle stably in the above-mentioned system, instable charging is noticed at the sixth cycle and even worse at higher current density. This may cause dendrite problem, short circuit induced safety issues, low material utilization and electrolyte decomposition, eventually the cell failure. Therefore, a stabilizer in the electrolyte is necessary for the cell. We applied SiO_2-IL-ClO_4 nanoparticles as additives to stabilize the electrolyte and protect sodium metal as indicated in electrolyte stability analysis previously.

We next add either 5 vol% or 10 vol% of the SiO_2-IL-ClO_4 in the electrolyte as a stabilizer and performed the galvanostatic test at 0.5 C. As expected, even as little as 5 vol% additives could stabilize charging to a large extent. Figure 40a and b show the voltage profile and cycling stability of the cell. The first discharge is performed at 0.1 C to fully activate the electrode. A discharge capacity of around 750 mAh/g is achieved initially and maintained to 600 mAh/g at the 100^{th} cycle, indicating a small capacity decay of 0.31 % per cycle, which is comparable to current Li-S batteries at the same C rate. The Coulombic efficiencies for the batteries with and without SiO_2-IL-ClO_4 are compared in Figure 40c and e to evaluate the stability of the systems. We have seen that, the cell without SiO_2-IL-ClO_4 show diverged Coulombic efficiency from 10^{th} to 60^{th} cycle, while cells with only small amount of SiO_2-IL-ClO_4 can improve the Coulombic efficiency to over 90 % each cycle, which is enhanced with increasing SiO_2-IL-ClO_4 amount. This improved stability can also improve the cycling discharge capacity as shown in Figure 40d because less side like electrolyte decomposition reaction is occurring.

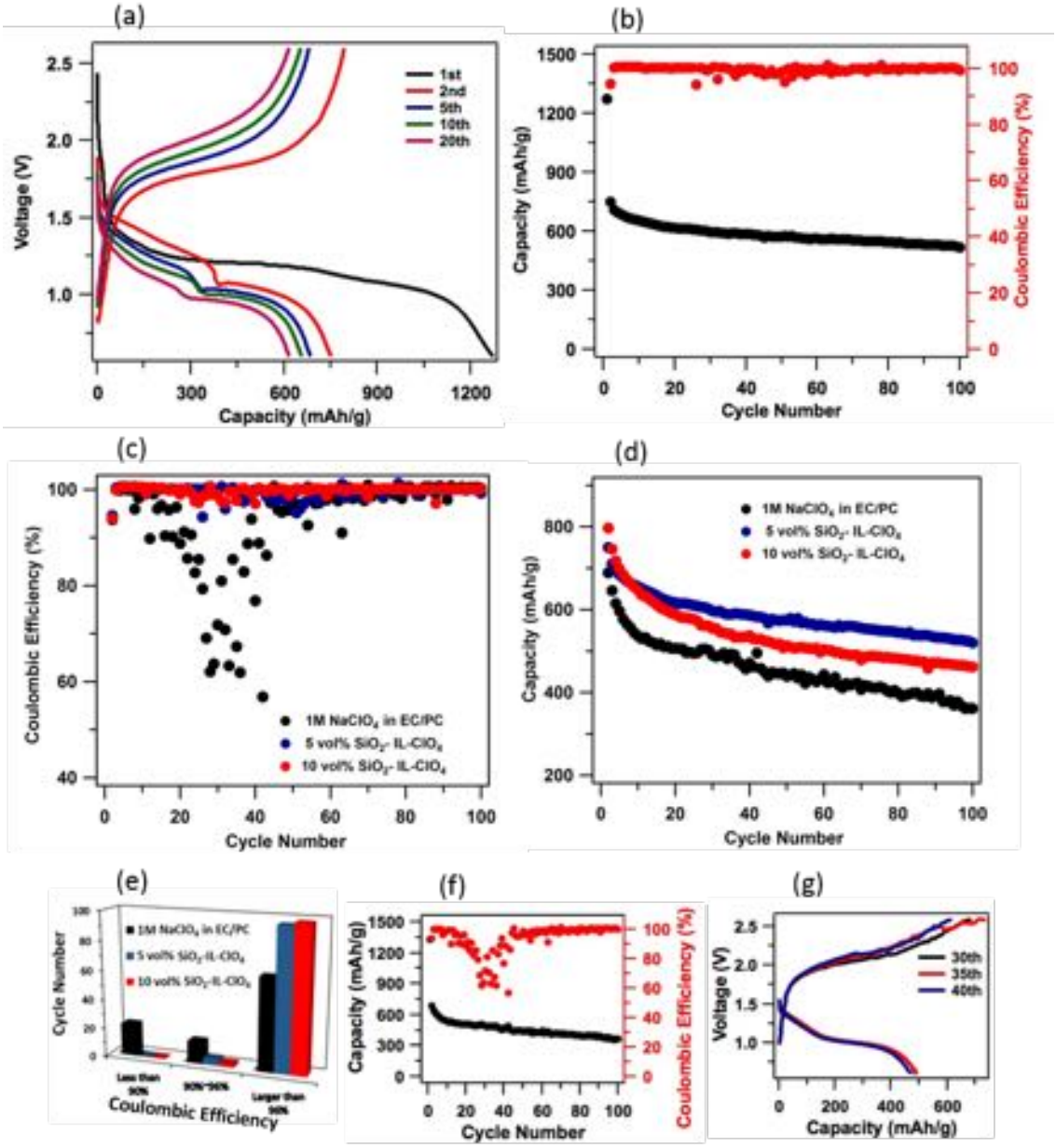

Figure 40: Galvanostatic cycling performance of the Na-S cell in a carbonate electrolyte with different amount of SiO_2-IL-ClO_4 . a, Electrochemical discharge and charge curves of the cell at various cycles with 5 vol% of SiO_2-IL-ClO_4 in the electrolyte. The tests were performed at 0.1 C for the first discharge and 0.5C for the following cycles in the potential range of 0.6–2.6 V vs Na/Na^+. b, Capacity and Coulombic efficiencies versus cycle number for the cell in a. c and d, Coulombic efficiency and capacity versus cycle number for the cell with different amount of SiO_2-IL-ClO_4 in the electrolyte respectively at 0.5C. e, Electrolyte stability analysis for the three cases in c in term of Coulombic efficiency. f and g, cycling stability and voltage profile of the cell without SiO_2-IL-ClO_4 in the electrolyte at 0.5C.

To investigate the discharge reaction mechanism, X-ray photoelectron spectroscopy (XPS) is applied on the cathode side after galvanostatic cycling at different stages study the species formed at each stage (Figure 41a). The pristine cathode exhibits an elemental-state sulfur doublelet with S2p 2/3 at 164 eV. When cell is discharged below 1 V, S2p 2/3 peaks at 162.1 eV and 160 eV representing Na_2S_2 and Na_2S rise. The peak beyond 166 eV is probably due to thiosulfate/sulfate complex species originating from oxidized sulfide species[132]. Upon fully discharge, elemental sulfur peak disappeared; only the sulfide peaks remain, suggesting the final discharge product of Na_2S. This can explain why the higher capacity is achieved compared to high temperature Na-S batteries, where the final discharge product is Na_2S_x ($x \geq 3$) because of the phase limitation[114]. To further understand the reaction mechanism, the energy dispersive X-ray (EDX) analysis of cathode after full discharge was performed (Figure 41b), the atomic ratio between Na and S is about 2 : 1, indicating almost fully reduction from S to Na_2S. UV-vis spectra of a dilute Na_2S_6 solution, battery cathode cycled in TEGDME and carbonate electrolyte soaked in TEGDME are shown in Figure 41c. In carbonate electrolyte, there are only insoluble S_2^{2-} or S^{2-} formed, while high order soluble PSs are formed when the cell are cycled in TEGDME. This again confirms that MCPS cathode coupled with carbonate electrolyte undergoes solid-state reaction with no soluble intermediated soluble polysulfide formed in Na-S batteries.

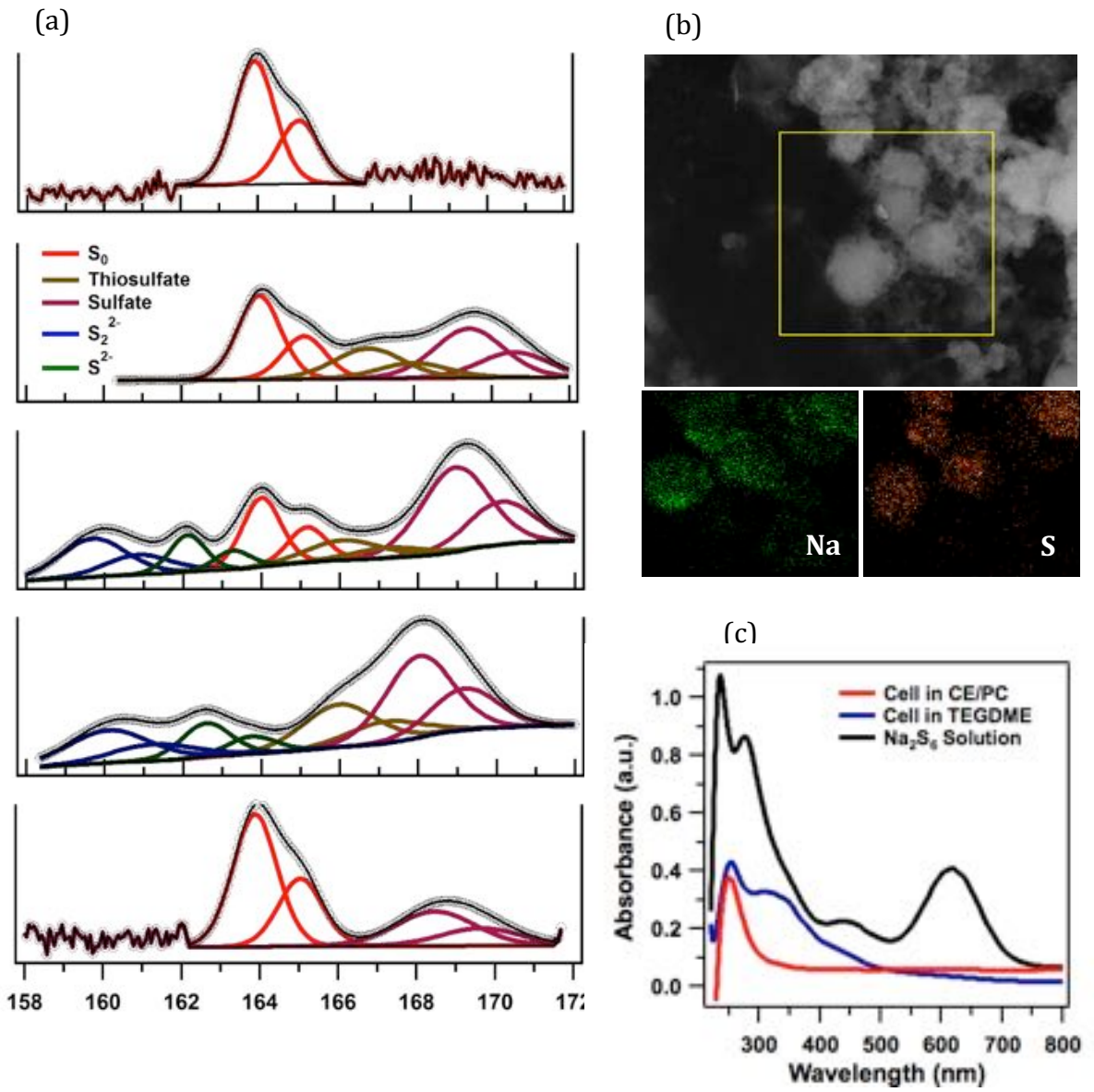

Figure 41: Post mortem characterization of the MCPS1 cathodes in carbonate electrolytes. a, Ex situ XPS spectra of S 2p in MCPS cathodes at pristine and different cycling states in a carbonate electrolyte. (From top to bottom: pristine cathode, cell was discharged to1.4 V, 1 V and 0.6 V and was recharged to 2.6 V at the first cycle respectively). Cathodes were disassembled in an argon filled grove-box and washed with electrolyte solvent before characterization. b, STEM image and EDX maps of the MCPS1 cathode after first discharge. The cathode was washed with electrolyte solvent and sonicated to form a homogeneous suspension in a sealed vial and then transferred to a Cu grid sample holder. c, UV-vis spectra of the cathodes solutions cycled in different electrolytes after 10 cycles at 0.1C. The MCP cathodes cycled in different electrolytes were all soaked in 2 mL TEGDME for 4 days to extract PS species. For the Na_2S_6 solution, 1M Na_2S_6, which is synthesized by mixing Na_2S and sulfur in a stoichiometric ratio of 2:6 in TEDME. It was diluted 200 times and subjected to test. Peak assignment: S^{2-} ,S_2^{2-}: 260 nm, S_6^{2-}: 340 nm and 450 nm, S_3^{2-}: 330 nm, $S_3^{\cdot-}$: 610 nm[133].

Based on the spectroscopic study above, we suspect that the electrochemistry on cathode side is occurred inside the MCPS only, indicating a solid-state reaction. To verify this, we approximate Na^+ diffusivity into the cathode based on electrochemical data. A galvanostatic intermittent titration technique (GITT) was performed by discharging the cell for 30 minutes at 0.1C followed by a 10-hour relaxation (Figure 42a). The diffusion coefficient (Figure 42b) during reversible charging and discharging can be calculated by the equation developed by Weppner and Huggins[134], which is in the range of solid-state diffusion. It is found to be the lowest at the plateau region, indicating a kinetics-controlled mechanism is simultaneously occurring. In addition, the equilibrium potential determined at the end of each titration step changes very slightly and all below 2 V, suggesting the formation of Na_2S_x ($x \leq 2$). This can also be verified by deriving diffusivity from Warburg element of a fitted equivalent circuit from the electrochemical impedance spectra (Figure 43). The calculated diffusivity shows the similar order of magnitude compared to that derived from GITT. The reason that in solid-state reaction occurs only in microporous carbons with extremely small pore size but not other carbon materials is probably due to that interaction between sulfur/sulfur species in the carbon is much stronger than the strength for sulfur/sulfur species solvation due to their poor solubility in carbonate electrolytes[135] and space confinement in carbon.

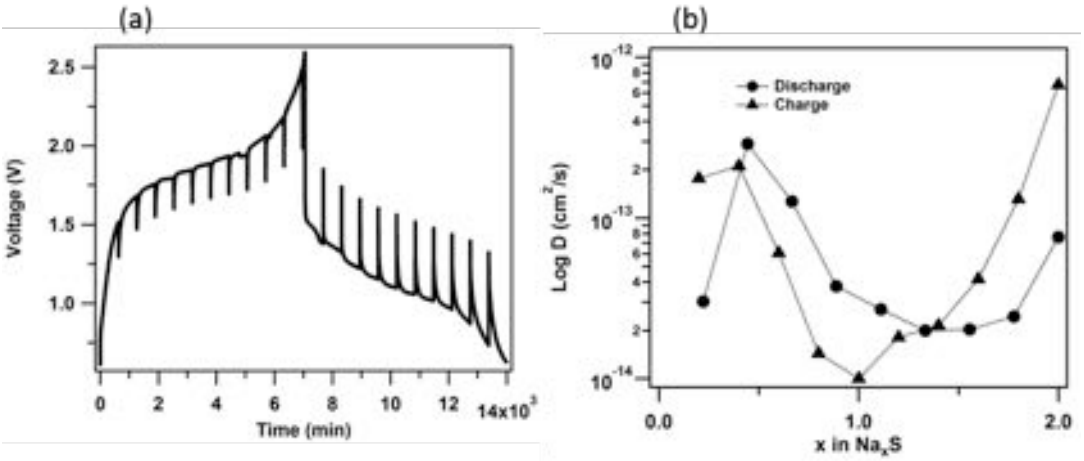

Figure 42: Diffusivity analysis of the Na-S cell. a, GITT curves of MCPS1 in EC/PC electrolyte and b, Diffusion coefficients derived from a.

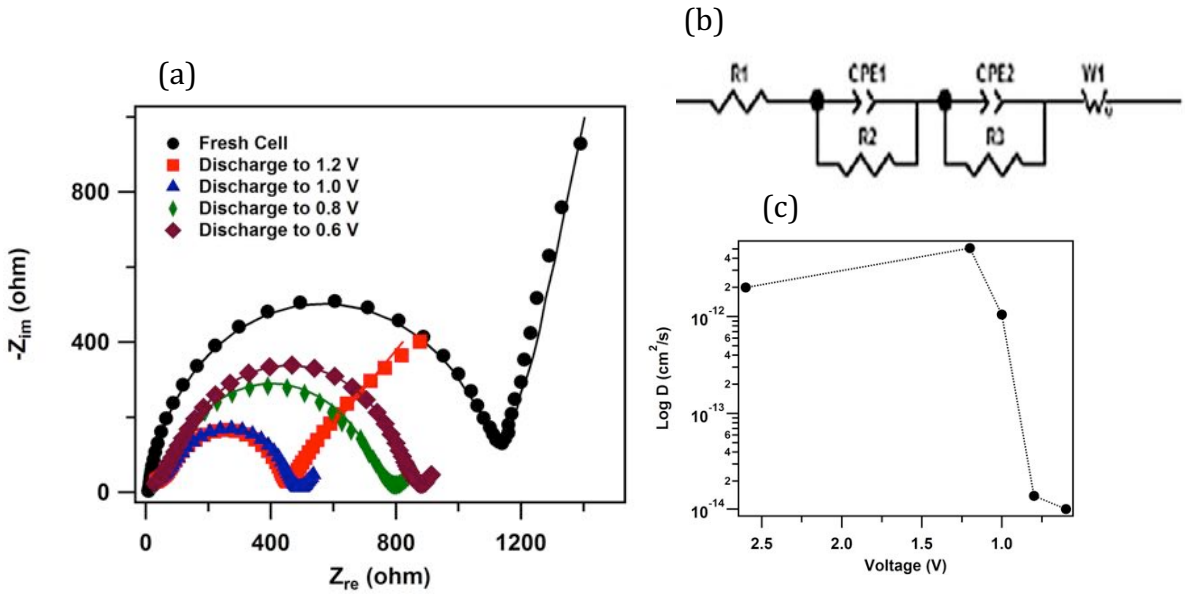

Figure 43: Impedance spectra a and derived diffusivity c of the MCPS1 cathode at pristine and different stages of discharge. b, equivalent circuit used to fit impedance spectra and to get Warburg element. The black like in a is the fitted impedance spectra by applying the circuit in b.

4.3 Conclusion

In conclusion, we constructed a sable cycling room temperature Na-S battery. The micoporous carbon sulfur composite provides strong physical confinement to ensure reaction to happen in all-solid state when coupled with non-solvent electrolyte for PSs. The unique small porous carbon shows strong affinity towards sulfur and can probably direct sulfur to exist in an unusual phase and avoid formation of high order PS during discharge. We use both spectroscopic and analytical tools to verify that the reaction occurs all inside the microporous carbon composite. The cell can stably cycling for over 100 cycles when adding SiO_2-IL-ClO_4 particles at a relatively high current density (0.5C), where the particle additives is seen to serve as a stabilizer to protect sodium metal and prevent dendrite formation through chemically deposition of a stable SEI layer as well as physically reducing electrical field by increasing the length scale to the size of particle and increase viscosity of the electrolyte. Our finding underscores the benefits of micorporous carbon-sulfur composite and nanoparticles for gridding new material designs for inexpensive rechargeable metal-sulfur batteries. Further investigations are needed to fully understand the effect and interaction of microporous carbon and sulfur species as well as the functionality of SiO_2-IL-ClO_4 on metal anode protection.

4.4 Methods

Materials Synthesis: MCPS and SiO_2-IL-ClO_4 electrolyte were synthesized according to the previous methods with modifications[26, 136]. Briefly, the synthesis of MCPS is the same except the final sulfur infusion step. A sealed Pyrex tube was used to hold samples and a ramp rate of 1 ºC/min was used for both heating and cooling. The final mass fraction of sulfur in the composites was determined by TGA (Q5000 IR Thermogravimetric Analyzer). The synthesis of

SiO_2-IL-ClO_4 was the same as well except the anion exchange step. In this work, $NaClO_4$ was used to as anion exchange source.

Material Characterization: The morphology and elemental mappings of the materials were studied using a FEI Tecnai F20 Transmission Electron Microscope and A LEO 1550 high resolution scanning electron microscopy. The nitrogen adsorption-desorption isotherms of the MCP and MCPS were obtained with a Brunauer-Emmett-Teller (Micromeritics ASAP2020). Raman spectra were collected using a Renishaw InVia Confocal Raman Microscope (λ= 488nm). UV-vis spectra were collected by Shimadzu UV-Vis-NIR Spectrometer. X-ray photoelectron spectroscopy (XPS) measurements were performed with a Surface Science SSX-100 spectrometer using a monochromatic Al Kα source (1486.6 eV). Non-linear least squares curve fitting was applied to high-resolution spectra, using CasaXPS software.

Electrochemical Measurements: The cathodes were prepared with MCPS1 or MCPS2, carbon black (Super-P, TIMCAL), and polymer binder (poly(vinylidene difluoride), PVDF, Aldrich) in a weight ratio of 8:1:1. A carbon-coated aluminum foil (0.004 in thick, MTI Corp.) was used as the current collector. The typical thickness of the active material film is ~20 μm. Sodium foil (Alfa Aesar) was used as the counter and reference electrode. A glass fiber filter paper (Watchman 934-AH) was used as separator. 80 μL 1M Sodium perchlorate in a mixture ethylene carbonate (EC) and diethyl carbonate (DEC) (v:v = 1 :1) or in tetraethylene glycol dimethyl ether (TEGDME) or in a mixture of EC and propylene carbonate (PC) (v:v = 1 :1) with different amount of SiO_2-IL-ClO_4 were used as electrolyte for the cells. Cell assembly was carried out in an argon-filled glove-box (MBraun Labmaster) by using coin cell 2032 type. The room-temperature cycling characteristics of the cells were evaluated under galvanostatic conditions using Neware CT-3008 battery testers and electrochemical processes in the cells were studied by

cyclic voltammetry using a CHI600D potentiostat. Electrochemical impedance and floating tests were conducted by using a Solartron Cell Test System model 1470E potentiostat/galvanostat. Ionic conductivities were measured using a Novocontrol N40 broadband dielectric spectrometer. For post-mortem studies, cells were disassembled in an argon-filled glove-box and the electrodes were harvested and rinsed thoroughly with the electrolyte solvent before analysis.

REFERENCE

1. Bruce, P.G., et al., *Li-O2 and Li-S batteries with high energy storage.* Nat Mater, 2012. **11**(1): p. 19-29.
2. Dunn, B., H. Kamath, and J.-M. Tarascon, *Electrical Energy Storage for the Grid: A Battery of Choices.* Science, 2011. **334**(6058): p. 928-935.
3. Tarascon, J.M. and M. Armand, *Issues and challenges facing rechargeable lithium batteries.* Nature, 2001. **414**(6861): p. 359-367.
4. Jiang, C., E. Hosono, and H. Zhou, *Nanomaterials for lithium ion batteries.* Nano Today, 2006. **1**(4): p. 28-33.
5. Lee, K.T. and J. Cho, *Roles of nanosize in lithium reactive nanomaterials for lithium ion batteries.* Nano Today, 2011. **6**(1): p. 28-41.
6. Hassoun, J. and B. Scrosati, *Moving to a solid-state configuration: a valid approach to making lithium-sulfur batteries viable for practical applications.* Adv Mater, 2010. **22**(45): p. 5198-201.
7. Yang, Z., et al., *In situ synthesis of lithium sulfide–carbon composites as cathode materials for rechargeable lithium batteries.* Journal of Materials Chemistry A, 2013. **1**(4): p. 1433.

8. Miller TJ (2009) Electrical Energy Storage for Vehicles: Targets and Metrics, Ford Motor Company

9. Gao, J. and H.D. Abruña, *Key Parameters Governing the Energy Density of Rechargeable Li/S Batteries.* The Journal of Physical Chemistry Letters, 2014. **5**(5): p. 882-885.

10. Meyer, B., *Solid Allotropes of Sulfur.* Chemical Reviews, 1964. **64**(4): p. 429-451.

11. Akridge, J.R., Y.V. Mikhaylik, and N. White, *Li/S fundamental chemistry and application to high-performance rechargeable batteries.* Solid State Ionics, 2004. **175**(1-4): p. 243-245.

12. Wang, J., *Sulfur-mesoporous carbon composites in conjunction with a novel ionic liquid electrolyte for lithium rechargeable batteries.* Carbon, 2008. **46**: p. 229-235.

13. Jayaprakash, N., et al., *Porous Hollow Carbon@Sulfur Composites for High-Power Lithium–Sulfur Batteries.* Angewandte Chemie International Edition, 2011. **50**(26): p. 5904-5908.

14. Zeng, Q., et al., *Synergy of nanoconfinement and surface oxygen in recrystallization of sulfur melt in carbon nanocapsules and the related Li–S cathode properties.* Journal of Materials Chemistry A, 2014. **2**(18): p. 6439.

15. Cunningham, P.T., S.A. Johnson, and E.J. Cairns, *Phase equilibria in lithium-chalcogen systems: Lithium-sulfur.* J. Electrochem. Soc., 1972. **119**: p. 1448-1450.

16. Choi, J.W., *Rechargeable lithium/sulfur battery with suitable mixed liquid electrolytes.* Electrochim. Acta, 2007. **52**: p. 2075-2082.

17. Zheng, G., et al., *Hollow Carbon Nanofiber-Encapsulated Sulfur Cathodes for High Specific Capacity Rechargeable Lithium Batteries.* Nano Letters, 2011. **11**(10): p. 4462-4467.

18. Guo, Y.-G., J.-S. Hu, and L.-J. Wan, *Nanostructured Materials for Electrochemical Energy Conversion and Storage Devices.* Advanced Materials, 2008. **20**(15): p. 2878-2887.

19. Wang, J.L., et al., *Sulfur–carbon nano-composite as cathode for rechargeable lithium battery based on gel electrolyte.* Electrochemistry Communications, 2002. **4**(6): p. 499-502.

20. Ma, L., et al., *Nanomaterials: Science and applications in the lithium–sulfur battery.* Nano Today, 2015. **10**(3): p. 315-338.

21. Xin, S., et al., *Smaller sulfur molecules promise better lithium-sulfur batteries.* J Am Chem Soc, 2012. **134**(45): p. 18510-3.

22. Wang, H., et al., *Graphene-Wrapped Sulfur Particles as a Rechargeable Lithium–Sulfur Battery Cathode Material with High Capacity and Cycling Stability.* Nano Letters, 2011. **11**(7): p. 2644-2647.

23. Ji, X., K.T. Lee, and L.F. Nazar, *A highly ordered nanostructured carbon-sulphur cathode for lithium-sulphur batteries.* Nat Mater, 2009. **8**(6): p. 500-506.

24. Zhao, Y., et al., *Encapsulating MWNTs into Hollow Porous Carbon Nanotubes: A Tube-in-Tube Carbon Nanostructure for High-Performance Lithium-Sulfur Batteries.* Advanced Materials, 2014. **26**(30): p. 5113-5118.

25. Zhang, C., et al., *Confining Sulfur in Double-Shelled Hollow Carbon Spheres for Lithium–Sulfur Batteries.* Angewandte Chemie International Edition, 2012. **51**(38): p. 9592-9595.

26. Wu, H.B., et al., *Embedding Sulfur in MOF-Derived Microporous Carbon Polyhedrons for Lithium–Sulfur Batteries.* Chemistry – A European Journal, 2013. **19**(33): p. 10804-10808.

27. Bruce, P.G., *Energy storage beyond the horizon: Rechargeable lithium batteries.* Solid State Ionics, 2008. **179**(21-26): p. 752-760.

28. Liang, C., N.J. Dudney, and J.Y. Howe, *Hierarchically Structured Sulfur/Carbon Nanocomposite Material for High-Energy Lithium Battery.* Chemistry of Materials, 2009. **21**(19): p. 4724-4730.

29. Ye, H., et al., *Tuning the porous structure of carbon hosts for loading sulfur toward long lifespan cathode materials for Li-S batteries.* Journal of Materials Chemistry A, 2013. **1**(22): p. 6602-6608.

30. Zhang, B., et al., *Enhancement of long stability of sulfur cathode by encapsulating sulfur into micropores of carbon spheres.* Energy & Environmental Science, 2010. **3**(10): p. 1531-1537.

31. Moon, S., et al., *Encapsulated Monoclinic Sulfur for Stable Cycling of Li–S Rechargeable Batteries.* Advanced Materials, 2013. **25**(45): p. 6547-6553.

32. Li, Z., et al., *A Highly Ordered Meso@Microporous Carbon-Supported Sulfur@Smaller Sulfur Core–Shell Structured Cathode for Li–S Batteries.* ACS Nano, 2014. **8**(9): p. 9295-9303.

33. Tao, X., et al., *Highly mesoporous carbon foams synthesized by a facile, cost-effective and template-free Pechini method for advanced lithium-sulfur batteries.* Journal of Materials Chemistry A, 2013. **1**(10): p. 3295-3301.

34. Schuster, J., et al., *Spherical Ordered Mesoporous Carbon Nanoparticles with High Porosity for Lithium–Sulfur Batteries.* Angewandte Chemie International Edition, 2012. **51**(15): p. 3591-3595.

35. Li, X., et al., *Optimization of mesoporous carbon structures for lithium-sulfur battery applications.* Journal of Materials Chemistry, 2011. **21**(41): p. 16603-16610.

36. Wang, J., et al., *Polymer lithium cells with sulfur composites as cathode materials.* Electrochimica Acta, 2003. **48**(13): p. 1861-1867.

37. Ji, X., et al., *Stabilizing lithium–sulphur cathodes using polysulphide reservoirs.* Nat Commun, 2011. **2**: p. 325.

38. Lai, C., et al., *Synthesis and Electrochemical Performance of Sulfur/Highly Porous Carbon Composites.* The Journal of Physical Chemistry C, 2009. **113**(11): p. 4712-4716.

39. He, G., X. Ji, and L. Nazar, *High "C" rate Li-S cathodes: sulfur imbibed bimodal porous carbons.* Energy & Environmental Science, 2011. **4**(8): p. 2878-2883.

40. Wei, S., et al., *Pig bone derived hierarchical porous carbon and its enhanced cycling performance of lithium-sulfur batteries.* Energy & Environmental Science, 2011. **4**(3): p. 736-740.

41. Ahn, W., et al., *Synthesis and electrochemical properties of a sulfur-multi walled carbon nanotubes composite as a cathode material for lithium sulfur batteries.* Journal of Power Sources, 2012. **202**(0): p. 394-399.

42. Yuan, L., et al., *Improvement of cycle property of sulfur-coated multi-walled carbon nanotubes composite cathode for lithium/sulfur batteries.* Journal of Power Sources, 2009. **189**(2): p. 1141-1146.

43. Chen, J.-j., et al., *A hierarchical architecture S/MWCNT nanomicrosphere with large pores for lithium sulfur batteries.* Physical Chemistry Chemical Physics, 2012. **14**(16): p. 5376-5382.

44. Zheng, W., et al., *Novel nanosized adsorbing sulfur composite cathode materials for the advanced secondary lithium batteries.* Electrochimica Acta, 2006. **51**(7): p. 1330-1335.

45. Elazari, R., et al., *Sulfur-Impregnated Activated Carbon Fiber Cloth as a Binder-Free Cathode for Rechargeable Li-S Batteries.* Advanced Materials, 2011. **23**(47): p. 5641-5644.

46. Ji, L., et al., *Porous carbon nanofiber-sulfur composite electrodes for lithium/sulfur cells.* Energy & Environmental Science, 2011. **4**(12): p. 5053-5059.

47. Zhang, X.-Q., et al., *Synthesis of superior carbon nanofibers with large aspect ratio and tunable porosity for electrochemical energy storage.* Journal of Materials Chemistry A, 2013. **1**(33): p. 9449-9455.

48. Miao, L.-X., et al., *A high sulfur content composite with core-shell structure as cathode material for Li-S batteries.* Journal of Materials Chemistry A, 2013. **1**(38): p. 11659-11664.

49. Ji, X., et al., *Stabilizing lithium-sulphur cathodes using polysulphide reservoirs.* Nat Commun, 2011. **2**: p. 325.

50. Evers, S., T. Yim, and L.F. Nazar, *Understanding the Nature of Absorption/Adsorption in Nanoporous Polysulfide Sorbents for the Li–S Battery.* The Journal of Physical Chemistry C, 2012. **116**(37): p. 19653-19658.

51. Sun, F., et al., *A high-rate lithium–sulfur battery assisted by nitrogen-enriched mesoporous carbons decorated with ultrafine La2O3 nanoparticles.* Journal of Materials Chemistry A, 2013. **1**(42): p. 13283.

52. Choi, Y.J., et al., *Electrochemical properties of sulfur electrode containing nano Al2O3 for lithium/sulfur cell.* Physica Scripta, 2007. **T129**: p. 62-65.

53. ARICÒ, A.S., et al., *Nanostructured materials for advanced energy conversion and storage devices.* NATURE MATERIALS, 2005. **4**.

54. Kim, S., et al., *Positive electrode for lithium-sulfur battery and lithium-sulfur battery fabricated using same*. 2007, Google Patents.

55. Ma, L., et al., *Tethered Molecular Sorbents: Enabling Metal-Sulfur Battery Cathodes.* Advanced Energy Materials, 2014: p. n/a-n/a.

56. Guo, J., et al., *Lithium-sulfur battery cathode enabled by lithium-nitrile interaction.* J Am Chem Soc, 2013. **135**(2): p. 763-7.

57. Tao, X., et al., *Strong Sulfur Binding with Conducting Magneli-Phase TinO2n-1 Nanomaterials for Improving Lithium-Sulfur Batteries.* Nano Lett, 2014. **14**(9): p. 5288-94.

58. Pang, Q., et al., *Surface-enhanced redox chemistry of polysulphides on a metallic and polar host for lithium-sulphur batteries.* Nat Commun, 2014. **5**: p. 4759.

59. Evers, S. and L.F. Nazar, *Graphene-enveloped sulfur in a one pot reaction: a cathode with good coulombic efficiency and high practical sulfur content.* Chem Commun (Camb), 2012. **48**(9): p. 1233-5.

60. Ji, L., et al., *Graphene oxide as a sulfur immobilizer in high performance lithium/sulfur cells.* J Am Chem Soc, 2011. **133**(46): p. 18522-5.

61. Sun, H., et al., *A composite material of uniformly dispersed sulfur on reduced graphene oxide: Aqueous one-pot synthesis, characterization and excellent performance as the cathode in rechargeable lithium-sulfur batteries.* Nano Research, 2012. **5**(10): p. 726-738.

62. Zhang, F.-f., et al., *Facile and effective synthesis of reduced graphene oxide encapsulated sulfur via oil/water system for high performance lithium sulfur cells.* Journal of Materials Chemistry, 2012. **22**(23): p. 11452.

63. Zhang, L., et al., *Electronic structure and chemical bonding of a graphene oxide-sulfur nanocomposite for use in superior performance lithium-sulfur cells.* Phys Chem Chem Phys, 2012. **14**(39): p. 13670-5.

64. Wang, B., S.M. Alhassan, and S.T. Pantelides, *Formation of Large Polysulfide Complexes during the Lithium-Sulfur Battery Discharge.* Physical Review Applied, 2014. **2**(3): p. 034004.

65. Sun, F., et al., *High efficiency immobilization of sulfur on nitrogen-enriched mesoporous carbons for Li-S batteries.* ACS Appl Mater Interfaces, 2013. **5**(12): p. 5630-8.

66. Sun, X.G., et al., *Lithium-sulfur batteries based on nitrogen-doped carbon and an ionic-liquid electrolyte.* ChemSusChem, 2012. **5**(10): p. 2079-85.

67. Xu, H., et al., *The superior cycle and rate performance of a novel sulfur cathode by immobilizing sulfur into porous N-doped carbon microspheres.* Chem Commun (Camb), 2014. **50**(72): p. 10468-70.

68. Yang, J., et al., *Functionalized N-Doped Porous Carbon Nanofiber Webs for a Lithium–Sulfur Battery with High Capacity and Rate Performance.* The Journal of Physical Chemistry C, 2014. **118**(4): p. 1800-1807.

69. Li, X., et al., *Tailoring interactions of carbon and sulfur in Li-S battery cathodes: significant effects of carbon-heteroatom bonds.* Journal of Materials Chemistry A, 2014. **2**(32): p. 12866-12872.

70. Hassoun, J., et al., *Nickel-Layer Protected, Carbon-Coated Sulfur Electrode for Lithium Battery.* Journal of The Electrochemical Society, 2012. **159**(4): p. A390.

71. Zheng, S., et al., *Copper-Stabilized Sulfur-Microporous Carbon Cathodes for Li-S Batteries.* Advanced Functional Materials, 2014. **24**(26): p. 4156-4163.

72. Chung, S.-H. and A. Manthiram, *Lithium–sulfur batteries with superior cycle stability by employing porous current collectors.* Electrochimica Acta, 2013. **107**: p. 569-576.

73. Demir-Cakan, R., et al., *Cathode composites for Li-S batteries via the use of oxygenated porous architectures.* J Am Chem Soc, 2011. **133**(40): p. 16154-60.

74. Zheng, J., et al., *Lewis acid-base interactions between polysulfides and metal organic framework in lithium sulfur batteries.* Nano Lett, 2014. **14**(5): p. 2345-52.

75. Bao, W., et al., *Confine sulfur in mesoporous metal–organic framework @ reduced graphene oxide for lithium sulfur battery.* Journal of Alloys and Compounds, 2014. **582**: p. 334-340.

76. Wang, Z., et al., *A Metal–Organic Framework with Open Metal Sites for Enhanced Confinement of Sulfur and Lithium–Sulfur Battery of Long Cycling Life.* Crystal Growth & Design, 2013. **13**(11): p. 5116-5120.

77. Zheng, G., et al., *Amphiphilic Surface Modification of Hollow Carbon Nanofibers for Improved Cycle Life of Lithium Sulfur Batteries.* Nano Letters, 2013. **13**(3): p. 1265-1270.

78. Xiao, L., et al., *A Soft Approach to Encapsulate Sulfur: Polyaniline Nanotubes for Lithium-Sulfur Batteries with Long Cycle Life.* Advanced Materials, 2012. **24**(9): p. 1176-1181.

79. Fu, Y. and A. Manthiram, *Enhanced Cyclability of Lithium–Sulfur Batteries by a Polymer Acid-Doped Polypyrrole Mixed Ionic–Electronic Conductor.* Chemistry of Materials, 2012. **24**(15): p. 3081-3087.

80. Wu, F., et al., *Sulfur/Polythiophene with a Core/Shell Structure: Synthesis and Electrochemical Properties of the Cathode for Rechargeable Lithium Batteries.* The Journal of Physical Chemistry C, 2011. **115**(13): p. 6057-6063.

81. Fanous, J., et al., *Structure-Related Electrochemistry of Sulfur-Poly(acrylonitrile) Composite Cathode Materials for Rechargeable Lithium Batteries.* Chemistry of Materials, 2011. **23**(22): p. 5024-5028.

82. Li, W., et al., *High-performance hollow sulfur nanostructured battery cathode through a scalable, room temperature, one-step, bottom-up approach.* Proceedings of the National Academy of Sciences, 2013. **110**(18): p. 7148-7153.

83. Yang, Y., et al., *Improving the Performance of Lithium-Sulfur Batteries by Conductive Polymer Coating.* ACS NANO, 2011. **5**(11): p. 9187-9193.

84. Fu, Y. and A. Manthiram, *Orthorhombic Bipyramidal Sulfur Coated with Polypyrrole Nanolayers As a Cathode Material for Lithium–Sulfur Batteries.* The Journal of Physical Chemistry C, 2012. **116**(16): p. 8910-8915.

85. Zhang, Y., et al., *One-step synthesis of branched sulfur/polypyrrole nanocomposite cathode for lithium rechargeable batteries.* Journal of Power Sources, 2012. **208**: p. 1-8.

86. Liang, X., et al., *A composite of sulfur and polypyrrole–multi walled carbon combinatorial nanotube as cathode for Li/S battery.* Journal of Power Sources, 2012. **206**: p. 409-413.

87. Liang, X., et al., *A nano-structured and highly ordered polypyrrole-sulfur cathode for lithium–sulfur batteries.* Journal of Power Sources, 2011. **196**(16): p. 6951-6955.

88. Qiu, L., et al., *Preparation and enhanced electrochemical properties of nano-sulfur/poly(pyrrole-co-aniline) cathode material for lithium/sulfur batteries.* Electrochimica Acta, 2010. **55**(15): p. 4632-4636.

89. Wang, J., et al., *A Novel Conductive Polymer–Sulfur Composite Cathode Material for Rechargeable Lithium Batteries.* Advanced Materials, 2002. **14**(13-14): p. 963-965.

90. Hwang, T.H., et al., *One-Dimensional Carbon–Sulfur Composite Fibers for Na–S Rechargeable Batteries Operating at Room Temperature.* Nano Letters, 2013. **13**(9): p. 4532-4538.

91. Yu, X.-g., et al., *Lithium storage in conductive sulfur-containing polymers.* Journal of Electroanalytical Chemistry, 2004. **573**(1): p. 121-128.

92. Yu, X., et al., *Stable-cycle and high-capacity conductive sulfur-containing cathode materials for rechargeable lithium batteries.* Journal of Power Sources, 2005. **146**(1–2): p. 335-339.

93. Yin, L., et al., *Polyacrylonitrile/graphene composite as a precursor to a sulfur-based cathode material for high-rate rechargeable Li-S batteries.* Energy & Environmental Science, 2012. **5**(5): p. 6966-6972.

94. Liu, Z., et al., *Lyotropic Liquid Crystal of Polyacrylonitrile-Grafted Graphene Oxide and Its Assembled Continuous Strong Nacre-Mimetic Fibers.* Macromolecules, 2013. **46**(17): p. 6931-6941.

95. Mo, Y., et al., *Preparation and tribological performance of chemically-modified reduced graphene oxide/polyacrylonitrile composites.* Composites Part A: Applied Science and Manufacturing, 2013. **54**(0): p. 153-158.

96. Li, J., et al., *A sulfur–polyacrylonitrile/graphene composite cathode for lithium batteries with excellent cyclability.* Journal of Power Sources, 2014. **252**(0): p. 107-112.

97. Zhang, Y.Z., et al., *Sulfur/polyacrylonitrile/carbon multi-composites as cathode materials for lithium/sulfur battery in the concentrated electrolyte.* Journal of Materials Chemistry A, 2014. **2**(13): p. 4652-4659.

98. Luo, C., et al., *Carbonized Polyacrylonitrile-Stabilized SeSx Cathodes for Long Cycle Life and High Power Density Lithium Ion Batteries.* Advanced Functional Materials, 2014. **24**(26): p. 4082-4089.

99. Ye, J., et al., *Sulfur/carbon nanocomposite-filled polyacrylonitrile nanofibers as a long life and high capacity cathode for lithium-sulfur batteries.* Journal of Materials Chemistry A, 2015. **3**(14): p. 7406-7412.

100. Xin, S., et al., *Smaller Sulfur Molecules Promise Better Lithium–Sulfur Batteries.* Journal of the American Chemical Society, 2012. **134**(45): p. 18510-18513.

101. Wang, Z., et al., *Enhancing lithium–sulphur battery performance by strongly binding the discharge products on amino-functionalized reduced graphene oxide.* Nat Commun, 2014. **5**.

102. Guo, J., et al., *Lithium–Sulfur Battery Cathode Enabled by Lithium–Nitrile Interaction.* Journal of the American Chemical Society, 2012. **135**(2): p. 763-767.

103. Armand, M. and J.M. Tarascon, *Building better batteries.* Nature, 2008. **451**(7179): p. 652-657.

104. WHITTINGHAM, M.S., *Electrical Energy Storage and Intercalation Chemistry.* Science, 1976. **192**(4244): p. 1126-1127.

105. Bruce, P.G., et al., *Li-O2 and Li-S batteries with high energy storage.* Nat Mater, 2012. **11**(1): p. 19-29.

106. Manthiram, A., S.-H. Chung, and C. Zu, *Lithium–Sulfur Batteries: Progress and Prospects.* Advanced Materials, 2015. **27**(12): p. 1980-2006.

107. Zhao, Q., et al., *Sulfur Nanodots Electrodeposited on Ni Foam as High-Performance Cathode for Li–S Batteries.* Nano Letters, 2015. **15**(1): p. 721-726.

108. Guo, J., et al., *Lithium–Sulfur Battery Cathode Enabled by Lithium–Nitrile Interaction.* Journal of the American Chemical Society, 2013. **135**(2): p. 763-767.

109. Aurbach, D., et al., *Prototype systems for rechargeable magnesium batteries.* Nature, 2000. **407**(6805): p. 724-727.

110. Lin, M.-C., et al., *An ultrafast rechargeable aluminium-ion battery.* Nature, 2015. **520**(7547): p. 324-328.

111. Yabuuchi, N., et al., *P2-type Nax[Fe1/2Mn1/2]O2 made from earth-abundant elements for rechargeable Na batteries.* Nat Mater, 2012. **11**(6): p. 512-517.

112. Manthiram, A. and X. Yu, *Ambient Temperature Sodium–Sulfur Batteries.* Small, 2015. **11**(18): p. 2108-2114.

113. Adelhelm, P., et al., *From lithium to sodium: cell chemistry of room temperature sodium–air and sodium–sulfur batteries.* Beilstein Journal of Nanotechnology, 2015. **6**: p. 1016-1055.

114. Sudworth, J.L., *The sodium sulfur battery*, A.R. Tilley, Editor. 1985, Chapman & Hall: London ;.

115. Hueso, K.B., M. Armand, and T. Rojo, *High temperature sodium batteries: status, challenges and future trends.* Energy & Environmental Science, 2013. **6**(3): p. 734-749.

116. Yang, Y., G. Zheng, and Y. Cui, *Nanostructured sulfur cathodes.* Chemical Society Reviews, 2013. **42**(7): p. 3018-3032.

117. Manthiram, A., et al., *Rechargeable Lithium–Sulfur Batteries.* Chemical Reviews, 2014. **114**(23): p. 11751-11787.

118. Yin, Y.-X., et al., *Lithium–Sulfur Batteries: Electrochemistry, Materials, and Prospects.* Angewandte Chemie International Edition, 2013. **52**(50): p. 13186-13200.

119. Hartmann, P., et al., *A rechargeable room-temperature sodium superoxide (NaO2) battery.* Nat Mater, 2013. **12**(3): p. 228-232.

120. Peng, H.-J. and Q. Zhang, *Designing Host Materials for Sulfur Cathodes: From Physical Confinement to Surface Chemistry.* Angewandte Chemie International Edition, 2015: p. n/a-n/a.

121. Xin, S., et al., *A High-Energy Room-Temperature Sodium-Sulfur Battery.* Advanced Materials, 2014. **26**(8): p. 1261-1265.

122. Zhang, S., et al., *Recent Advances in Electrolytes for Lithium–Sulfur Batteries.* Advanced Energy Materials, 2015: p. n/a-n/a.

123. Lu, Y., et al., *Ionic-Liquid–Nanoparticle Hybrid Electrolytes: Applications in Lithium Metal Batteries.* Angewandte Chemie International Edition, 2014. **53**(2): p. 488-492.

124. Lu, Y., et al., *Ionic liquid-nanoparticle hybrid electrolytes and their application in secondary lithium-metal batteries.* Adv Mater, 2012. **24**(32): p. 4430-5.

125. Lu, Y., Z. Tu, and L.A. Archer, *Stable lithium electrodeposition in liquid and nanoporous solid electrolytes.* Nat Mater, 2014. **13**(10): p. 961-969.

126. Zheng, G., et al., *Interconnected hollow carbon nanospheres for stable lithium metal anodes.* Nat Nano, 2014. **9**(8): p. 618-623.

127. Slater, A.G. and A.I. Cooper, *Function-led design of new porous materials.* Science, 2015. **348**(6238).

128. Cravillon, J., et al., *Controlling Zeolitic Imidazolate Framework Nano- and Microcrystal Formation: Insight into Crystal Growth by Time-Resolved In Situ Static Light Scattering.* Chemistry of Materials, 2011. **23**(8): p. 2130-2141.

129. Erlich, R.H. and A.I. Popov, *Spectroscopic studies of ionic solvation. X. Study of the solvation of sodium ions in nonaqueous solvents by sodium-23 nuclear magnetic resonance.* Journal of the American Chemical Society, 1971. **93**(22): p. 5620-5623.

130. Ong, S.P., et al., *Voltage, stability and diffusion barrier differences between sodium-ion and lithium-ion intercalation materials.* Energy & Environmental Science, 2011. **4**(9): p. 3680-3688.

131. Cohn, G., L. Ma, and L.A. Archer, *A novel non-aqueous aluminum sulfur battery.* Journal of Power Sources, 2015. **283**: p. 416-422.

132. Liang, X., et al., *A highly efficient polysulfide mediator for lithium–sulfur batteries.* Nat Commun, 2015. **6**.

133. Manan, N.S.A., et al., *Electrochemistry of Sulfur and Polysulfides in Ionic Liquids.* The Journal of Physical Chemistry B, 2011. **115**(47): p. 13873-13879.

134. Weppner, W. and R.A. Huggins, *Determination of the Kinetic Parameters of Mixed-Conducting Electrodes and Application to the System Li3Sb.* Journal of The Electrochemical Society, 1977. **124**(10): p. 1569-1578.

135. Kamlet, M.J., et al., *Linear solvation energy relationships. 13. Relationship between the Hildebrand solubility parameter, .delta.H, and the solvatochromic parameter, .pi.*.* Journal of the American Chemical Society, 1981. **103**(20): p. 6062-6066.

136. Lu, Y., et al., *Ionic liquid-nanoparticle hybrid electrolytes.* Journal of Materials Chemistry, 2012. **22**(9): p. 4066-4072.